Chair of Reservoir Engineering

Master's Thesis

# Mechanistic Study of the Carbonated Smart Water in the Naturally Fractured Reservoir

Loay Al Kafry, BSc

February 2020

*To my parents, brothers, and my wife.*

# AFFIDAVIT

I declare on oath that I wrote this thesis independently, did not use other than the specified sources and aids, and did not otherwise use any unauthorized aids.

I declare that I have read, understood, and complied with the guidelines of the senate of the Montanuniversität Leoben for "Good Scientific Practice".

Furthermore, I declare that the electronic and printed version of the submitted thesis are identical, both, formally and with regard to content.

Date 03.02.2020

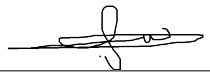

Signature Author
Loay, Al Kafry

# Acknowledgments

*I would love to thank my supervisor Prof. Kharrat for his great help, encouragement, and guidance, to finish this research.*

*A vast and limitless thanks to Gabi and Herbert, who lighted this way for me in a hard time. GIG members! I cannot forget to thank you for everything you did for me to reach this stage.*

*A special thanks to my friends Mr. Dipl.-Ing. Walid Hamad and Mohammad Alfares, BSc. All of my friends! Thank you very much.*

.

# Abstract

Carbonated Smart Water Injection (CSMWI) has a lot of interest, especially in the last decade. This interest stems from its results in the recovery factor enhancement and the permanent storage capacity of the carbon dioxide. This method has been mainly studied for sandstone formations, and less attention has been given in the carbonates and especially in the naturally fractured carbonates. In this thesis, the effect of the CSMWI on the recovery factor in the naturally fractured carbonates has been investigated. Furthermore, the capability of the CSMWI to store the $CO_2$ permanently and safely in the reservoir has been studied.

This work has been established based on core flooding experimental data, and it has been extended to a five spots model. CMG simulator has been used to generate the CSMWI model, and the sensitivity analysis tool has been used to identify the optimum water composition and salinity. To determine the $CO_2$ molality and solubility in the obtained smart water, the PHREEQC simulator has been used, and the results have been introduced in the CMG model. Furthermore, the PHREEQC database has been used to define the geochemical reactions that could occur in the carbonates when the CSMWI is injected.

CSMWI in the core scale showed more oil recovery than Smart Water Injection (SMWI), Carbonated Seawater injection (CSWI), and Seawater injection (SWI) by 14, 7.6, 26.8 %, respectively. In the pilot-scale model, CSMWI recovered more oil than the SMWI by 5 to 8% based on the heterogeneity and fractures availability. The mechanisms behind this increment are; mineral dissolution, ion exchange, viscosity reduction, and wettability alteration, which have been described and analyzed in this work. These mechanisms were studied in the fractures and matrices to illustrate the effect of the fractures on the oil recovery.

More than 50% of the injected $CO_2$ within the CSMWI has been permanently captured in the residual oil and water in the reservoir. It has been concluded that the stored $CO_2$ in the reservoir depends on the amount of residual oil saturation. Where the higher the remaining oil in the reservoir, the higher the stored $CO_2$ amount.

# Zusammenfassung

Carbonated Smart Water Injection (CSMWI) hat vor allem im letzten Jahrzehnt großes Interesse geweckt. Dieses Interesse ergibt sich aus den Ergebnissen der Verbesserung des Rückgewinnungsfaktors und der permanenten Speicherkapazität des Kohlendioxids. Diese Methode wurde hauptsächlich für Sandsteinformationen untersucht, wobei den Carbonaten und insbesondere den natürlich gebrochenen Carbonaten weniger Aufmerksamkeit geschenkt wurde. In dieser Arbeit wurde der Einfluss des CSMWI auf den Rückgewinnungsfaktor in den natürlich gebrochenen Carbonaten untersucht. Zusätzlich wurde die Fähigkeit des CSMWI untersucht, das CO2 dauerhaft und sicher im Reservoir zu speichern.

Diese Arbeit wurde auf der Grundlage von experimentellen Kernflutungsdaten erstellt und auf ein Pilot-Modell erweitert. Die Simulationssoftware von CMG wurde verwendet, um das CSMWI-Modell zu generieren, und mit dem Sensitivitätsanalysetool die optimale Wasserzusammensetzung und der optimale Salzgehalt ermittelt. Zur Bestimmung der CO2-Molalität und -Löslichkeit in dem erhaltenen SMW wurde der PHREEQC-Simulator verwendet und die Ergebnisse in das CMG-Modell integriert. Darüber hinaus wurde die PHREEQC-Datenbank verwendet, um die geochemischen Reaktionen zu definieren, die in den Carbonaten auftreten können, wenn das CSMWI injiziert wird.

CSMWI in der Größenordnung des Kerns zeigten eine höhere Ölrückgewinnung als Smart Water Injection (SMWI), Carbonated Seawater Injection (CSWI) und Seawater Injection (SWI) um jeweils 14, 7,6 bzw. 26,8%. Im Modell des Pilotexperiments gewann CSMWI um 5 bis 8% mehr Öl zurück als SMWI, basierend auf der Heterogenität und der Verfügbarkeit von Frakturen. Die Mechanismen hinter diesem Zuwachs, wie z. B. die Auflösung von Mineralien, der Ionenaustausch, die Verringerung der Viskosität und die Änderung der Benetzbarkeit, wurden beschrieben und analysiert. Diese Mechanismen wurden in den Frakturen und Matrizen untersucht, um die Auswirkung der Frakturen auf die Ölgewinnung zu veranschaulichen.

Mehr als 50% des im CSMWI eingespritzten CO2 wurden dauerhaft im Rest-Öl und dem Wasser in der Lagerstätte gebunden. Es wurde der Entschluss gezogen, dass das in der Lagerstätte gespeicherte CO2 von der Menge der verbleibenden Ölsättigung abhängt. Je höher das verbleibende Öl im Reservoir ist, desto höher ist die gespeicherte CO2-Menge.

# Table of Contents


Declaration ..... iii
Erklärung ..... iii
Acknowledgments ..... iv
Abstract ..... v
Zusammenfassung ..... vi
Table of Contents ..... vii
List of Figures ..... ix
List of Tables ..... xi
Abbreviations ..... xiii
Chapter 1 ..... 15
1.1 Background and Context ..... 18
1.2 Scope and Objectives ..... 18
1.3 Achievements ..... 18
1.4 Technical Issues ..... 19
1.5 Overview of Dissertation ..... 19
Chapter 2 ..... 21
2.1 Potential Mechanisms of CSMWI ..... 21
2.1.1 Multi-Ion Exchange (MIE) ..... 21
2.1.2 Mineral dissolution ..... 22
2.1.3 Wettability Alteration and IFT Reduction: ..... 24
2.1.4 The Solubility of $CO_2$ in Brine and Oil Swelling: ..... 25
2.1.5 Diffusion coefficient of $CO_2$ ..... 28
2.2 $CO_2$ Capturing (sequestration) ..... 29
2.3 Effect of the injection rate ..... 30
2.4 Effect of the temperature on the recovery factor ..... 31
2.5 Effect of the pressure on the recovery factor ..... 31
2.6 Simulation Works ..... 31
Chapter 3 ..... 33
3.1 Overview of the Related Experiment ..... 33
3.2 Model Building ..... 34
3.2.1 Core scale model ..... 34
3.2.2 Smart Water Injection (SMWI) ..... 40
3.2.3 Carbonated Smart Water Injection (CSMWI) ..... 46
3.2.4 Pilot-scale model ..... 46
Chapter 4 ..... 51
4.1 Results Section ..... 51
4.1.1 Recovery Factor of Smart water ..... 51

4.1.2 Recovery Factor of Carbonated Smart water ..... 51
4.1.3 $CO_2$ Storage ..... 56
4.2 Discussion Section ..... 58
4.2.1 Mechanisms ..... 58
Chapter 5 ..... 73
5.1 Summary ..... 73
5.2 Evaluation ..... 74
5.3 Future Work ..... 74
Chapter 6 ..... 75
References ..... 75

# List of Figures

Figure 1: P, T Effect on $CO_2$ Solubility, PHREEQC Tutorial after (Parkhurst et al., 2013) ... 27
Figure 2: 1-D Core Model ... 35
Figure 3: P-T Diagram from WINPROP Simulator ... 36
Figure 4: History Matching of Oil Recovery - Core results, Water with 40,000ppm NaCl ... 38
Figure 5: Water Oil Relative Permeability Curves ... 39
Figure 6: History Matching of Oil Recovery in the Core, using CW with 40,000ppm NaCl. . 39
Figure 7: Oil Recovery changing by changing the $SO_4^{2-}$ Composition ... 40
Figure 8: Oil Recovery changing in the CW by changing the $SO_4^{2-}$ Composition ... 40
Figure 9: Seawater Optimization Study ... 42
Figure 10: A Sensitivity Analysis Study of the water compositions. ... 43
Figure 11: SMW- Sensitivity Analysis Results ... 44
Figure 12: Morris Analysis - the most effective components in the sensitivity analysis. ... 45
Figure 13: Sobol Analysis. ... 46
Figure 14: Permeability in the Homogeneous Pilot Scale Model ... 47
Figure 15: Porosity Distribution in the Heterogeneous Five Spots Model. ... 48
Figure 16: Permeability Distribution in the Heterogeneous Five Spots Model. ... 48
Figure 17: Water and Oil Relative Permeability curves in the matrix and fracture ... 49
Figure 18: RF in Core Scale, NaCl, SWI, SMAWI, and CSMWI ... 52
Figure 19: RF in CSWI and CSWI Cases in the Core Scale Case ... 53
Figure 20: Recovery Factor in the Secondary and Tertiary Stages in the Core Scale Case ... 54
Figure 21: Field Oil Recovery in the Heterogeneous Reservoir ... 55
Figure 22: Field Oil Recovery in the Homogeneous System ... 55
Figure 23: $CO_2$ Storage in the Core model ... 56
Figure 24: $CO_2$ Storage in the Core model after 6 PV injection (CSMWI) ... 57
Figure 25: Stored $CO_2$ in the Fractured and Non-Fractured Reservoirs ... 57
Figure 26: Oil Saturation in the Fractured and Non-Fractured Heterogeneous Reservoirs. ... 58
Figure 27: Aqueous Components Change in the Core ... 59
Figure 28: Aqueous Components Change in the CSMWI and SMWI in the fractured heterogeneous Reservoir ... 60
Figure 29: Aqueous Components Change in the Non-Fractured Reservoir ... 60
Figure 30 Aqueous Components Change in the Fractured Reservoir ... 61
Figure 31: $NaSO_4^-$ Change in the Heterogeneous Reservoir. ... 61
Figure 32: Pore Volume Change in the Core after 5 PVI. ... 62
Figure 33: Pore Volume change in the Reservoir Cases (Field) ... 63
Figure 34: Pore Volume change in the Fractured Reservoir Cases (Fractures and Matrices) . 64
Figure 35: Mineral Dissolution in the Fractured Homogeneous Reservoir ... 65
Figure 36: Mineral Dissolution % in the Several Cases of the Reservoir ... 65
Figure 37: Mineral Dissolution in the CSMWI and SMWI ... 66
Figure 38: Oil Viscosity in the injector (inlet), Core Case ... 67
Figure 39: Oil Viscosity in the Producer (outlet), Core Case ... 67
Figure 40: Oil Viscosity and Saturation in the injector, Pilot Case. ... 68
Figure 41: Oil Viscosity and Saturation in the Producer, Pilot Case ... 68
Figure 42: Oil Viscosity, in the CSMWI and SMWI cases in the Fractured Heterogeneous Reservoir ... 69
Figure 43: Water Cut in the Core Scale for SMWI and CSMWI ... 70
Figure 44: Water Cut in the Pilot Scale for SMWI and CSMWI. ... 70
Figure 45: Wettability Alteration in the Matrix by Using CSMWI ... 71
Figure 46: Wettability Alteration in the Fractures by Using CSMWI ... 71
Figure 47: PH Change in the Core ... 72
Figure 48: PH Change in the Reservoir ... 72

# List of Tables

Table 1: Experimental Data (Bakhshi et al., 2018) ..... 34
Table 2: Core Dimensions ..... 35
Table 3: Reservoir P, T, and Oil Components ..... 36
Table 4: The used Water Compositions ..... 44
Table 5: Pilot Properties ..... 47
Table 6: The obtained RF for each scenario. ..... 51
Table 7: Pore Volume Increase Values in Different Cases in the Pilot-Scale ..... 63

# Abbreviations

| | |
|---|---|
| FE | Finite Element |
| $CO_2$ | Carbon Dioxide |
| EOR | Enhanced Oil Recovery |
| WAG | Water Alternating Gas |
| SWAG | Simultaneous Water and Gas |
| CW | Carbonated Water |
| CWI | Carbonated Water Injection |
| CWF | Carbonated Water Flooding |
| CLSWI | Carbonated Low Salinity Water Injection |
| CSMWI | Carbonated Smart Water Injection |
| LSWI | Low Salinity Water Injection |
| TCWI | Tertiary Recovery - Carbonated Water Injection |
| SCWI | Secondary Recovery - Carbonated Water Injection |
| P | Pressure |
| T | Temperature |
| IFT | Interfacial Tension |
| Z | Zeta |
| NMR | Nuclear Magnetic Resonance |
| RF | Recovery Factor |
| MIE | Multicomponent Ion Exchange |
| SW4S | Seawater with Four Times Sulfate |
| PSD | Pore Size Distribution |
| ICP | Inductively Coupled Plasma |
| SEM | Scanning Electron Microscope |

| | |
|---|---|
| Nc | Capillary Number |
| ΔG | Gibbs Free Energy |
| Aq | Aqueous Phase |
| OIIP | Oil Initially in Place |
| NP | Net Oil Production |
| CMG | Computer Modelling Group Ltd |
| E300 | Eclipse 300 |
| SRK | Soave-Redlich-Kwong Equation of State |
| IMPES | Implicit Pressure Explicit Saturation |
| PVT | Pressure Volume Temperature Analysis |

# Chapter 1

## Introduction

Carbonate reservoirs represent more than two-thirds of oil and gas reserves in the world, while the sandstones and other lithologies acquire the residual reservoirs (Afekare & Radonjic, 2017). For several decades, the conventional water injection was the commonly used method to increase the recovery factor after the primary recovery due to its high feasibility compared to other methods. The new environmental situations, regulations, and oil price fluctuation required new aspects to be considered in the used recovery methods; therefore the attentions were turned to which called the co-optimization methods such as carbon dioxide $CO_2$ injection, water alternating gas WAG, simultaneous water and gas SWAG, and carbonated water injection CWI as enhanced oil recovery EOR methods and $CO_2$ storage processes.

However, carbonated water injection proved significant enhancement of the oil recovery and typical decrease of the residual oil saturation over the traditional seawater injection (Bakhshi et al. 2018; Kilybay et al., 2017; Lee et al., 2017; Seyyedi & Sohrabi, 2016; Sohrabi et al., 2011; Esene et al., 2019).

In 1958 in United States ORCO (Oil Recovery Cooperation) performed the first commercial implementation of CWF in the Dewey-Bartlesville Field, Washington County, Northeast Oklahoma, which was the K&S project (Hickok et al., 1960; Lee et al., 2017).

Carbonated low salinity water injection CLSWI or carbonated smart water injection CSMWI in the carbonate was the latest method in this field of industry. It is a combination of low salinity water and $CO_2$ co-existing in the same phase ($P > 1072$ Psi and $T > 31.1°C$), where under those conditions, the $CO_2$ will be in its supercritical status ( Kechut et al., 2011; Nunez et al., 2017). This method was developed as a tertiary or quaternary recovery method to enhance the oil recovery and to store the $CO_2$ permanently in the reservoir formation (Lee, Jeong, et al., 2017). The CLSWI takes advantage of the high ability of the low salinity water to dissolve the $CO_2$ (salting-out phenomenon). This ensures more mass transfer of the $CO_2$ from the CW to the

oil, based on the high affinity of $CO_2$ to be dissolved in the oil more than water (3 to 7 times) until the fugacity of $CO_2$ becomes equivalent in all existing phases (Bakhshi et al., 2018; Kilybay et al., 2017; Lee, Jeong, et al., 2017).

An improved sweep efficiency is obtained by using the CLSWI because of the stable front of W-O with almost the same viscosity value (Esene et al., 2019), and because of the ability of CW to overcome the shielding phenomenon of water. The shielding prevents the $CO_2$ (free phase) from being in contact with the oil, wherein the carbonated water, the $CO_2$ is dissolved in the water as an aqueous phase (Bakhshi et al., 2018; Honarvar et al., 2017; Mosavat & Torabi, 2014b). On the other hand, CLSW requires a lower pressure injection system and vanquishes the problems of gravity segregation and poor sweep efficiency.

Several experiments and measurements, such as interfacial tension (IFT), contact angle, Nuclear Magnetic Resonance NMR, Zeta ζ-potential, imbibition test, and core flooding tests have been conducted to determine the responsible mechanisms for the high recovery when CLSWI is applied. The proposed mechanisms for the obtained high recovery can be summarized as follows (Al Mesmari et al. 2016; Bakhshi et al., 2018; Honarvar et al., 2017; Kechut et al. 2010; Kilybay et al., 2017; Lee, Jeong, et al., 2017; Luo et al., 2018; Mahzari et al., 2018; Seyyedi & Sohrabi, 2016; Sohrabi et al. 2015):

1- Mineral dissolution due to the reaction between the CW and the reservoir rocks.
2- The solubility of the $CO_2$ into oil that can trigger the liberation of light components in the form of a new gaseous phase that can result in a reduction of the oil viscosity (the main recovery mechanism in the heavy oil).
3- Alteration of the water/oil contact angle, which is a direct indicator of wettability alteration of the crude oil/water/rock system (wettability alteration toward more water-wet).
4- IFT reduction of the water-oil interface.
5- Swelling of oil due to $CO_2$ diffusion results in a coalescence of the isolated oil ganglia (Lashkarbolooki et al. 2018), thus enhancement of the macroscopic sweep efficiency (the main mechanism in the light oil).
6- Fluid redistribution
7- Ions exchange
8- Increase the viscous force of the injecting fluid

One other mechanism was suggested by Perez et al. (1992), which can take place when the pressure decreases in the reservoir below the carbonation pressure. Some $CO_2$ will release and create a gas drive system, which induces a substantial increase in oil production. This occurs only in a case when the amount of gas evolving exceeds the maximum escaping velocity

of the gas. Gas relative permeability in the matrix rock is an important parameter to be known, where the minimum speed of depletion is directly proportional to it. This method could be used cyclically to give better results. Esene et al. (2019) stated that when the pressure declines, the released free $CO_2$ formation gas from the CW solution will connect with the oil droplets forming a thick layer of oil between the brine and free $CO_2$. This oil will flow toward the producer with the free gas ($CO_2$ clusters).

The usage of the CLSWI in the carbonate reservoir could increase the recovery factor to a significant amount based on the water components concentrations, $CO_2$ fraction in the water, oil density, oil viscosity, reservoir pressure, reservoir temperature, and the stage of the implementation (Bakhshi et al., 2018; Honarvar et al., 2017; Kechut et al. 2011; Shakiba et al., 2015). It has been proved that the recovery factor of the CLSWI could reach a higher level when used as a secondary stage and less when used as a tertiary or quaternary stage. The reason behind this increment is: Firstly, the injected CLSW will flow in the previously flooded water pathways, and consequently, it will be in contact with the flooded pores only. Reaching the remaining unflooded oil after conventional WF is more complicated than reaching the remaining oil in the case of secondary CWF. Secondly, in the secondary stage case, $CO_2$ will be continuously transferred from carbonated brine into the oil, where no water prevents the connection. Oil swelling is more effective due to the larger transferred mass of the $CO_2$ that diffuses into the oil. In the secondary flooding, long contact time between the CLSW and oil is available, and the contact starts from the beginning of flooding (Bakhshi et al., 2018; Kilybay et al., 2017; Sohrabi et al., 2011).

Kilybay et al. (2016) obtained the oil recovery factor in carbonate rocks in cores with different permeability values. They found out that permeability had no direct impact on the overall recovery factor. However, the obtained curves indicated that the higher permeable samples had higher mineral dissolution than the low permeable one, especially in the macro-porosity region. This dissolution can be attributed to the higher flow speed due to the lower resistance forces in the large pores and pore throats.

Despite the advantages of the carbonated water, there are some difficulties and restrictions which could limit the usage of this method, such as the availability of the $CO_2$ in the injection regions, $CO_2$ transfer from the $CO_2$ production areas to the field and the incurred costs. Several challenges have been reported and faced, such as corrosion, and the precipitation of the asphaltene around the wellbore region, scale formation, effect of water weakening, and high incurred costs (capital, operating, and maintenance) (Esene et al., 2019).

## 1.1 Background and Context

In the petroleum industry, $CO_2$ has been used for decades to enhance oil recovery. The commonly used method in the EOR was the $CO_2$ gas injection, which has some advantages by increasing the recovery and store the $CO_2$ into the geological formations, but it has, at the same time, some disadvantages, especially the early breakthrough, shielding phenomena, and the gas escaping risk. Those problems afterword have been solved partially by using WAG and SWAG methods, but the need for more effective methods remains urgent. Carbonated water injection was the new method generated from a combination of $CO_2$ flooding and water injection. This method overcame some flaws of the previous methods, such as the shielding phenomena and the early breakthrough. After the magnificent results of the LSWI usage, CW injection has been developed to CLSWI, which proved more oil recovery due to the higher $CO_2$ volume that can be dissolved into the injected water because of the low salinity (PPM) of the water (salting-out phenomena). Furthermore, most of the mechanisms of the LSWI will remain active when the $CO_2$ is dissolved in the water.

The CLSWI research has been mainly focused on sandstone reservoirs until recently due to a better understanding of its behaviors and mechanisms. Limited work has been reported on carbonate reservoirs. The reported results have mainly focused on the core scale experiments and simulations, and rarely on the global heterogeneity but until now, no research has investigated the effect of the CLSWI on the fractured carbonate reservoirs. As known, most of the carbonates are naturally fractured, therefore the demand to study the behavior and effects of the CSMWI on the fractures still exists. This is what has been conducted in this research to shed light on the impact of the CSMWI on the fractures, and to which extent could the heterogeneity affect the results.

## 1.2 Scope and Objectives

The objective of the present work is to study the effects of the carbonated smart water (CSMWI) injection on the naturally fractured carbonate reservoirs regarding the oil recovery factor and $CO_2$ storage in the reservoir formations and to shed light on the potential mechanisms behind these effects.

## 1.3 Achievements

The mechanisms behind the increase of the oil recovery by using the CSMW were studied carefully and compared with other results of the previous works. A novel work in this thesis has been achieved by studying the impact of the fractures and heterogeneity presence on the

results of the CSMWI in the carbonates. This impact has not been studied before in the previous projects.

## 1.4 Technical Issues

The results of this novel work still questionable until its validity is ascertained by the results of the experiments, especially the mechanisms of the production, mineral dissolution, and ion exchange in the fracture-matrix system. This is because of some shortcomings in the simulator, such as the inability to simulate the separated oil ganglia after the production using conventional water flooding. All of the developed models and simulators assume an instantaneous equilibrium state and complete mixing of the $CO_2$ leading to an overestimation in the RF and processes occurred in the system.

## 1.5 Overview of Dissertation

The main purpose of this work was to find the effects of the carbonated smart water on the carbonate rocks and to which extent it can be used to enhance the oil recovery in the naturally fractured carbonate reservoirs. The analysis of the potential mechanisms behind the increase of the recovery was the main part of this thesis. This work has been conducted based on experimental data to validate the generated model using the history matching methods. The established model was developed by including a new water composition obtained from the sensitivity analysis study that was conducted on the Seawater.

$CO_2$ has been dissolved in the smart water to generate carbonated smart water, and the new engineered water was injected in the generated model, and the results have been compared with other types of water that have been used too. The obtained model was expanded to a five spots pilot model. The effect of the carbonated smart water was studied in four pilot cases which are:

1- Non-fractured homogeneous reservoir
2- Non-fractured heterogeneous reservoir
3- Fractured homogeneous reservoir
4- Fractured heterogeneous reservoir.

The impact of the heterogeneity and fractures in the system was studied as well.

# Chapter 2

# Literature Review

## 2.1 Potential Mechanisms of CSMWI

### 2.1.1 Multi-Ion Exchange (MIE)

Multicomponent ion exchange (MIE) is considered in many studies to be the main mechanism of the low salinity water as an EOR method. The mechanism behind this importance is the wettability alteration of the oil-wet or mixed-wet reservoir rocks toward water-wet, allowing a release of the absorbed electrically polar oil components (carboxylic oil component) from the rock surface. This mechanism occurs by replacing the cations of the rock surface with the divalent ions from the injected low salinity water, thus changing the surface charge of the rock.

In other words, MIE in carbonates is a process of reactions of surface potential determining ions (PDIs), where $SO_4^{2-}$ will absorb on the positive rock surface, attracting the positive divalent ions ($Mg^{2+}$, $Ca^{2+}$). This absorption of $SO_4^{2-}$ will affect the system in two ways: firstly, sulfate services as a catalyst. Therefore, a co-adsorption of $Ca^{2+}$ and/or $Mg^{2+}$ will happen on the stern layer of $SO_4^{2-}$ due to the reduction of the electrostatic repulsive force (positive ions and the positive rock surface), forming an electrical double layer on the carbonate rock surface. Secondly, it will release the negative carboxylic oil component because the negatively charged sulfate ion is relatively strongly attracted to the carbonate rock surface compared to the carboxylic acids rendering the rock surface less oil-wet and allowing the oil to flow through the pore throats (Kilybay et al., 2017; Yousef et al., 2011; Zhang & Sarma, 2012).

The resultant and effectiveness of the ions exchange depend on some factors such as the ions themselves in the system and the temperature, where some ions have more repulsion or attraction force than others. In this context, it has been observed that calcium ion presented significant changes in concentration, which resulted in an increase in the rock porosity and

dolomite surface dissolution which is caused by the carbonic acid (Nunez et al., 2017). In addition, magnesium ions have high hydration energy, which allows it to form a tight bond to the first hydration shell $[Mg\ (H_2O)_6]^{2+}$, and consequently increases the effective size at the interface, hence reduce IFT (Hamouda & Bagalkot, 2019).

One other factor which impacts the Ions exchange mechanism is temperature. Increasing the temperature, in turn, will promote the Ions exchange, where these ions become more reactive with the chalk-rock surface (Yousef et al., 2011).

However, the researchers indicated that in order to get the best results from LSW utilization, Zeta Potential tests have to be done on the water to know the potential performance of this water in the water-Rock-Oil system. Since the used water should be able to bring the surface charge of the R-B-O system towards positive value (Bakhshi et al., 2018; Qiao et al., 2016). A dilution or a modification of the seawater could attain good results working as LSW. It has been shown that the SW4S (Seawater with four times sulfate) has the highest efficiency in this context due to the presence of four times increased sulfate ions in the seawater coupled with higher concentration of $Ca^{2+}$ & $Mg^{2+}$ ions, forming an electrical double layer consequently on the carbonate rock surface (Kilybay et al., 2017)

As a result of the reactions and mineral dissolution/precipitation, ionic species in the aqueous phase will be consumed or generated. The rate of the generated or consumed Ions is related to the mineral reaction (Lee et al., 2017).

$$\gamma_{k,\beta} = v_{k,\beta}\, r_\beta$$

where;

$\gamma_{k,\beta}$ : Mineral production or consumption rate of ionic species in brine due reaction

$v_{k,\beta}$ : The stoichiometric coefficients indicator,

$r_\beta$ : The reaction rate.

In contrast, it has been claimed that ion exchange is not the dominant factor in the enhanced oil recovery when using LSWI because of the slight change of ionic concentration ($Ca^{2+}$, $Mg^{2+}$, and $SO_4^{2-}$) after the core flooding with LSW (Lee et al., 2017). They found out that oil swelling and oil viscosity reduction have more effects than wettability modification or Ion exchange.

### 2.1.2 Mineral dissolution

The dissolution of $CO_2$ in water forms a carbonic acid, which can dissolve the reservoir rocks when it reacts with its minerals. An increase of 16.15% in porosity was reported when the CW

was injected in the carbonate cores, but no appreciable permeability change was noticed (Esene et al., 2019). While Perez et al. (1992) reported an increase of 20.33 % over the original permeability. However, pores with relatively small diameters disappeared for some samples (Kono et al., 2014).

The increase in pore volume due to calcite dissolution is calculated as follow (Kono et al., 2014):

$$V_{pore} = \frac{m_{Calcite}}{\rho_G}$$

where $V_{pore}$, $m_{Calcite}$, and $\rho_G$ are the increased pore volume ($cm^3$), the mass of dissolved calcite (g), and calcite density ($g/cm^3$), respectively.

The result of those reactions could be minerals and ions dissolution or precipitation. One of the used methods to monitor the pore size distribution (PSD) is the Inductively Coupled Plasma (ICP). By analyzing and comparing pre-flooding and post-flooding brines, the ion variation can be obtained. This can provide the knowledge to understand rock dissolution and/or mineral deposition during the core flooding. Additional methods can be used to determine if there is a change in the porosity due to the mineral dissolution or not such as Scanning Electron Microscope (SEM) image, liquid chromatography analysis of dissolved ion, Nuclear Magnetic Resonance (NMR) analysis, and elastic wave velocity measurements (Kilybay et al., 2017; Kono et al., 2014; Perez et al., 1992).

The dissolution (if occurs) will result in a larger pores diameter, thus lower capillary pressure in those pores, which could enhance the microscopic sweep efficiency (Bakhshi et al., 2018; Yousef et al., 2011). Kilybay et al. (2017) reported some noticeable changes in the PSD based on the NMR studies of the cores. This change occurs in the micro and macro scale, where they noticed a reduction in the micro-pores refers to blockages of porosity due to deposition of sulfate scales or produced fines. The observed increase in the macro-pores can refer to the carbonate dissolution (mainly $Ca^{2+}$ and $Mg^{2+}$). The overall measured porosity in the experiments indicated an increase in the porosity which can be explained by the higher volume of the dissolved minerals than the precipitated in the small pores.

Nunez et al. (2017) conducted a core-flooding experiment, which composed of two connected samples to study the effects of carbonated water injection on dolomite porous media. They reported an increase in the porosity in the nearby area from the injector for the first sample, due to the mineral dissolution. However, no porosity variation was observed in the second sample for the entire experiment. In contrast, a constant permeability was observed in the first core, while lower permeability was obtained in the second one due to the precipitation of the transferred dissolved minerals from the first sample.

The heterogeneity of the studied rock has an important effect on mineral dissolution, as found out by the work of Nunez et al. (2017). They reported that the mineral dissolution increases in the higher porosity region and decreases in the lower one. This can be clarified based on the interstitial velocity variation, where the carbonated water flow presented lower interstitial velocity in the high porosity area, providing a longer time for the CW to be in contact with the minerals, increasing the dissolution rate. The opposite happened in lower porosity regions. This conclusion has also been obtained from the experimental results of (Kilybay et al., 2017), although they did not report it in their observations, it can be seen in the PSD curves and NMR plots, where the higher the permeability, the more the dissolved minerals, especially in the macro-porosity region.

Nunez et al. (2017) indicated in the experiment results that rock dissolution performs better at low temperatures. This might be due to the higher solubility of $CO_2$ as temperature decreases, where the kinetic energy will increase between the $CO_2$ and water molecules at the high temperature.

### 2.1.3 Wettability Alteration and IFT Reduction

Yousef et al. (2011) observed a change in the contact-angle measurements in the core flooding experiments on the carbonate rocks when they changed the ionic composition and the salinity of the injected water. They found out that this change has a significant impact on the rock surface wettability due to the pH increase, which leads to IFT reduction. Consequently, this effect on the contact angle indicates to the wettability alteration to a more water-wet system. Lee et al. (2018) as well, claimed that the usage of the LSWF could change the wettability to a more water-wet system, where a shift of the intersection of the relative permeability curves resulted from initial to final wetness state. The same results were reported when the CW was used in a microscale system. They improved that the CW reduces the IFT leading to an increase in capillary number (Nc) by orders of magnitude enhancing, in turn, the oil recovery significantly.

Cleverson et al. (2019) found out that due to a very low IFT between the CW and oil, a stable front at the phase interface was generated during the displacement process. This can be attributed to the almost same fluid viscosity for both of them. In contrast, Eidan et al. (2017) concluded from a set of repeatable experiments that carbonated water would not alter the wettability effectively. Furthermore, Ruidiaz et al. (2017) reported that the wettability alteration is independent of the brine concentration and the presence of the $CO_2$ in the water. They concluded as well that the $CO_2$ or its derived ions might prevent the wettability alteration mechanism.

The IFT reduction due to CLSW injection has been investigated, and some explanation has been provided (Honarvar et al. 2017; Esene et al. (2019), Rezaei, et al. (2019). The dissolved $CO_2$ tends to move to the surface (oil/water interface) due to the low reactivity toward polar water molecules. When $CO_2$ molecules reach the surface, they will decrease the available space for water molecules, imposing some spatial (conformational) constraints onto water molecules. In response, IFT is reduced as a result of the weakened of hydrogen bonds among water molecules. Consequently, IFT in the CW/oil interface is less than it in the brine/oil system (Honarvar et al. 2017). On the other hand, the transferred $CO_2$ molecules to the residual oil could modify the oil-solid interactions at the micromodel surface. Hamouda & Bagalkot (2019) reported the same observation when they used carbonated water with $MgCl_2$. This was attributed to the reduction of interfacial tension and to higher hydration energy of $Mg^{2+}$ . Hence, a tight bond to the first hydration shell $[Mg(H2O)6]^{2+}$ might be generated. Consequently, this increases the effective size at the interface, and diminishes the IFT.

Several water compositions and concentrations were used in the experimental work of Esene et al. (2019) to study the effect of the salinity on the IFT and recovery. They found out that CW with about 1500 to 2000 ppm displays the minimum IFT, especially by using 2000 ppm $K_2SO_4$ (48% IFT decreasing). Furthermore, they reported some factors that affect the IFT, where the IFT decreases with increasing temperature, pressure, and $CO_2$ content in the oil. Hamouda & Bagalkot, (2019) observed that CW+$MgCl_2$, specifically $Mg^{2+}$ ion, leads to lower IFT compared to other used salts or ions such as CW+$Na_2SO_4$ that increased the IFT.

Moreover, it has been found out that the dynamic IFT decreases with increasing temperature, where the minimum value of IFT was reached at 100 °C, and the maximum IFT value was at 40 °C (Honarvar et al. 2017). Increasing the temperature will increase the kinetic energy and mobility of the molecules. This increase will, in turn, inherently increases the two-phase surface total entropy and, diminishing the free energy (ΔG), leading to a lower IFT. Another factor that was reported Honarvar et al. (2017) is the dissolved $CO_2$ in the oil, where they found out that, the higher the solubility, the lower the IFT. Increasing the pressure will increase, in turn, the $CO_2$ solubility leading to an IFT reduction.

### 2.1.4 The Solubility of $CO_2$ in Brine and Oil Swelling

The solubility of carbon dioxide in brine at a constant salinity increases with pressure increasing and temperature decreasing until certain values. Above those values (for example, at a pressure above 2500 psi), a slight and minimal change could occur (Honarvar et al. 2017). Esene et al. (2019) found out from a series of experiments that the more the $CO_2$ concentration in the injected water, the higher the recovery factor due to the high mass transport of $CO_2$.

Salinity and temperature effect on the CO2 solubility can be seen in Henry's law as follow (Lee et al., 2017):

$$f_{CO2,o} = f_{CO2,g} = f_{CO2,aq}$$

$$f_{CO2,aq} = H_{salt,CO2} x_{CO2,aq}$$

$$ln\left(\frac{H_{salt,CO2}}{H_{CO2}}\right) = k_{salt,CO2} m_{salt}$$

$$k_{salt,CO2} = 0.11572 - 0.00060293T + 3.5817 * 10^{-6} T^2 - 3.7772 * 10^{-9} T^3$$

Where:

$f_{CO2,j}$ represents the $CO_2$ fugacity in phase j

$H_{salt,CO2}$ is Henry's constant of $CO_2$ at specific salinity

$x_{CO2,aq}$ is the molar fraction of $CO_2$ in the aqueous phase

$H_{CO2}$ is Henry's constant of $CO_2$ at zero salinity

$k_{salt,CO2}$is the salting-out coefficient of $CO_2$

$m_{salt}$ is the molality of salt

T is the temperature

Subscripts o, g, and aq represent the oil, gas, and aqueous phases

The inverse effect of the temperature on the solubility is due to the kinetic energy that increases when the temperature increases. This kinetic energy leads to a more rapid motion between the molecules, breaking the intermolecular bonds, which in turn allows molecules to escape to the gas phase. Thus, $CO_2$ solubility reduces when the temperature increases independently on the pressure or water salinity (Honarvar et al., 2017).

Kechut et al. (2010) also reported a correlation to calculate the $CO_2$ solubility based on what Chang et al. (1996) published. This correlation was then confirmed by the direct measurement of $CO_2$ solubility.

$$log\left(\frac{R_{sb}}{R_{sw}}\right) = -0.028ST^{-0.12}$$

Where $R_{sb}$is the $CO_2$ solubility in the brine with salinity S in SCF/STB, $R_{sw}$is the $CO_2$ solubility of water in SCF/STB, S is the salinity in weight % of solid and T is the temperature (°F).

Figure 1 describes the effect of temperature and pressure on the solubility of $CO_2$ in pure water. In this figure, the temperature range is 25–150 °C and the pressure range is 0–1000 atm.

The effect of the salinity can be observed by studying several water salinities at constant T and P. The lower the water salinity, the higher the solubility of $CO_2$, due to the salting-out phenomenon. However, the composition of the salt has an important effect on the volume of the dissolved $CO_2$ at the same level of salt ionic strength (mol/kg), where the salts influence the magnitude of $CO_2$ solubility in the following order: $KCl < CaCl_2 < MgCl_2 < NaCl < Na_2SO_4$ (Esene et al., 2019).

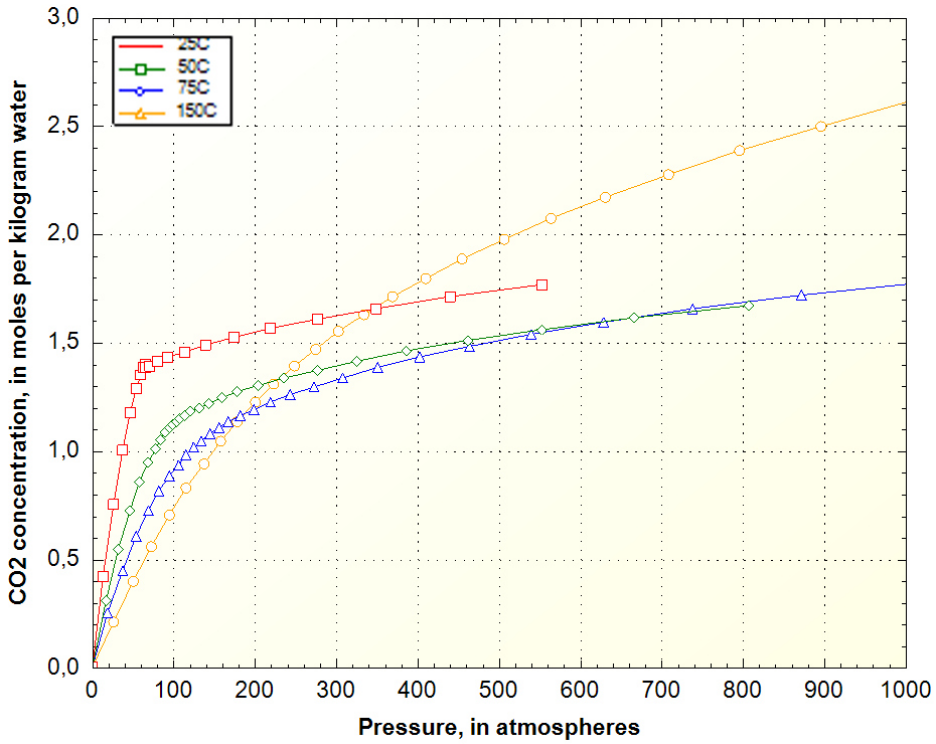


Figure 1: P, T Effect on $CO_2$ Solubility, PHREEQC Tutorial after (Parkhurst et al., 2013)

The swelling phenomenon appears when the CLSWI is used due to the $CO_2$ diffusion in the oil. Zhao et al. (2015)reported that the behavior of the solved $CO_2$ in the oil has two different regions. In the first region, when the temperature increases, the $CO_2$ solubility decreases, leading to a lower oil swelling. Reversely in the second region, the $CO_2$ solubility increased at a given pressure and increased temperature. The same results were obtained by Lashkarbolooki et al. (2018), where they divided the response of the oil to be swelled into two regions: the initial one, where when the temperature increases, the oil swelling decreases. The second region tacks place when the pressure is above a certain level and when the meso-equilibrium is reached. Oil swelling in this region will be higher when the temperature increases.

Perez et al. (1992), in contrast, reported that oil swelling and $CO_2$ solubility increase by increasing the pressure, diminishing the temperature, and when the water salinity is lower. Esene et al. (2019) added the effect of the PH on the $CO_2$ solubility. They reported that above a certain value of the pH (8.3), $HCO_3$ and $CO_3^{2-}$ ions will be generated by a complete dissociation of the $CO_2$ (aq). They stated also that the oil swelling will be higher when the injection rate of the CW is lower, where at the low injection rate, the $CO_2$ has more time to be in a contact with the oil, thus more solubility and swelling occur.

### 2.1.5 Diffusion coefficient of $CO_2$

When the $CO_2$ enriched water is in touch with the oil, the $CO_2$ will diffuse from the aqueous phase to the oleic phase, leading to an oil swelling, thus decreasing the oil viscosity, which could enhance the ultimate recovery. This diffusivity is controlled by the $CO_2$-brine diffusion coefficient, which is a function of temperature, pressure (small effect), salinity, porosity, tortuosity, and salt composition. The diffusion coefficient of $CO_2$ in pure water is about $1.86 \pm 0.26 \times 10^{-9}$ $m^2/s$, and it will decrease as a power-law correlation at 5M NaCl salinity to become one-third of that of the pure water at the same temperature (Esene et al. 2019; Hamouda & Bagalkot, 2019).

The time, in this case, is the most important factor, where the longer the connection time between the $CO_2$ and oil, the higher the diffusion efficiency, and hence, the recovery will increase because of the mobilization of the residual oil ganglia. This increment could indicate a change in the surface area at the interface of the CW/oil moving the fluid-fluid interface. This assumption is the opposite of the assumption of the static interface. In the work of Hamouda & Bagalkot (2019), it was indicated that there is an inaccuracy in the estimation of the diffusion coefficient when assuming the statistical interface model, where the error reaches approximately 2% at 10 bars to a significant 36% at 60 bars.

The partition of the $CO_2$ between the oil and water can be calculated using the partition coefficient of $CO_2$. The $CO_2$ partition coefficient is defined as the ratio of concentration of $CO_2$ in the oil phase to that in the water (CW) phase.

$$k_{CO2,OW} = \frac{C_{CO2;O}}{C_{CO2;W}}$$

Where: $k_{CO2,OW}$ denotes the oil-water partition coefficient of $CO_2$; $C_{CO2;O}$ is the concentration of $CO_2$ in the oil phase, and $C_{CO2;W}$ represents the concentration of $CO_2$ in the CW phase (Esene et al., 2019).

The mass transfer of $CO_2$ to and from the water depends on the temperature and the water salinity. The ionic composition of the dissolved salt into the water has a significant effect on the mass transfer too. The ions could stop the coalesces of $CO_2$ bubbles, thus increasing the surface area between $CO_2$ and water, enhancing the mass transfer. Some theories of how the salt ions enhance the mass transfer are reported by Hamouda & Bagalkot (2019). They reported that the existence of the salt in the water would have several effects such as, increasing the entropy of the solution, enhancing the mobility, leading to a convective movement in bulk liquid, and may enhance the mass transfer.

Another effect is the ionic and atomic connection between the $SO_4^{2-}$, $CO_2$, water, and hydrogen. The $SO_4^{2-}$ is surrounded by up to 14 hydration ions. Each hydrogen atom interacts with $SO_4^{2-}$ or the oxygen atom of another water molecule that has free OH groups. The local OH groups at the interface are suggested to reduce lightly and locally IFT promoting the transfer of $CO_2$ into the n-decane drop (Hamouda & Bagalkot, 2019).

## 2.2 $CO_2$ Capturing (Sequestration)

$CO_2$ is one of the most potent emitted greenhouse gases, where it contributes to 72-77% (Haard, 2006). Because of this problem, the dispose of this gas was indispensable. The best way to dispose of $CO_2$ is to store it in the underground or the ocean, permanently. Over the past decades, $CO_2$ was either stored in the underground geological traps or used in the EOR methods by injecting a pure $CO_2$ gas. Applying those methods has complications and flaws such as gas leakage and the low sweep efficiency. For those reasons, some new methods had to be created to overcome those problems and to gather the advantages of those old methods (Bakhshi et al. 2018; Shakiba et al. 2016). Based on the conducted laboratory experiments and the simulation models, $CO_2$ storage in the formation as $CO_2$-enriched water and/or dissolved in the residual oil was a very secure and beneficial application for the environment and to recover more oil (Esene et al. 2019). Moreover, this technique requires a significantly lower pressure system and $CO_2$ amount than that was used in the pure $CO_2$ injection method (Kechut et al. 2010).

A combination of the LSWI and $CO_2$ injection methods resulted in a CLSWI method, which proved in the core flooding experiments more efficient to produce oil and to store $CO_2$. In the CLSWI, some experiments showed that up to 17-45% $CO_2$ volume was captured in the formation due to the salting-out phenomenon (Lee et al. 2017). When the $CO_2$ is dissolved in the water, water will have lower mobility due to the higher viscosity; therefore, the stored $CO_2$ in the remained water will have no risk to escape. The exsolved $CO_2$, in turn, has low mobility due to the dispersed morphology of its bubbles in the pore space; therefore, there is no risk of leaking out. As a result, it can be safely stored in porous media (Zuo & Benson, 2014).

Furthermore, the remaining oil will have a considerable amount of $CO_2$, which will still be captured in the reservoir safely and permanently (Zuo & Benson, 2014; Kechut et al. 2010).

The fraction of the stored $CO_2$ differs based on which stage of recovery it is applied. It is reported that it is higher in the tertiary mode TCWI than the secondary one SCWI due to the more amount of the residual oil that could sequestrate the $CO_2$. Bakhshi et al. (2018) and Mosavat & Torabi (2014a) found out that in the tertiary mode, the stored $CO_2$ was 61% from the injected volume, while it was 40.7% in the secondary scenario. This conclusion did not match what Shakiba et al. (2015) reported in the experimental investigation. They found out that TCWI and SCWI captured the same amount of $CO_2$ (more than half of the injected $CO_2$) with similar physical properties. Bakhshi et al. (2018) reported that $CO_2$ proved more solubility and retention in a case of light oil than in the heavy oil. This will boost the capacity of residual light oil to store $CO_2$.

To estimate the amount of the storable $CO_2$ in the reservoir, following the $CO_2$ retention equation can be used. This equation uses the amount of injected $CO_2$ instead of the total capacity of $CO_2$ in the reservoir (Bakhshi et al., 2018):

$$CO_2\ Retention = \frac{M^I_{CO2} - M^P_{CO2}}{M^I_{CO2}} = \frac{M^S_{CO2}}{M^I_{CO2}}$$

where $M^I_{CO2}$, $M^p_{CO2}$, and $M^S_{CO2}$ are respectively the mass of $CO_2$ injected in, produced from, and stored in a reservoir. The previous equation can be combined with the dimensionless oil recovery $\frac{N_p}{OIIP}$ to form an objective function (f) (Bakhshi et al., 2018):

$$f = w1\frac{N_p}{OIIP} + w2\frac{M^S_{CO2}}{M^I_{CO2}}$$

where $w1 + w2 = 1$ with $0 \leq w1 \leq 1$, $w1$ and $w2$ are respectively the weighting factors for oil recovery and $CO_2$ storage, NP is the net oil production, OIIP is the oil initially in place. The fraction of the CO2 can be controlled using this function, either to be stored or inserted as an EOR agent. $w1 = 1$ means that all CO2 is used to maximize oil recovery through diffusion and dispersion. While $w2 = 1$ means that all $CO_2$ will be stored in the reservoir.

## 2.3 Effect of the injection rate

The injection rate has a significant effect on the recovery mechanisms; therefore, a balance between the injection rate and the other factors has to be considered. For instance, some researchers found out that some high injection rates produced more significant changes in porosity and permeability than the lower flow rates (Nunez et al. 2017). On the other hand, the lower the injection rate, the higher the available time for $CO_2$ to be dissolved into the oil, hence increasing the RF. A disadvantage of the high injection rates is the earlier breakthrough in the

core flooding scale and earlier breakthrough and coning in the pilot-scale, which could, in turn, decrease the ultimate oil recovery (Esene et al., 2019; Cleverson et al., 2019)

## 2.4 Effect of the temperature on the recovery factor

It was evident that in the conventional recovery methods, that the higher the operating temperature, the higher the oil recovery due to the proportional reduction in the oil viscosity and the dynamic IFT (Yousef et al. 2011; Honarvar et al. 2017). However, in the carbonated water, the temperature has a reverse effect on the recovery to some degree. The increase in the temperature will decrease the capacity of the water to dissolve the $CO_2$ as mentioned in the $CO_2$ solubility par; thus, the lower the transferred $CO_2$ mass into the oleic phase (Bakhshi et al. 2018) reducing the recovery factor. Perez et al. (1992) reported that the decline in the $CO_2$ value could be compensated by the viscosity reduction due to the high temperature, which, in turn, leads to an increase in the ultimate recovery factor.

Esene et al. (2019) reported that the temperature effect would appear after the start of the injection. They found out that the oil recovery when CW is injected at a low temperature is more than the recovery at higher temperature conditions and at the same time. They reported, as well, that the temperature increase would impede the performance of CWI partially.

## 2.5 Effect of the pressure on the recovery factor

Increasing the operating pressure will enhance the $CO_2$ dissolution in the water. The $CO_2$ - enriched water with higher $CO_2$ concentration will results in more mineral dissolution and lower IFT than the same water with a lower $CO_2$ ratio (Nunez et al., 2017). The same results were concluded by Mosavat & Torabi, (2014b) and Fathollahi & Rostami (2015), where they reported that increasing the pressure will increase the ultimate recovery factor due to the increase of the $CO_2$ solubility. Furthermore, they reported that this increase of the pressure in the secondary stage would enhance the recovery more than it in the tertiary stage. Perez et al. (1992), in contrast, found out from their imbibition experiments that the pressure has no effect on the recovery factor.

## 2.6 Simulation Works

Based on developed mathematical models, educational and commercial software have been constructed to study the CWI in sandstones and carbonates reservoirs. Some simulators included the thermodynamic equilibrium (such as CMG), and some did not (such as the UTCOMP). The UTCOMP simulator was developed by the University of Texas at Austin,

recently (Sanaei et al. 2019). All of the developed models and simulators assumed an instantaneous equilibrium state of $CO_2$. Due to this instantaneous equilibrium and complete mixing, the commercial simulators overestimated the RF by almost 10 % for CWI processes (Esene et al. 2019).

One of the first models in the CWI has been achieved by De Nevers (1964), where it was based on the Buckley–Leveret type linear flow model to predict the CWI performance. The capillary and gravity forces are ignored in the model; however, the effects of oil viscosity reduction and oil swelling due to the CO2 dissolving into the oil were considered. They concluded from this model that the viscosity reduction is the main mechanism of the oil recovery enhancement, and oil swelling contributes to a lower extent. Ramesh & Dixon (1973) developed a 2-D dynamic three-phase flow mathematical model, including the solubility of $CO_2$ in oil. They used the implicit method for pressure equation discretization.

Mansoori (1982) developed a compositional simulator to identify the effect of the solubility of $CO_2$ in the water on oil recovery by $CO_2$ flooding. Based on the Soave-Redlich-Kwong (SRK) equation of state, the phase equilibrium and $CO_2$ solubility in water were calculated. This model was developed to simulate 1-D and 2-D displacement processes, and Newton's method was used to discretize and solve sets of equations until convergence was achieved. In this model, the water and $CO_2$ were separately injected, and the $CO_2$ dissolved into the water during the injection and in the reservoir in different proportions. They concluded that the higher the solubility of $CO_2$ in water, the higher the recovery factor.

Chang et al. (1996) presented a 3-D, three-phase compositional model to simulate the $CO_2$ flooding, including $CO_2$ solubility in water, where the gravity and capillary terms were also included. Fully implicit and IMPES formulations are included in the model, and a cubic equation of state was utilized to model the Oil- and gas-phase densities and fugacities. In this model, the $CO_2$ was dissolved into the water in an aqueous phase before the injection.

Kechut et al. (2011) conducted a series of carbonated water flood experiments and used Eclipse 300 (E300) simulator to simulate those experiments. They injected the water and the $CO_2$ separately in two wells, and the model included another well as a producer. The model assumed homogeneous porosity and permeability, and capillary pressure was assumed to be - predicted the oil recovery during the carbonated water flooding by 5%. This was contributed to a miss matching of the PVT data, and the assumptions of the instantaneous equilibrium and complete mixing. Lee et al. (2017) used GEM software developed by CMG to model LSWI core flooding experiments. GEM simulator takes into account the geochemical reactions and Multi-Ion Exchange theory (MIE), they used the PHREEQC simulator to calculate the solubility of $CO_2$ in the salinity water at the reservoir pressure and temperature conditions.

# Chapter 3

# Technical Chapters

## 3.1 Overview of the Related Experiment

This work has been established based on the core-flooding experimental data published by Bakhshi et al. (2018). They studied the effects of the carbonated water injection on carbonate plugs by injecting 2.5 PV water with a salinity of 40,000 PPM of NaCl. Thereafter, they repeated the process by injecting 3.7 PV carbonated NaCl-water at the same salinity. The carbonated water injection (CWI) caused an oil recovery increment by 13.6% more than the conventional water flooding. Moreover, they proved that the injection of the carbonated water into the carbonate plugs led to a 50.6 % $CO_2$ storage after 3.7 PV injection, where the injected water was fully saturated with the $CO_2$, and the concentration of the $CO_2$ in the water under the operational pressure and temperature conditions was 0.983 mole/kg water. The mineral dissolution, porosity changes, ion exchange, and viscosity reduction have not been widely investigated in their research, which will be considered in this simulation work. The core and oil properties, in addition to the detail of the experiment work, are given in Table 1. These properties and experimental results will be used in the simulation work.

Table 1: Experimental Data (Bakhshi et al., 2018)

| Core Properties | | | | | |
|---|---|---|---|---|---|
| D (cm) | L (cm) | PV (cc) | K (md) | Φ | |
| 3.785 | 14.48 | 15.6 | 0.901 | 0.096 | |
| Oil Properties | | | | | |
| API° | Density (g/cc) | μ (cp) | T (°F) | P (Psi) | |
| 33.8 | 0.8277 | 0.4168 | 140 (60 °C) | 2000 (138 bar) | |
| Water Properties | | | Results | | |
| NaCl (PPM) | Injection rate (m3/day) | μ (cp) | | RF % | Injected-PV |
| 40 000 | 0.000144 | 0.63 | NaCl-Water | 39.4 | 2.5 |
| | | | Carbonated NaCl-Water | 53 | 3.7 |

## 3.2 Model Building

### 3.2.1 Core scale model

A 1-D core-flooding model was constructed to represent the data of the carbonated water flooding experiment published by Bakhshi et al., (2018). A 100 x 1 x 1 cartesian grids model in the x, y, and z directions was used to overcome the numerical dispersion that appeared in the less-grids model (Figure 2). No considerable change was observed when the number of cells was increased by more than 100 cells. The core dimensions are shown in Table 2. Table 3 presents the reservoir pressure and temperature and the lumped oil components used to generate the PVT model. PVT oil model has been generated in the WINPROP simulator based on the experimental oil composition and under the same P and T conditions, too (Figure 3). The compositions have been lumped into seven groups to match the allowable number of the outputs in the GEM simulator. The generated PVT model was imported into the CMG-Builder simulator and inserted into the previously generated core model. Peng-Robinson equation was chosen to represent the model equation of state. The core position was supposed to be 10 meters

above the oil-water contact to ensure that no external water influx contributed to the production results, and no external forces affected the work.

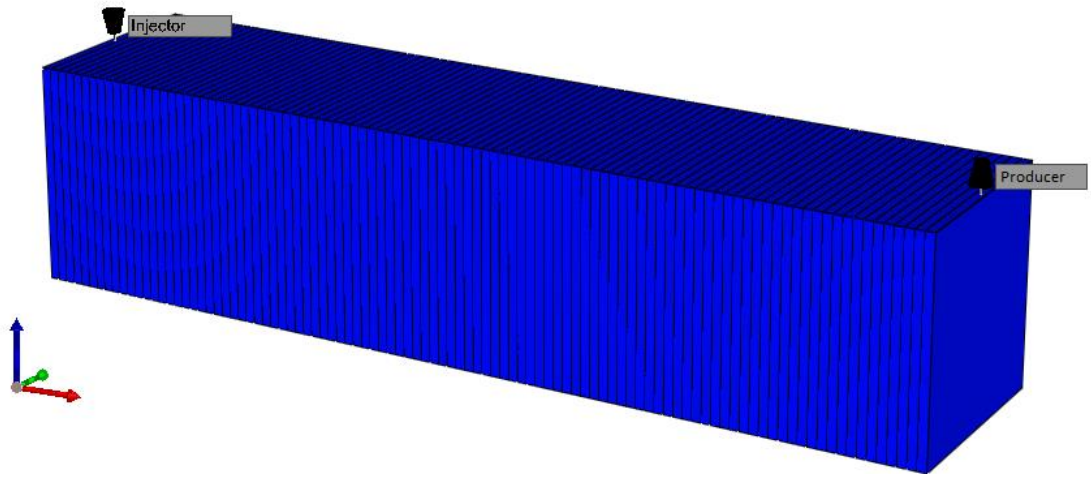


Figure 2: 1-D Core Model

Table 2: Core Dimensions

| Core Dimensions | | | |
|---|---|---|---|
| | I | J | K |
| Number of Cells | 100 | 1 | 1 |
| Dimension of Each Cell (m) | 0.001448 | 0.03354 | 0.03354 |

$CO_2$ solubility was activated in the PVT model, and $CO_2$ Henry's constant was obtained from the WINPROP simulator with a value of 371225.22 KPa. Henry's constant values of the $N_2$, $H_2S$, and other hydrocarbon phase components have been specified as a zero to represent an insolubility state in the water. $N_2$ was selected as a trace component, where $CO_2$ cannot be used as a trace in the CWI case because the CMG assumes that the used trace component will be considered as an insoluble component in the system.

Table 3: Reservoir P, T, and Oil Components

| **PVT Data** | |
|---|---|
| P (Psi) | 2000 |
| T(°F) | 140 |
| **Composition** | **Mole Fraction** |
| $CO_2$ | 0.00080 |
| H2S | 0.00010 |
| N2 | 0.00560 |
| C1 to C3 | 0.08769 |
| IC4 to NC5 | 0.15998 |
| FC6 | 0.74483 |
| **Total** | 1.00 |

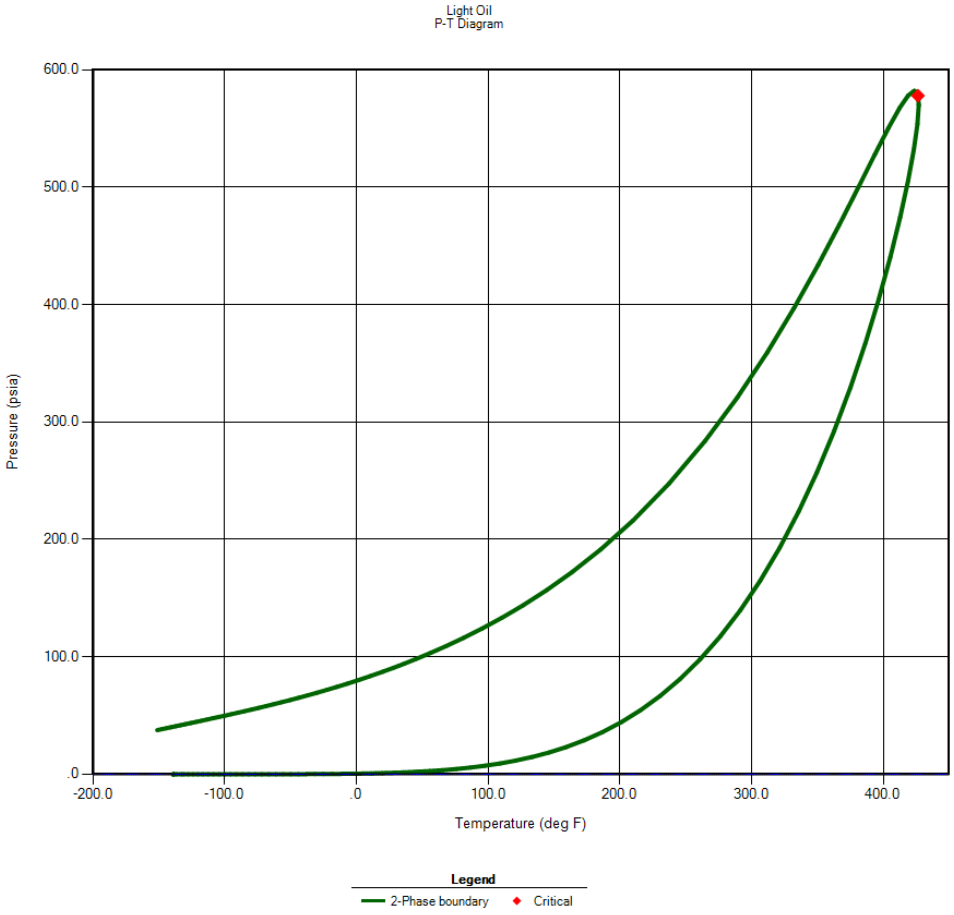


Figure 3: P-T Diagram from WINPROP Simulator

A geochemical-reactions model was implemented based on the database of the PHREEQC simulator. The following general chemical reactions have been used based on mineralogy of the rocks:

Geochemical reactions:

$$H^+ + OH^- \leftrightarrow H_2O$$

$$CO_2(aq) + H_2O \leftrightarrow H^+ + HCO_3^-$$

$$H^+ + CaCO_3 \leftrightarrow Ca^{2+} + HCO_3^-$$

$$H^+ + MgCO_3 \leftrightarrow Mg^{2+} + HCO_3^-$$

$$H^+ + NaCO_3^- \leftrightarrow Na^+ + HCO_3^-$$

$$CaHCO_3^+ \leftrightarrow Ca^{2+} + HCO_3^-$$

$$MgHCO_3^+ \leftrightarrow Mg^{2+} + HCO_3^-$$

$$NaCO_3 \leftrightarrow Na^+ + HCO_3^-$$

$$H^+ + MgOH^+ \leftrightarrow H_2O + Mg^{2+}$$

$$H^+ + NaOH \leftrightarrow Na^{2+} + H2O$$

$$CaSO_4 \leftrightarrow Ca^{2+} + SO_4^{2-}$$

$$NaSO_4^- \leftrightarrow Na^+ + SO_4^{2-}$$

$$MgSO_4 \leftrightarrow Mg^{2+} + SO_4^{2-}$$

$$SrHCO_3^+ \leftrightarrow Sr^{2+} + HCO_3^-$$

$$SrSO_4 \leftrightarrow \mathrm{Sr}^{2+} + \mathrm{SO}_4^{2-}$$

Mineral dissolution / precipitation:

$$\mathrm{Calcite} + \mathrm{H}^+ \leftrightarrow \mathrm{Ca}^{2+} + \mathrm{HCO}_3^-$$

$$\mathrm{Dolomite} + 2(\mathrm{H}^+) \leftrightarrow \mathrm{Ca}^{2+} + 2(\mathrm{HCO}_3^-) + \mathrm{Mg}^{2+}$$

A 50% Calcite and 50% Dolomite rock model is used as an oil-wet carbonate reservoir to study the mineral dissolution, geochemical reactions, ion exchanges, viscosity reduction, and wettability alteration when the carbonated water is injected. A constant water injection rate was assigned in the injector (core inlet), and constant bottom hole pressure was applied in the producer (core outlet).

The Builder model was then exported and run into the GEM simulator to consider the geochemical reactions and the ion exchange processes. In the first case, the composition of the brine and the injected water was 40,000 ppm NaCl-water. About 2.5 PV water was injected, and the recovery factor was obtained. Thereafter, 3.5 PV carbonated NaCl-water with the same salinity was injected in a separate model, and the results have been presented in the CMG-Results tool.

Based on the results of the generated model and using the history matching tool in the CMG simulator (*Figure 4*), the relative permeability curves (Figure 5) were adjusted to match those in the waterflooding experiment and to be used in further works. Capillary pressure was ignored in this study as well as in the five spots studied models. The history matching step was conducted to ensure the validity of the generated model.

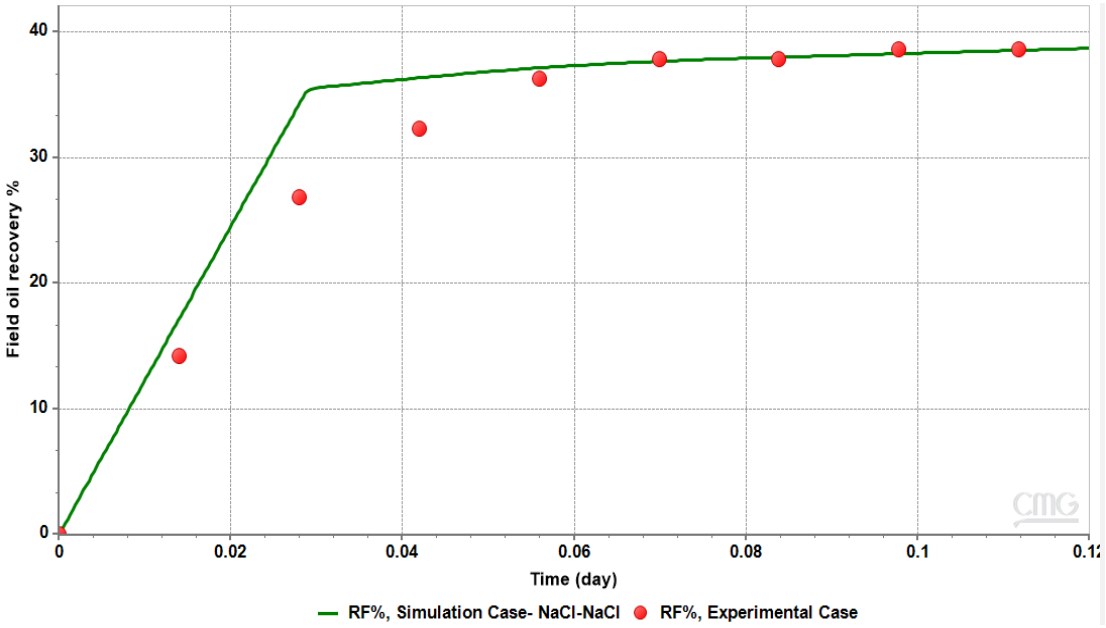


Figure 4: History Matching of Oil Recovery - Core results, Water with 40,000ppm NaCl

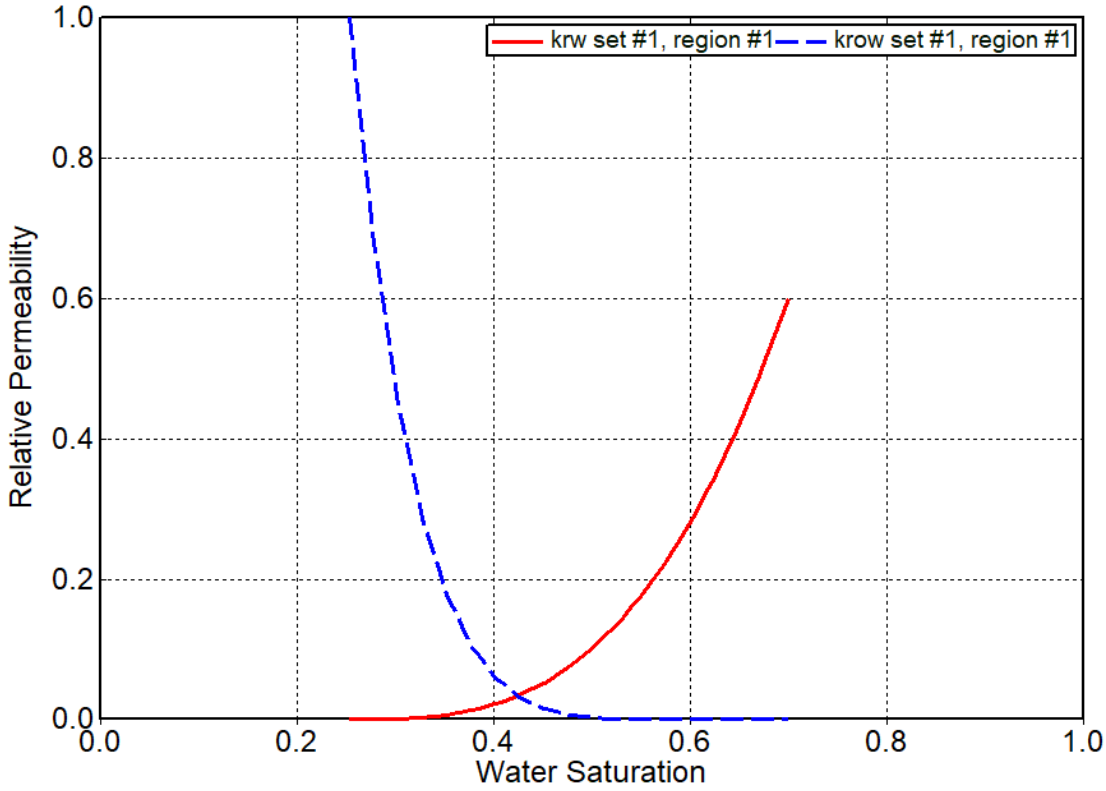


Figure 5: Water Oil Relative Permeability Curves

For more history matching study accuracy, carbonated water with 40,000 ppm Sodium chloride (NaCl) has been studied and plotted in Figure 6. As can be seen, a good match was obtained with respect to the carbonated water core flooding experimental data.

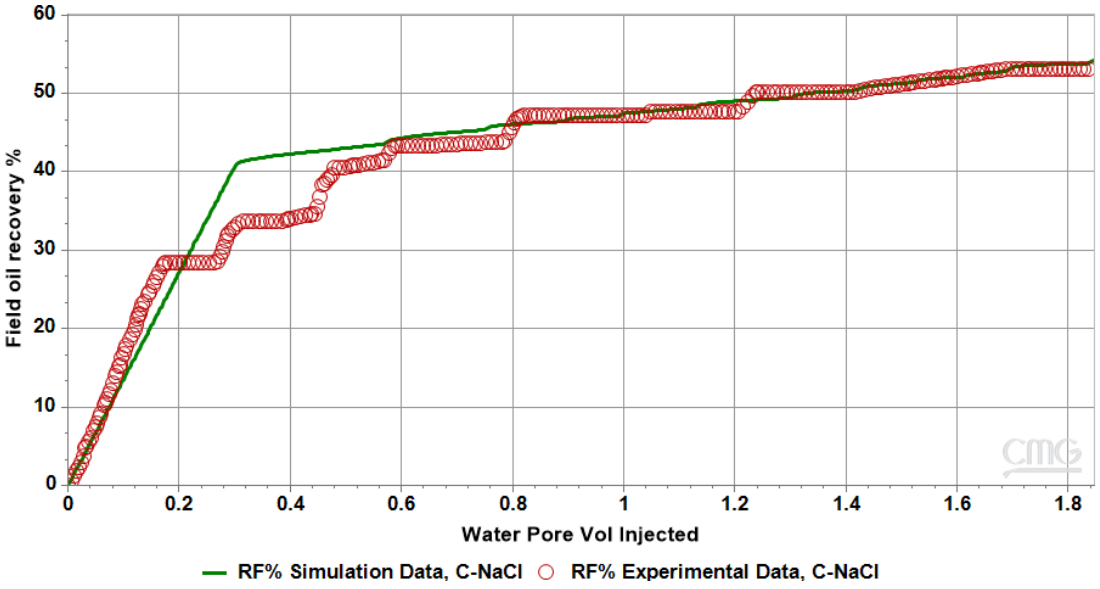


Figure 6: History Matching of Oil Recovery in the Core, using CW with 40,000ppm NaCl.

The next step in this methodology will be changing the composition of the used water starting by using the sulfate concentration since it is the most effective element as explained before. Figure 7 shows the increment in the oil recovery by adding $SO_4^{2-}$ in different concentrations to the used brine.

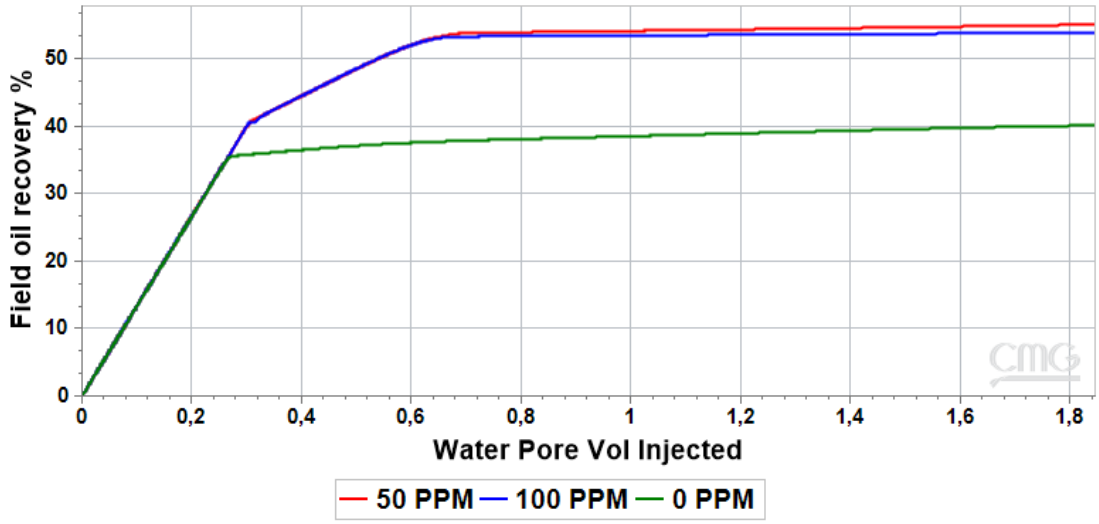


Figure 7: Oil Recovery changing by changing the $SO_4^{2-}$ Composition

Changing the composition of the carbonated NaCl-water by adding 50 PPM of the Sulfate indicated that there is an increase in the recovery, Figure 8. Therefore, the other compositions will be studied to form the smart water to be used in the pilot scale.

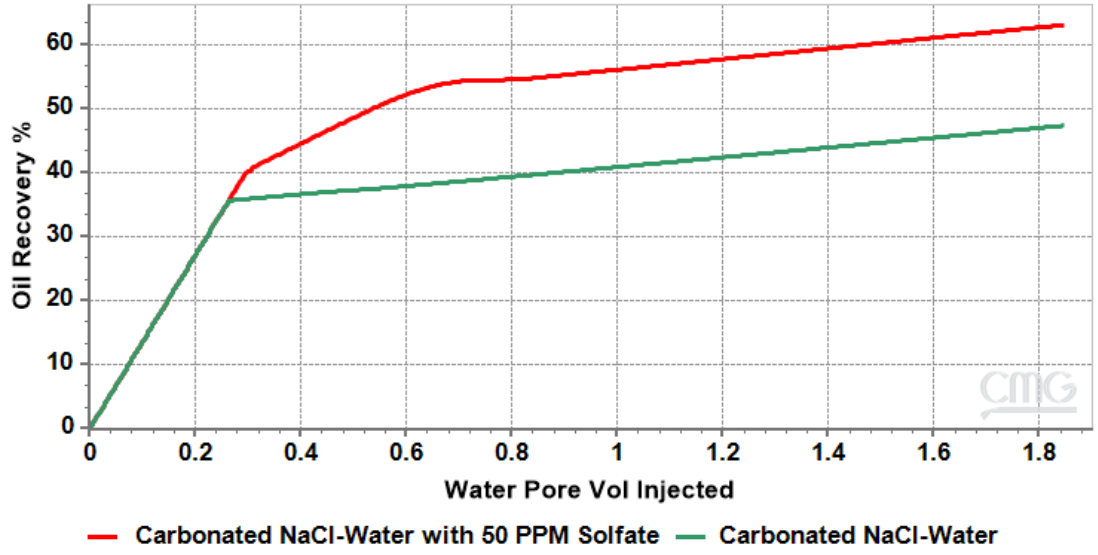


Figure 8: Oil Recovery changing in the CW by changing the $SO_4^{2-}$ Composition

### 3.2.2 Smart Water Injection (SMWI)

After establishing the waterflooding model, the formation and injection waters have been replaced with real formation water and seawater, respectively. The water compositions data were published by Lee et al. (2017). The formation water (FW) salinity is 26,958 PPM, and a Seawater SW salinity is 36,808 PPM (Table 4). $SO_4^{2-}$ was selected as the main studied aqueous component for relative permeability interpolation between the low and high salinity water.

A sensitivity analysis study (SAS) and an optimization study using the CMOST tool were conducted to find out the optimum composition and salinity of the smart water that gives the highest oil recovery and to be used in the pilot-scale model cases. This study was performed in three steps to ensure the validity and consistency of the selected smart water. The first step is the optimization of the seawater, and the second step is to minimize the salinity range if the optimization results indicated that there is a possibility to enhance the seawater, and the third step is to use the SAS in the range with the highest potential to enhance the recovery.

Seawater was optimized in the optimization function in CMG to detect if there are possibilities to have higher recovery when other ratios of the water compositions and salinity are used. Based on the results illustrated in Figure 9, there is a high potential to recover more oil by changing the water composition and salinity value in the low salinity range. The results indicated an optimum case (red line) which gave the highest recovery, but it cannot be considered the absolute optimum solution due to the random distribution of the values for each water ion in the given salinity range. The salinity of the optimal solution (simulator suggestion) is almost 5000 PPM. However, from this optimization study and from the distribution of the concentrations of the most important ions in this study ($SO_4^{2-}$, $Mg^{2+}$, and $Ca^{2+}$) versus the recovery factor, it can be observed that the low values gave the high recovery factors, Figure 10 (a, b, and c). Therefore, and due to the other main aim of this study which is $CO_2$ injection and storage, the range of the salinity has been restricted to 6000 PPM and the intervals in this range were reduced for more intensive study and more potential compositions.

A new study was conducted in a range of 2000 to 6000 PPM using the sensitivity analysis tool. The results were compared and the optimum value of each ion has been chosen to form the smart water composition. From the SAS, the optimum water salinity was found to be 3,963.3 PPM, as given in Table 4. As a confirmation step of the sensitivity analysis, the obtained water has been used as a base-case to see if there is another and better composition to be used because of the random distribution in the tool results. In this step (Figure 11), smart water (black line) displayed the best recovery factor between 15 generated cases (blue lines). Therefore, this composition has been used as the smart water for the later parts of this research. Some other compositions gave good results near to the used SMW, which means that in this range, the desirable compositions could be used based on the field situation and equipment and materials availability.

Moreover, ten times diluted water (0.1SW) and ten times diluted water with four times $SO_4^{2-}$ (0.1SW+4 times $SO_4^{2-}$ ) were studied, as well. The results were compared with the obtained smart water recovery to prove that the low salinity water, represented as the diluted

water, cannot always be used as smart water. When the ten times diluted seawater has been used with the same $SO_4^{2-}$, $Mg^{2+}$, and $Ca^{2+}$ ion concentrations of the obtained smart water, the recovery factor increased from 68.7 to 75%. This indicates that the diluted seawater could be used with some enhancement on the most effective ions.

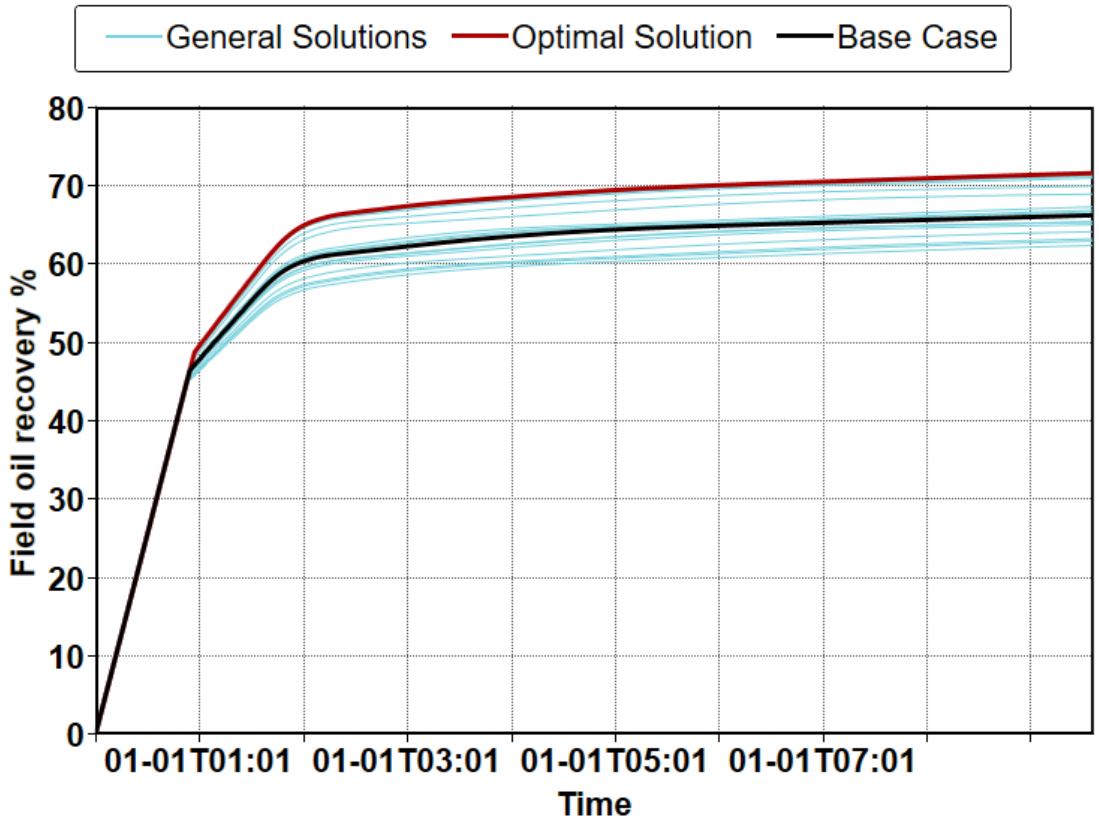


Figure 9: Seawater Optimization Study

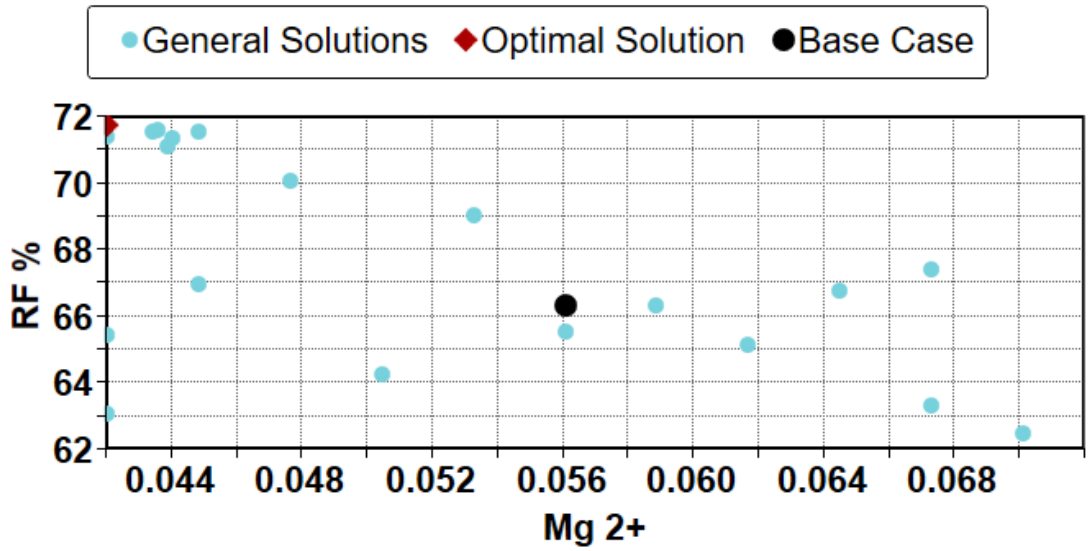


Figure 10-a: A Sensitivity Analysis Study of the $Mg^{2+}$ Component

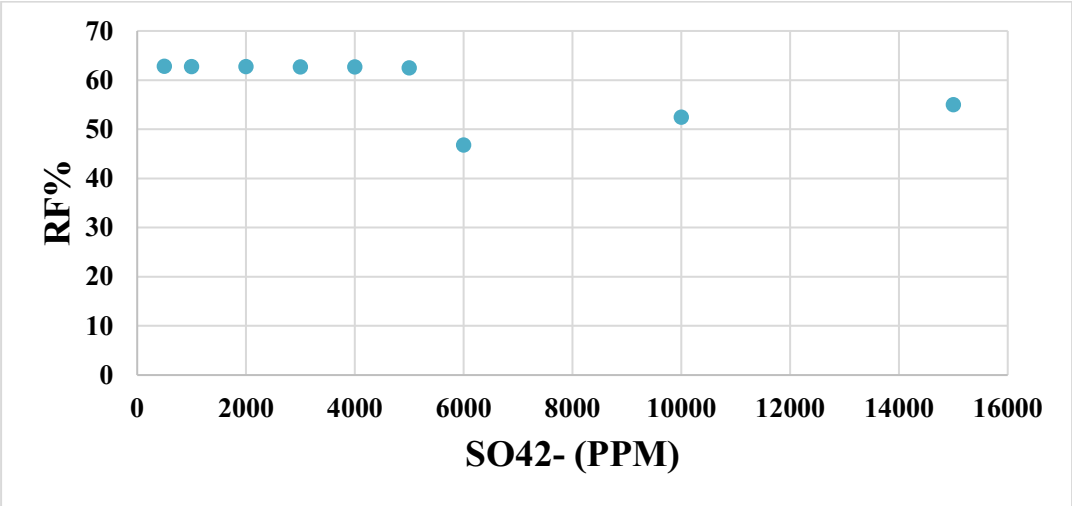


Figure 10-b: A Sensitivity Analysis Study of the $SO_4^{2-}$ Component

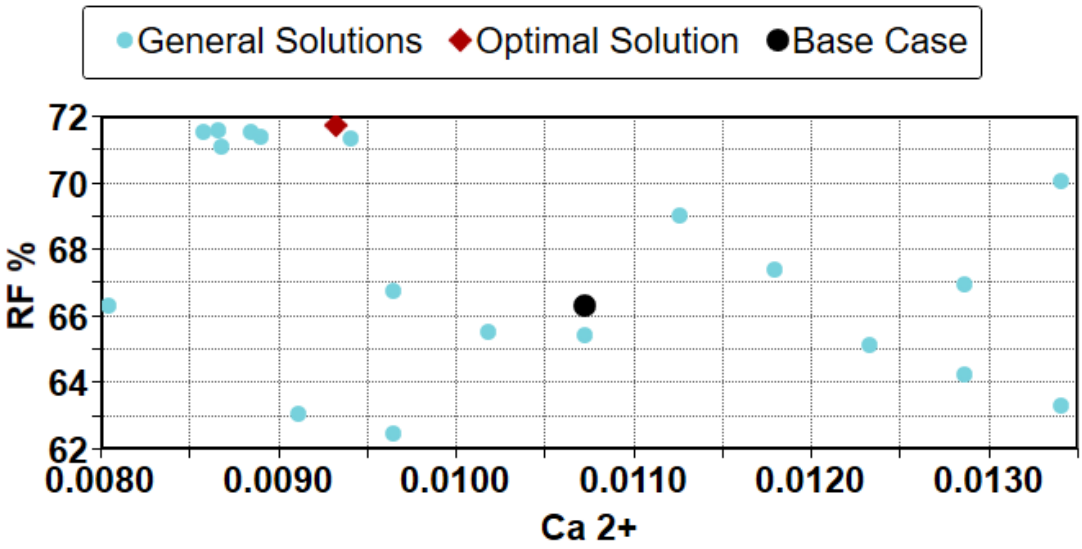


Figure 10-c: A Sensitivity Analysis Study of the $Ca^{2+}$ Component

Figure 10: A Sensitivity Analysis Study of the water compositions.

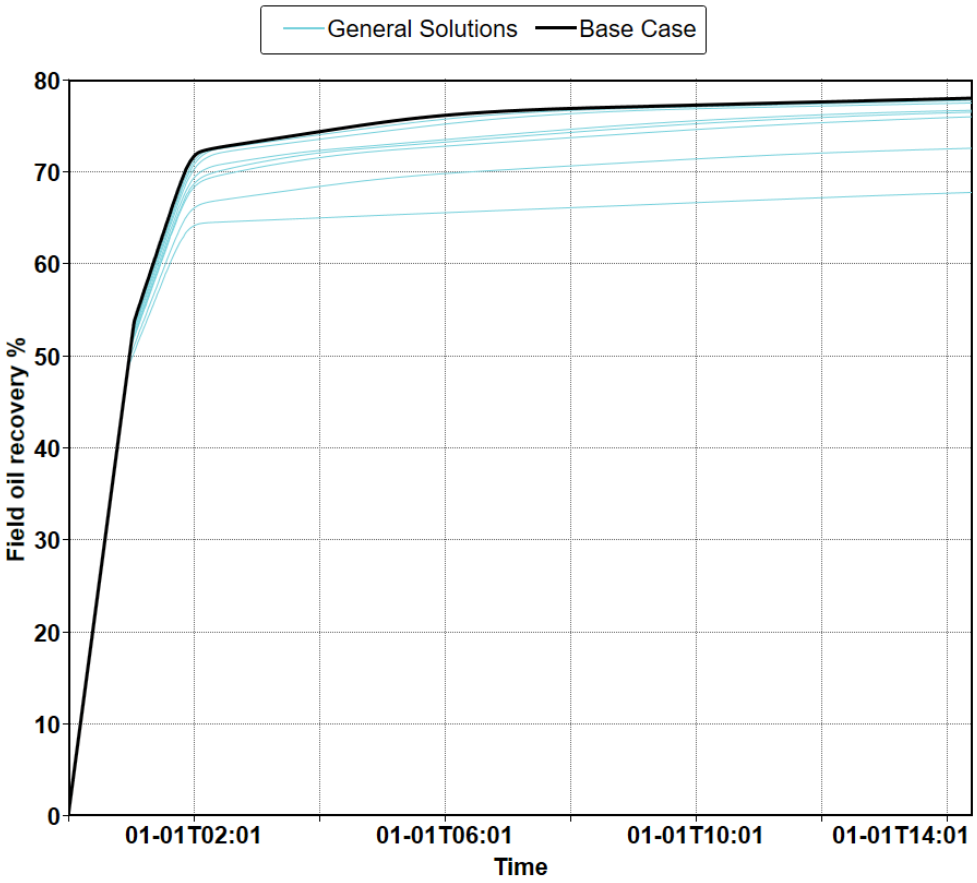


Figure 11: SMW- Sensitivity Analysis Results

Table 4: The used Water Compositions

| Composition | FW | SW | 0.1SW | 0.1SW+ $4SO_4^{2-}$ | Enhanced 0.1SW | SMW |
|---|---|---|---|---|---|---|
| $Ca^{2+}$ | 320.4 | 429.6 | 42.96 | 42.96 | 25.77 | 25.77 |
| $Cl^-$ | 15117.2 | 20040 | 2004 | 2004 | 2004 | 1202.4 |
| $HCO_3^-$ | 1135.9 | 47.6 | 4.758 | 4.758 | 4.758 | 1.9 |
| $Mg^{2+}$ | 219 | 1361.6 | 136.2 | 136.16 | 27.2 | 27.2 |
| $Na^+$ | 9615 | 11430 | 1143 | 1143 | 1143 | 2286 |
| $SO_4^{2-}$ | 550.6 | 3500 | 350 | 1400 | 420 | 420 |
| Sum (PPM) | 26958 | 36809 | 3681 | 4731 | 3624.7 | 3963 |

Some other interesting features in the CMG have been used to define and evaluate the most effective elements in the SAS. Those tools are Morris and Sobol Analysis (Figure 12 and Figure 13). The Morris method (The elementary effects (EE) method) of global sensitivity analysis is a screening method. This method is used to identify the inputs of the model that have the greatest influence on its outputs. It screens the important input factors from the used overall factors by the model proposing the construction of sensitivity measures to identify which input factors have effects which were 1-negligible, 2-linear and additive, or 3-nonlinear or involved in interactions with other factors (Andrea Saltelli, 2008). Morris Analysis replicates and randomizes the "one-at-a-time" (OAT) experiment design. One input parameter is assigned as a new value in each run. This simplifies the global sensitivity analysis by changing different points *xi* locally. Those points are selected from the given range of the possible input values.

The Sobol method (Sobol 1993) is a type of variance-based sensitivity analysis. It is used to quantify the variance amount each input factor contribution to the unconditional variance of output. The tool is useful for computational models for the estimation of the relative importance of the input parameters on the output result (Glen & Isaacs, 2012). In this study, Sobol Analysis was used to distribute the recovery factor enhancement ability on the effective components. From those analyses, $SO_4^{2-}$ found to be the most effective parameter in this study, as was observed by others (Al-Attar et al. 2013; Zhang et al. 2007). The $Ca^{2+}$ and $Mg^{2+}$ found to have the next significant effect.

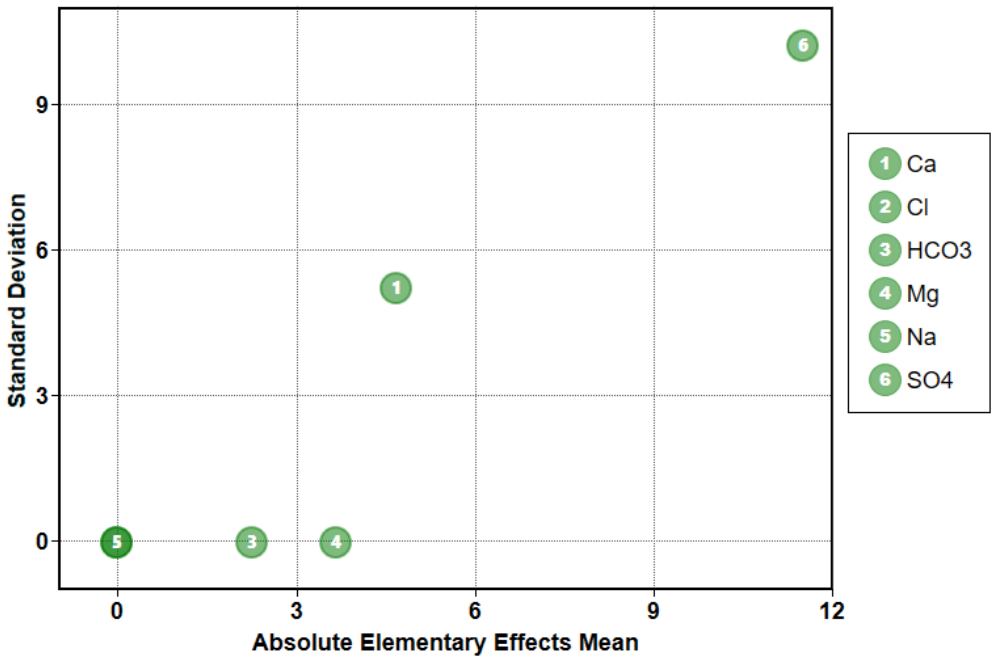


Figure 12: Morris Analysis - the most effective components in the sensitivity analysis.

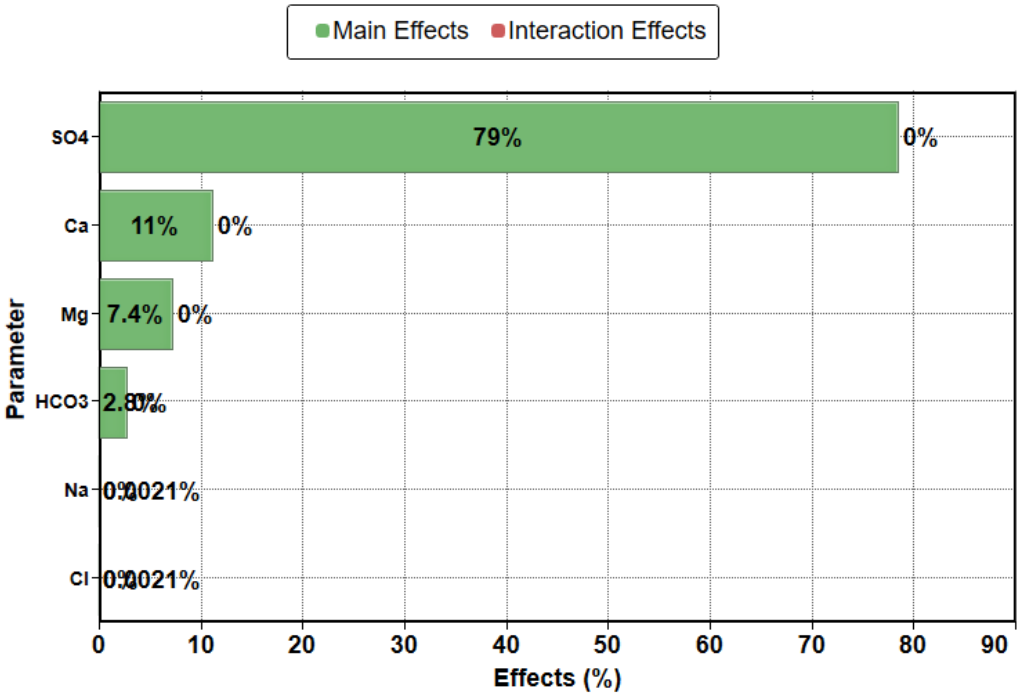


Figure 13: Sobol Analysis.

### 3.2.3 Carbonated Smart Water Injection (CSMWI)

The designed smart water was fully saturated with $CO_2$ to configure the carbonated smart water. $CO_2$ saturation value, under the experiment P and T conditions, is specified by the PHREEQC simulator and has been included in the GEM model. The smart water capacity to dissolve the $CO_2$ is more than the high salinity water due to the salting-out phenomena. The solubility of the $CO_2$ in the water has been calculated and obtained from the PHREEQC simulator, where it was in the optimum smart water 1.13 mole/kg water, and 0.983 mole/kg water in the 40,000 PPM NaCl water. The $CO_2$-saturated smart water or the carbonated smart water (CSMW) was injected in the carbonate core, and the results were compared to the SMWI case.

### 3.2.4 Pilot-scale model

The model was expanded to a (300 x 300 x 8 m) 3D, five spots, two layers pilot model, as can be seen in Table 5. One injection well and four production wells were designed in the model, where the same porosity and permeability, as in the core scale model, were assigned in the first model (Figure 14). An injection rate of 15 $m^3$/day was assigned in the injector, and the same bottom hole pressure was applied in producers, as in the outlet of the core. The obtained CSMW was injected into the pilot with a higher injection rate (15 $m^3$/day) to fit the new dimensions and pore volume (scale-up). To study the effect of the reservoir heterogeneity on the recovery factor, the porosity and the permeability subsequently were randomly distributed in each layer

of the second model, as shown in Figure 15 & Figure 16. The same CSMW and SMW were used in the models.

Table 5: Pilot Properties

| Direction | I | J | K |
|---|---|---|---|
| Distance (M) | 300 | 300 | 6 |
| Cells | 11 | 11 | 2 |
| Matrix-Porosity | 10% | 10% | 10% |
| Fracture-Porosity | 5% | 5% | 5% |
| Matrix-Permeability (md) | 0.901 | 0.901 | 0.901 |
| Fracture -Permeability (md) | 1000 | 1000 | 500 |
| Fracture Spacing (m) | 0.4 | 0.4 | 0.2 |

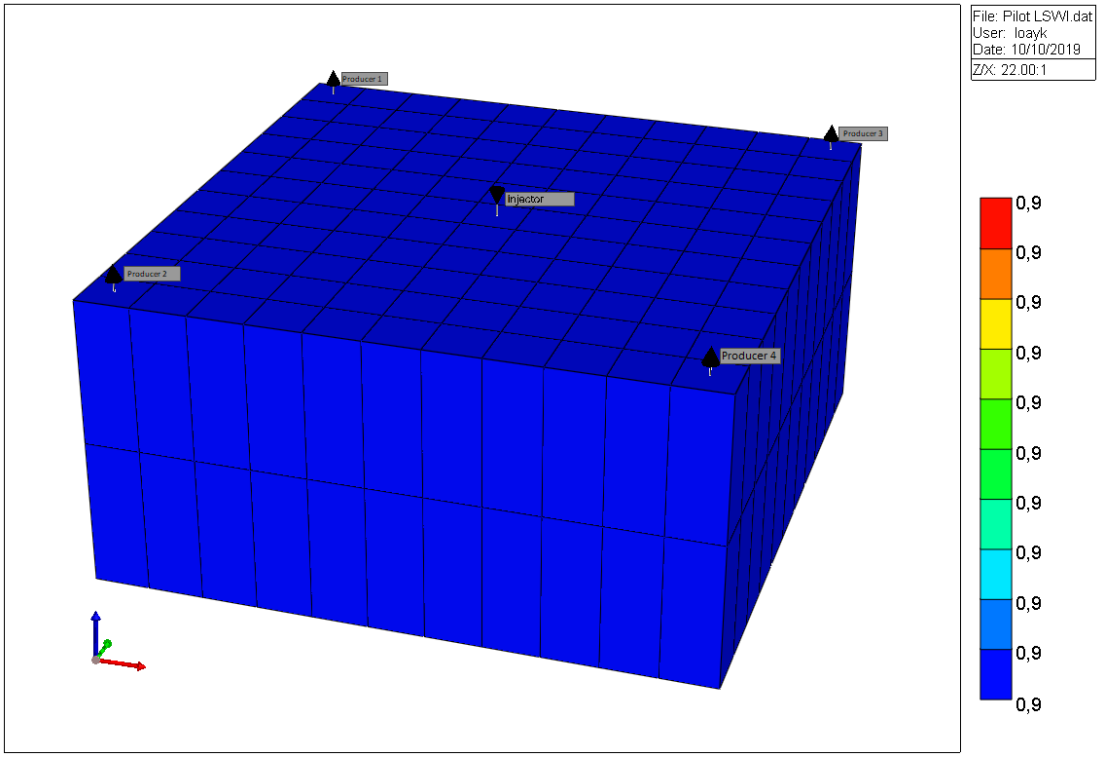


Figure 14: Permeability in the Homogeneous Pilot Scale Model

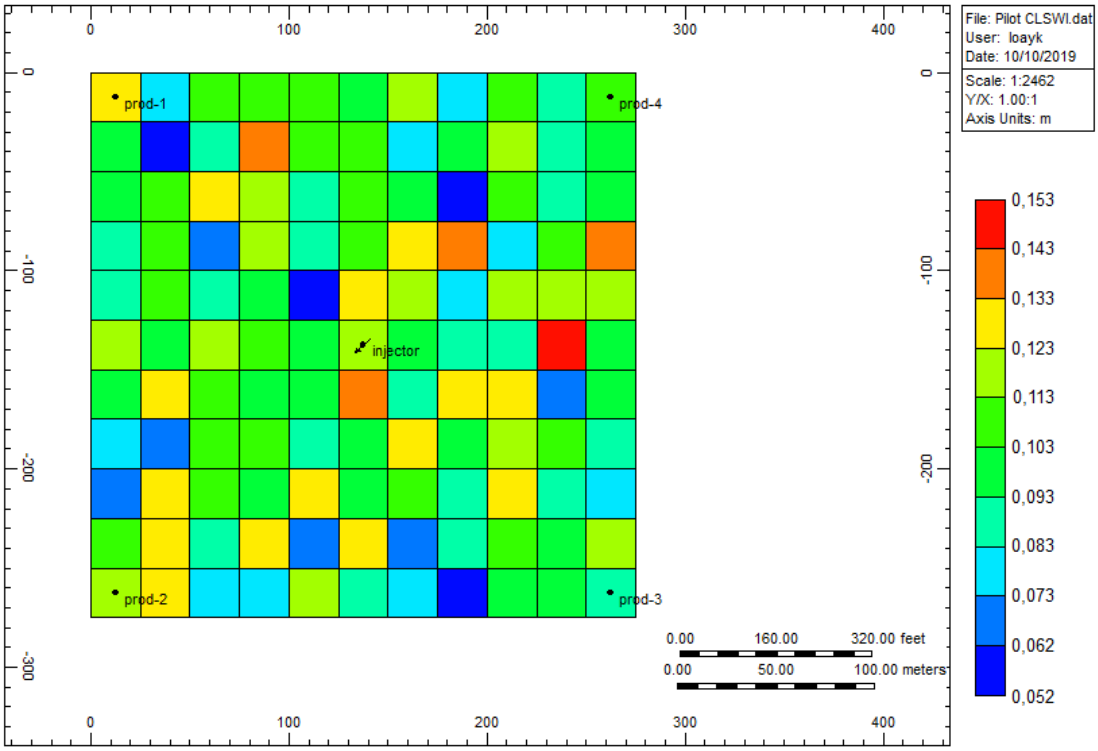


Figure 15: Porosity Distribution in the Heterogeneous Five Spots Model.

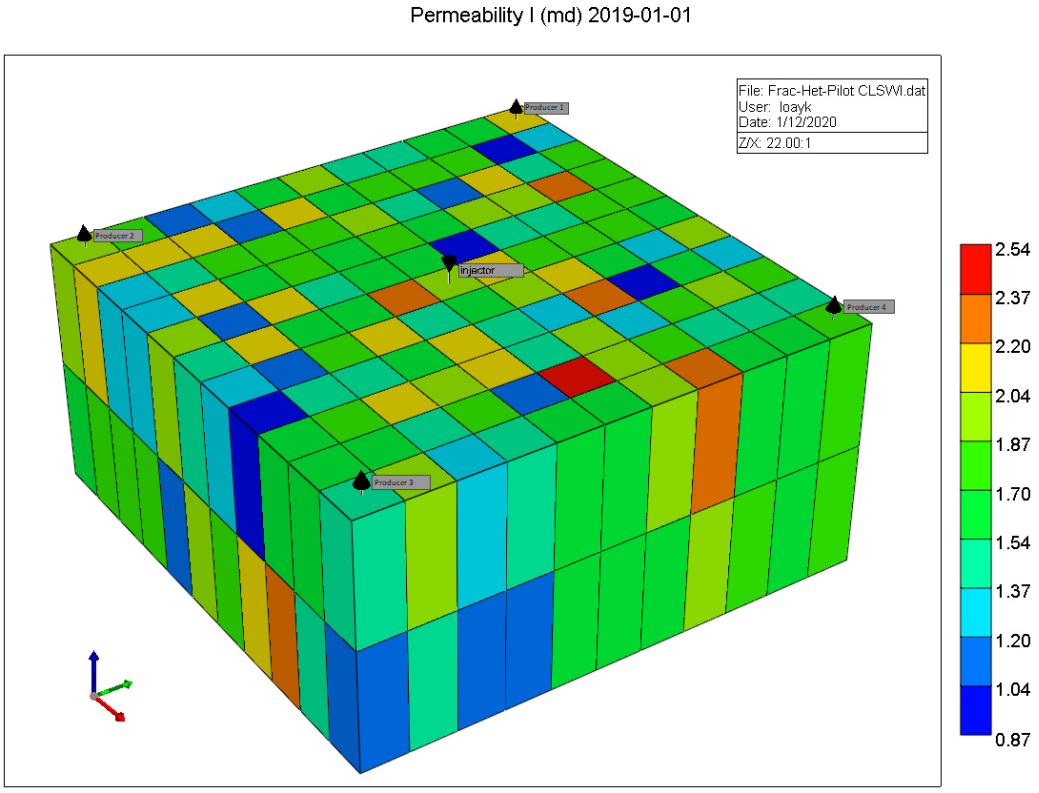


Figure 16: Permeability Distribution in the Heterogeneous Five Spots Model.

To simulate the real case of the carbonate reservoirs, the fractures were included in the homogeneous and heterogeneous models, and the effects of the CSMWI on the minerals, fractures, matrix, and the RF were analyzed and compared with SMWI cases. New relative permeability curves for the fractures were included in the prior non-fractured model, and the Dual Porosity- Dual Permeability model was implemented to represent the fracture system (Figure 17 ).

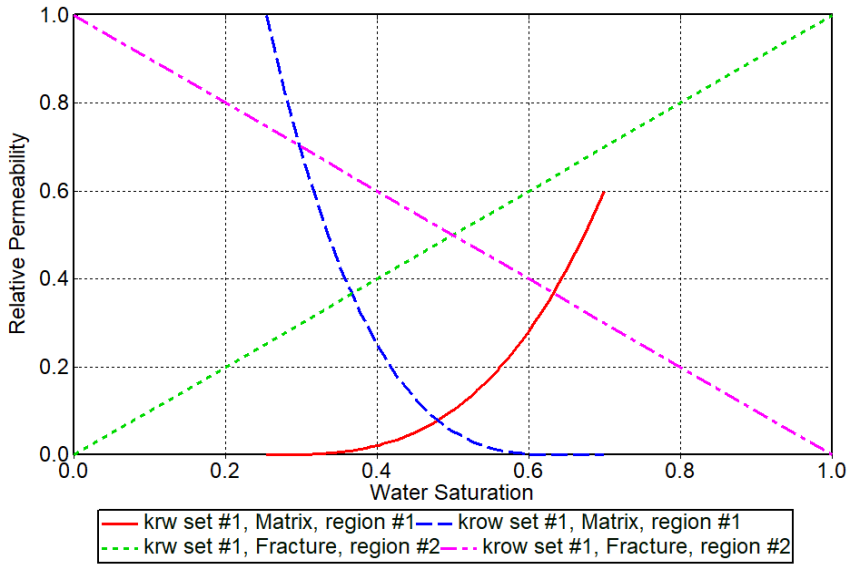


Figure 17: Water and Oil Relative Permeability curves in the matrix and fracture

# Chapter 4

# Results and Discussion

## 4.1 Results Section

### 4.1.1 Recovery Factor of Smart water

Table 6 shows the recovery factors of the tested different water systems from the core flooding simulation. As can be seen, the best-case scenario is related to the SMWI. Whereas the worst-case scenario is related to the 40.000 ppm NaCl and then SWI.

Table 6: The obtained RF for several scenarios.

| Composition | NaCl | SW | 0.1SW | 0.1SW+4$SO_4^{2-}$ | Enhance 0.1SW | SMW |
|---|---|---|---|---|---|---|
| Ultimate Recovery % | 39.4 | 63.7 | 68.7 | 70 | 75 | 77.8 |

### 4.1.2 Recovery Factor of Carbonated Smart water

In this section, at first, the oil recovery of the core flooding in the secondary and tertiary stages will be presented, then the result of the pilot will be discussed.

#### 4.1.2.1 Core scale

##### 4.1.2.1.1 Secondary Stage

Carbonated smart water injection (CSMWI) in the core case (Figure 18) recovered 14, 26.8, and 44.35 % more oil than Smart water injection (SMWI), Seawater injection (SWI), and brine with 40,000 ppm of NaCl, respectively. As can be seen in Figure 18, the main oil volume has been produced before the breakthrough, which is between 0.33 and 0.42 PV for all cases. The different values of the recovery factor could be attributed to the differences in the sweep efficiency for several types of water, as will be explained later in the Mobility Enhancement section. After the breakthrough, other responsible mechanisms are triggered in addition to the mobility enhancement. Those mechanisms are widely explained in the Potential Mechanisms of CSMWI part.

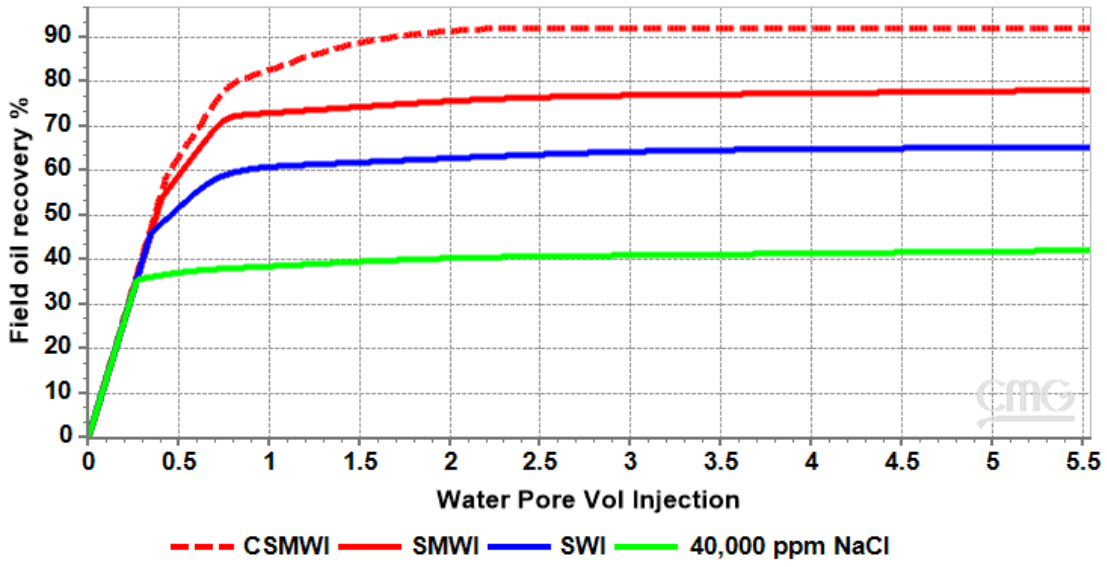


Figure 18: RF in Core Scale, NaCl, SWI, SMAWI, and CSMWI

This increase in the oil recovery in the carbonated water depends mainly on the $CO_2$ saturation, where the more the dissolved $CO_2$ in the injected water, the more the oil recovery. However, in the field, the injected carbonated water is usually fully saturated with $CO_2$. The aim of that is to get the maximum advantages of oil recovery and $CO_2$ storage.

Figure 19 shows the RF of the CSMWI and Carbonated seawater injection (CSWI). The CSMWI recovered 7.6 % more oil than the CSWI due to the higher amount of dissolved $CO_2$ in the CSMW combined with the other mechanisms that are explained later. This increase in the $CO_2$ capacity is attributed to the salting-out phenomena.

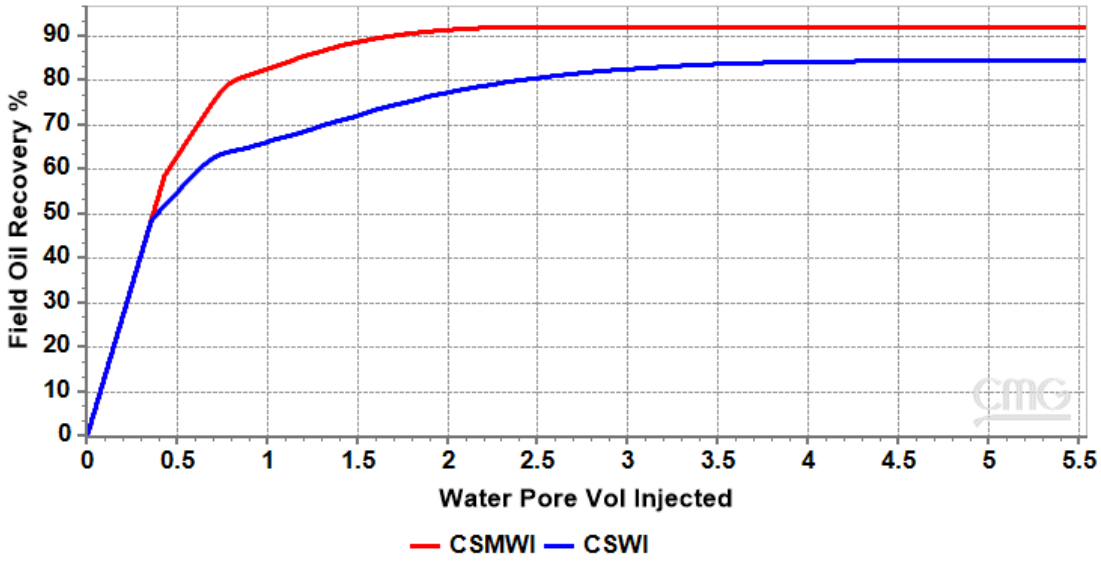


Figure 19: RF in CSWI and CSWI Cases in the Core Scale Case

#### 4.1.2.1.2 Tertiary Stage

The ultimate recovery of the oil depends on in which stage the carbonated water is injected. As mentioned before in the literature review in Chapter 1, the recovery in the secondary stage is higher than it in the tertiary stage.

In the present study, a volume of 2 PV seawater was injected in the core as secondary recovery. The carbonated waters were injected as a tertiary recovery after the plateau was reached in the SWI and no more oil was recovered. The results are compared with the results of the CSMWI and CSWI that have been injected in the secondary stages. Figure 20 depicted the recovery of the CSMWI, SMWI, CSWI, and SWI in the secondary and tertiary stages. It is evident that the recovery factor in the secondary stage of the CSMWI is more than it in the tertiary stage by 4 %. These results match the experimental results obtained by other researchers (Mosavat & Torabi, 2014; Fathollahi & Rostami, 2015; Shakiba et al., 2015; Esene et al., 2019).

From the same figure, it can be seen that the performance of the injected water began to appear shortly after the tertiary injection. This delay is due to the required time to replace the previously existed water in the core. Furthermore, the low salinity mechanisms and $CO_2$ diffusion, by using the carbonated water, need time to be active.

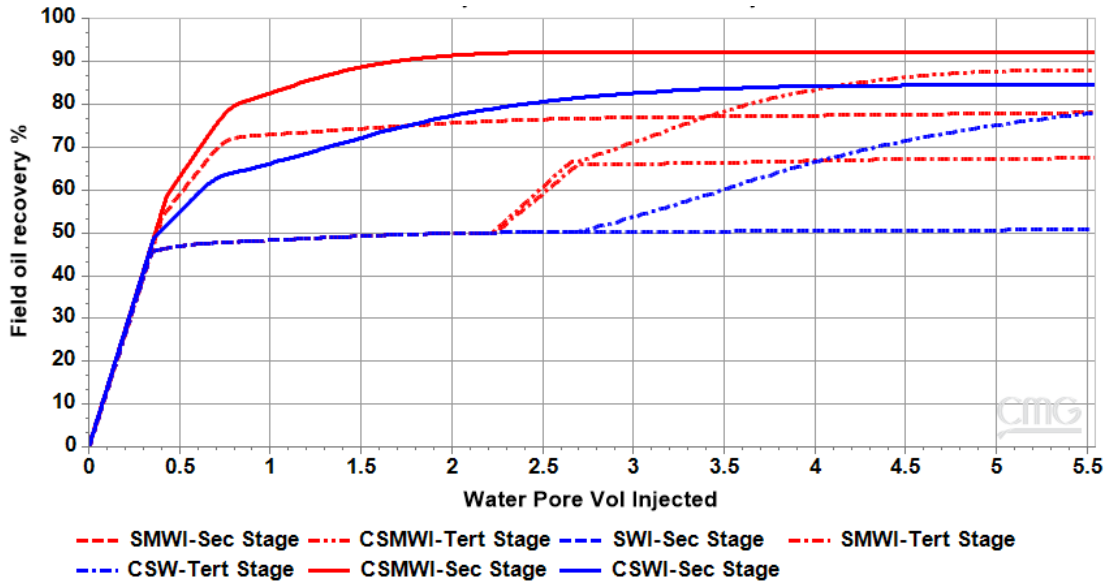


Figure 20: Recovery Factor in the Secondary and Tertiary Stages in the Core Scale Case

#### 4.1.2.2 Pilot-Scale

As in the core scale case, the CSMWI proved more oil recovery in the extended five spots model than the SMWI in the heterogeneous non-fractured & fractured reservoirs and homogeneous non-fractured & fractured reservoirs as well, but with different values. CSMWI recovered 6.6 % and 8 % oil more than the SMWI in the heterogeneous non-fractured and fractured reservoirs, respectively, Figure 21. In the homogeneous reservoirs, CSMWI recovered 5.5 % and 5 % oil more than the SMWI in the non-fractured and fractured reservoirs, respectively, as illustrated in Figure 22.

The recovery increment after the breakthrough can be attributed to some mechanisms such as viscosity reduction and mineral dissolution. From Figure 21, BT of the fractured reservoir occurred at 0.4 PV, while in the non-fractured happened at 0.6 PV. The very early BT can be attributed to the high water's mobility in the channels (the fractures). In the non-fractured reservoir, it can be observed that only a small volume of the oil has been recovered after BT due to the bypassing of the oil by the water. In the fractured reservoir, a higher recovery is obtained after the BT due to the $CO_2$ diffusion from the fractures into the matrices and the spontaneous imbibition process, where those mechanisms need a long time to act effectively and start paying off after the BT.

At the early time after the BT, the recovery rate was high due to the combined effects of the co- and counter-current spontaneous imbibition flow regimes. However, the recovery rate starts to be less at the late time due to the domination of the co-current spontaneous

imbibition flow regime. Moreover, the mixed-current regime could be observed as well in the middle time (Hamad, 2019).

From Figure 22, it can be seen that the fractures have a slight effect on the ultimate recovery, where both cases recovered almost the same ultimate oil recovery. The breakthrough occurred in the fractured reservoir earlier than the non-fractured one by 0.1 PV, but it recovered more oil after the BT than the non-fractured as well. Based on the observation of Figure 21 and Figure 22, the heterogeneity effect might be the reason for the lower recovery of the heterogeneous fractured reservoir.

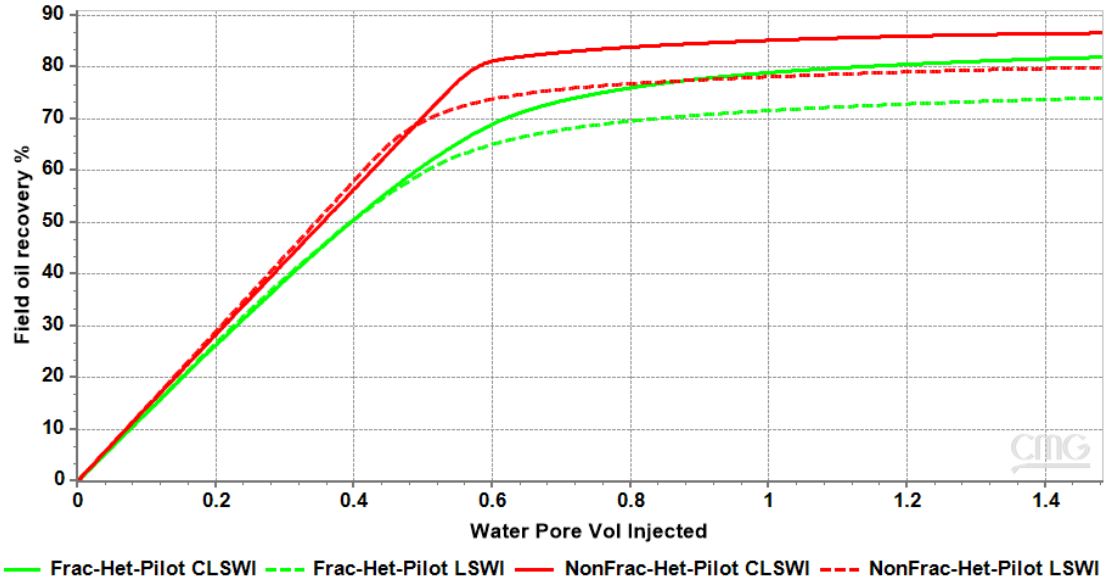


Figure 21: Field Oil Recovery in the Heterogeneous Reservoir

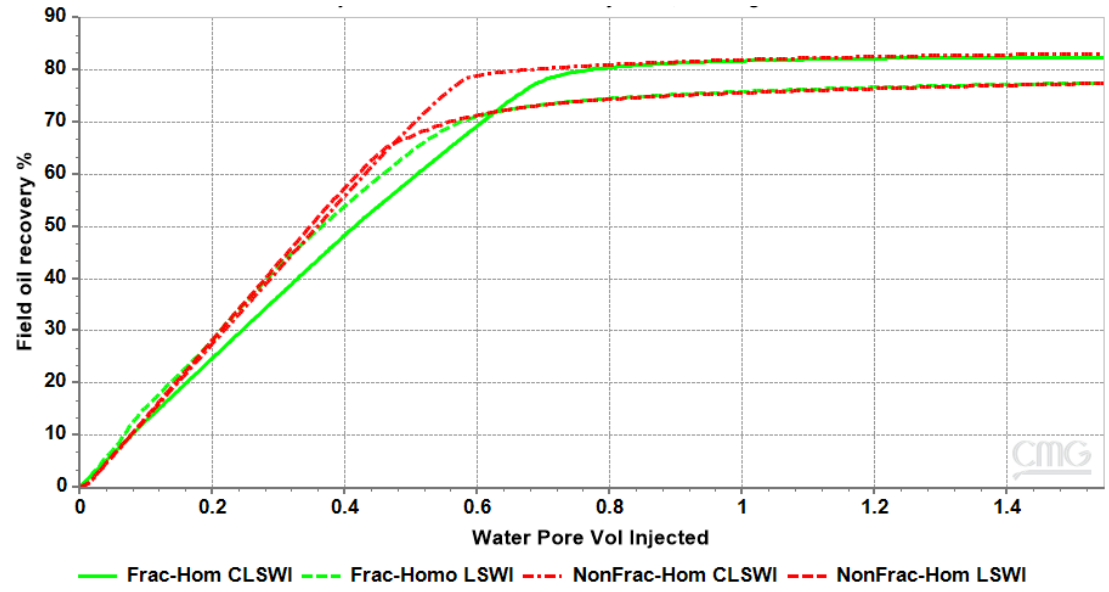


Figure 22: Field Oil Recovery in the Homogeneous System

### 4.1.3 $CO_2$ Storage

#### 4.1.3.1 Core Scale

When the $CO_2$-saturated water is injected in the reservoir, and due to the higher affinity of the $CO_2$ to be dissolved in oil more than water, the $CO_2$ will transfer from the water into the oil until the equilibrium state is reached. After the final production stage, the remaining oil and water in the reservoir will capture a considerable amount of the $CO_2$ in the underground. In the core scale, 40 % of the injected $CO_2$ was stored in the CSMWI case, while in the CSW case, 50.5% was trapped in the reservoir (Figure 23). The CSWI showed higher storage of $CO_2$ than the CSMWI case due to the higher remaining oil in the CSWI, as shown in the RF result's part.

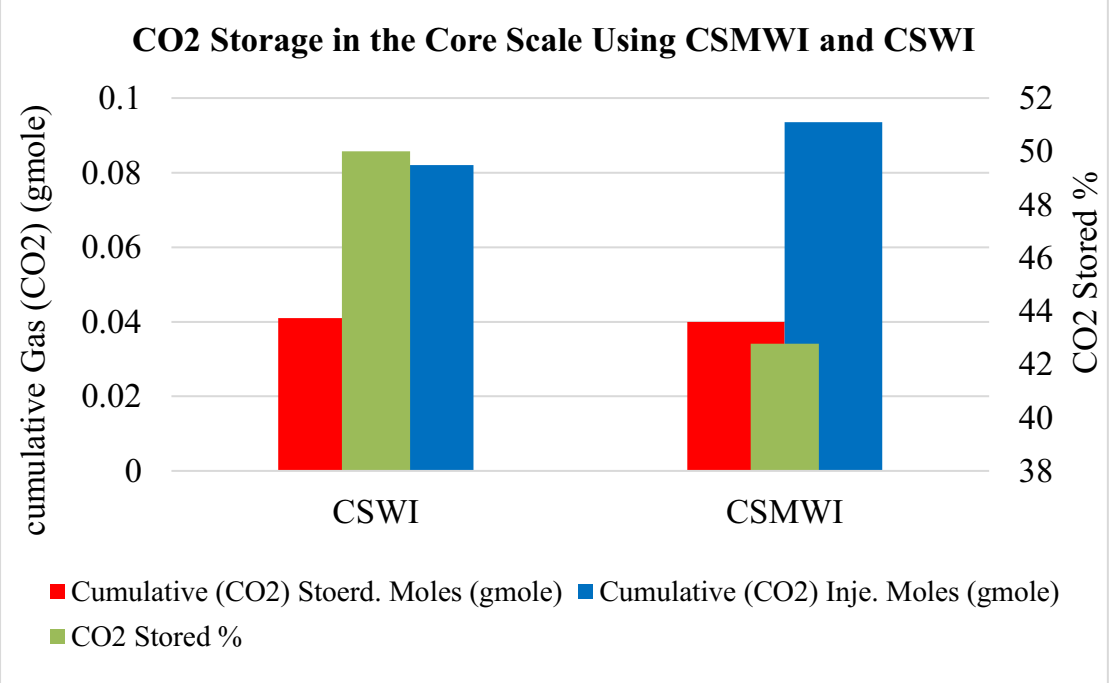


Figure 23: $CO_2$ Storage in the Core model

Figure 24 depicted a very long injection time case in the core-scale (12 PV). This case has been run to show that $CO_2$ storage has a direct relationship with the residual oil in the reservoir. The stored $CO_2$ became constant after the oil production reached the plateau, and no more oil was produced.

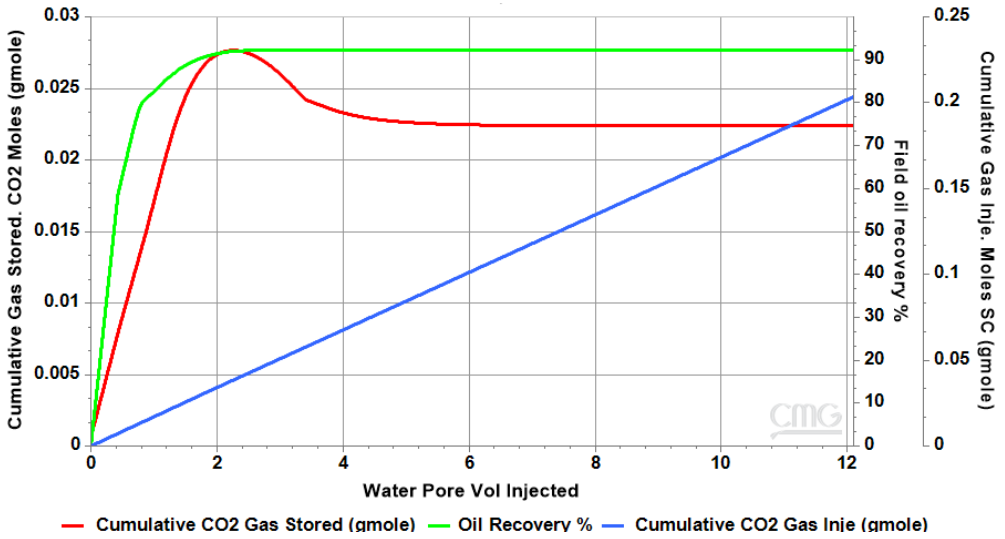


Figure 24: $CO_2$ Storage in the Core model after 6 PV injection (CSMWI)

### 4.1.3.2 Pilot Scale

In the pilot-scale scenario, 56% and 45.5% of the injected $CO_2$ have been stored in the fractured and non-fractured heterogeneous reservoirs, respectively, as shown in Figure 25. This difference in the trapped $CO_2$ can be attributed to the residual oil saturation in the fractured reservoir. The residual oil saturation in the fractured reservoir is higher than in the non-fractured, as depicted in Figure 26. The remaining oil in the non-fractured reservoir is 10 %, while in the fractured reservoir 15%. The remaining oil in the fractures is almost zero, but the oil volume in the fractures is 9 % of the total oil in the reservoir, and the rest 91 % is located in the matrix pores with a residual oil saturation of 16.5 %.

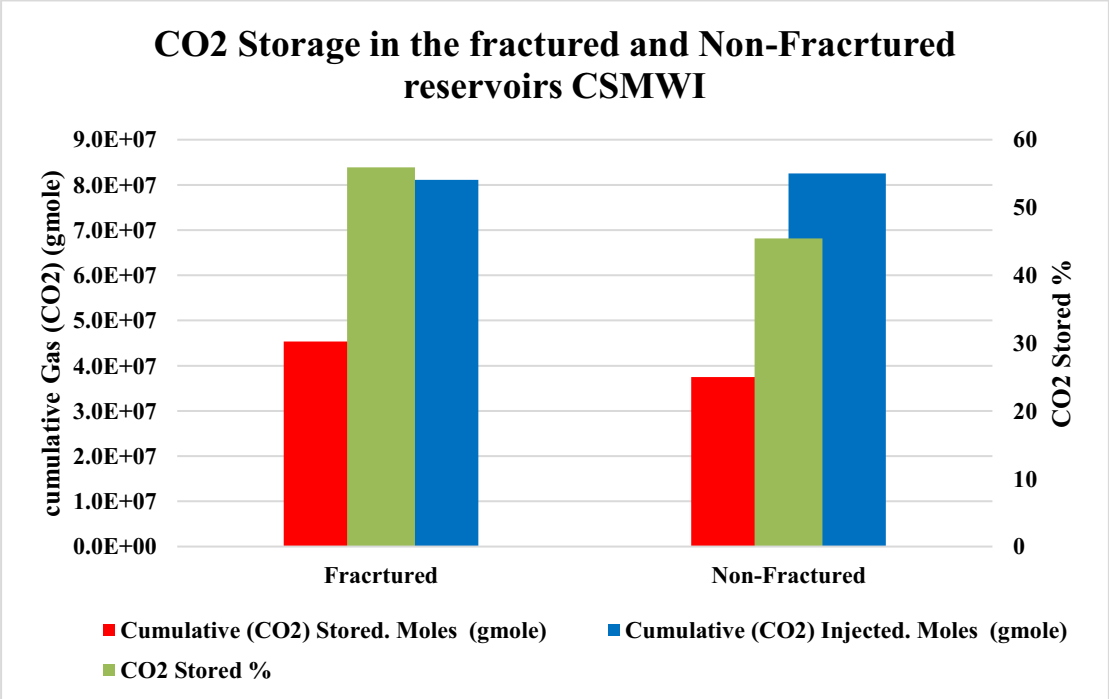


Figure 25: Stored $CO_2$ in the Fractured and Non-Fractured Reservoirs

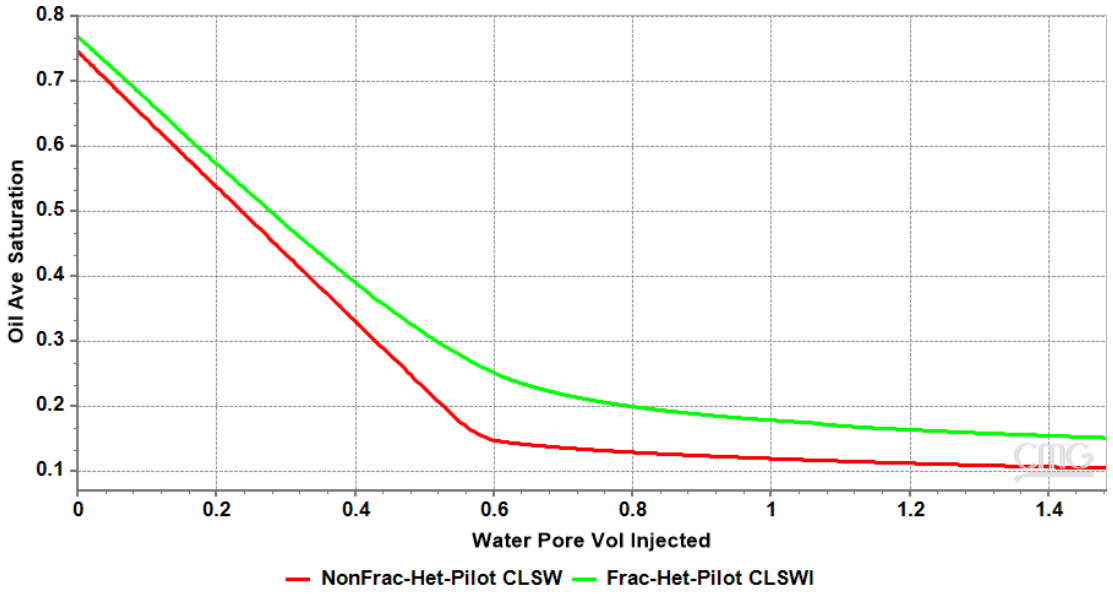


Figure 26: Oil Saturation in the Fractured and Non-Fractured Heterogeneous Reservoirs.

## 4.2 Discussion Section

### 4.2.1 Mechanisms

#### 4.2.1.1 Ion exchange

Concentration differences between ions in the injected and formation waters result in mineral dissolution/precipitation and ions exchange. Some of the ion concentrations increased, and some others decreased due to the different processes that occurred in place. Ion concentrations changes of $Ca^{2+}$, $Mg^{2+}$, and $SO_4^{2-}$ in the core is shown in Figure 27. From this figure, it can be seen that there is no significant change in the concentrations between the SMWI and the CSMWI, which leads to the conclusion that ion exchange is due to the low salinity of the carbonated water. This conclusion has been adopted based on the results obtained from the present core case study, and because it matches the previous conclusions from other researchers published in this context. Due to the time scale and dimensions scale restrictions of the core flooding case, the ion exchanges have been studied in the pilot-scale, and the results have been compared with the core results.

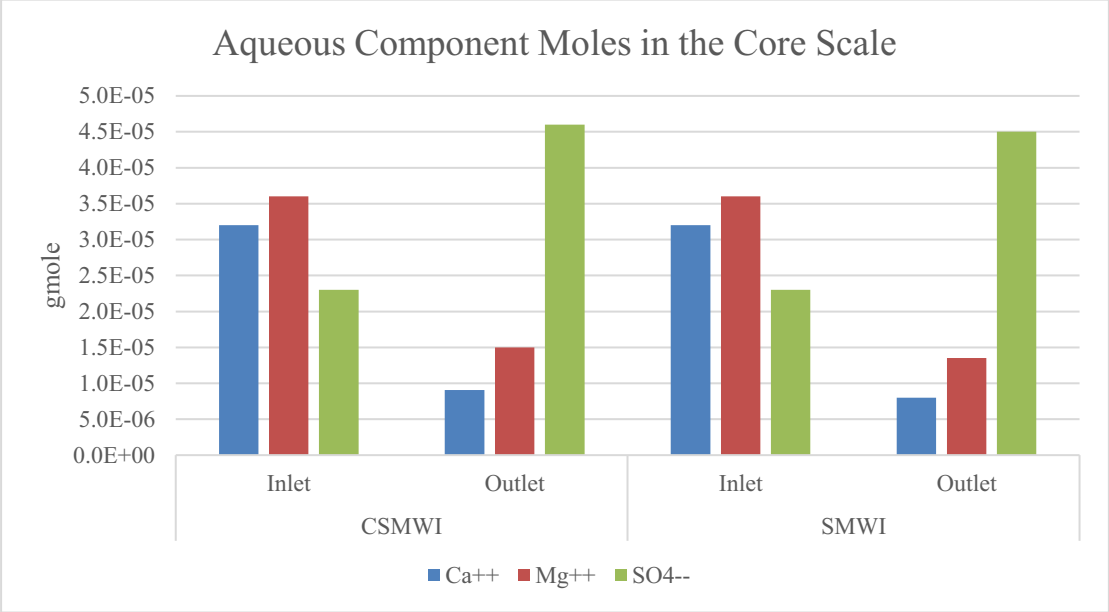


Figure 27: Aqueous Components Change in the Core

Figure 28 depicts the ions exchange on the fractured heterogeneous reservoir. The behavior of the ions change in the pilot is obviously different from it in the core scale, where all of the divalent ions are increasing in both scenarios, SMWI and CSMWI, but with different values. However, the increase of $Ca^{2+}$ and $Mg^{2+}$ concentration is more pronounced in the CSMWI. This increment could be attributed to the Dolomite and Calcite dissolution, as will be explained in the Mineral dissolution and Porosity Changes part.

The $SO_4^{2-}$ decreased by 27.5 % when the CSMWI was injected compared to the SMWI. The reduction of the $SO_4^{2-}$ in the CSMWI compared to the SMWI refers to the consumption of the sulfate in the processes that occurred in the CSMWI, such as the electrical double layer expansion, where the $SO_4^{2-}$ replaces the adsorbed carboxylic group of the oil from the rock surface. Consequently, it will be bonded with the positive charged divalent ($Ca^{2+}$ and $Mg^{2+}$), forming an electrical double layer. Based on the previous explanation and from Figure 28, it can be concluded that the ion exchange process in the SMWI is not active like in the CSMWI. However, it can be considered as an important mechanism of the enhanced oil recovery in the CSMWI method.

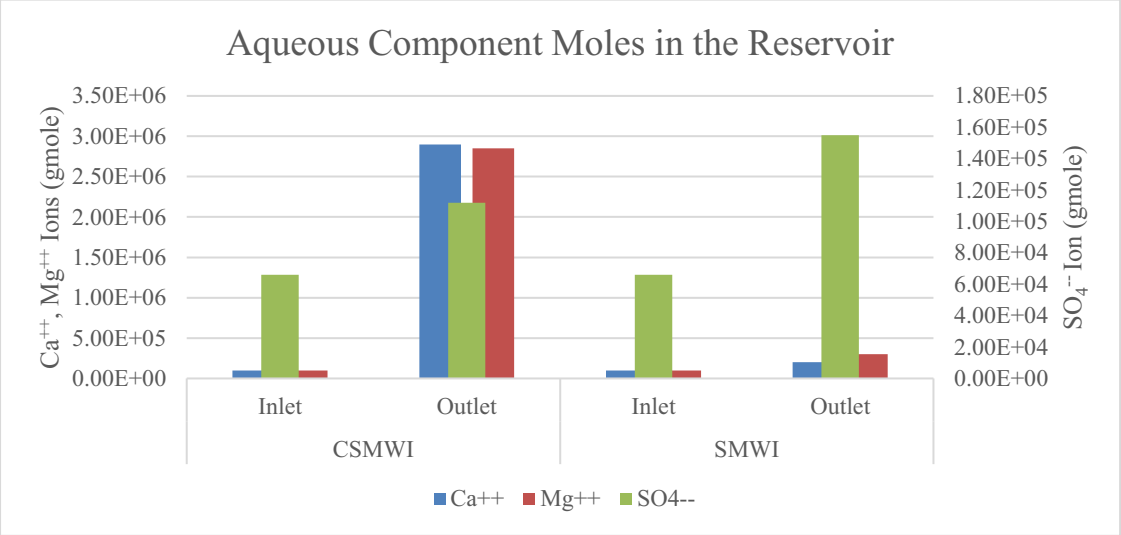


Figure 28: Aqueous Components Change in the CSMWI and SMWI in the fractured heterogeneous Reservoir

Figure 29 and Figure 30 show the ion exchange in the non-fractured and fractured reservoirs, respectively. The $SO_4^{2-}$ in the non-fractured reservoir did not change as much as it in the fractured reservoir due to the precipitation of the $NaSO_4^-$ as can be seen in Figure 31.

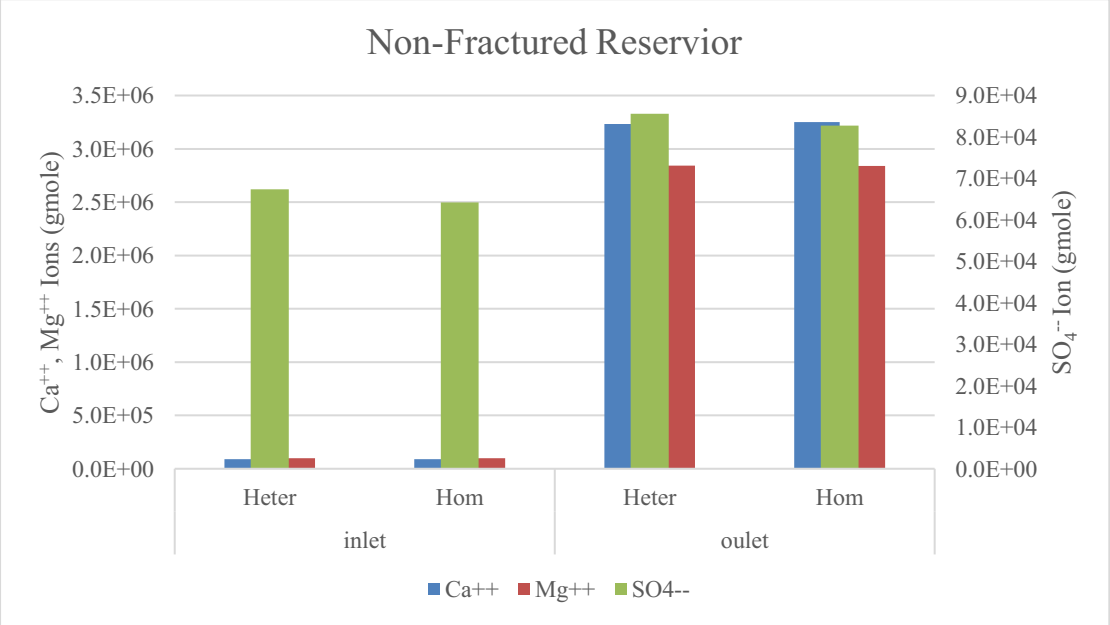


Figure 29: Aqueous Components Change in the Non-Fractured Reservoir

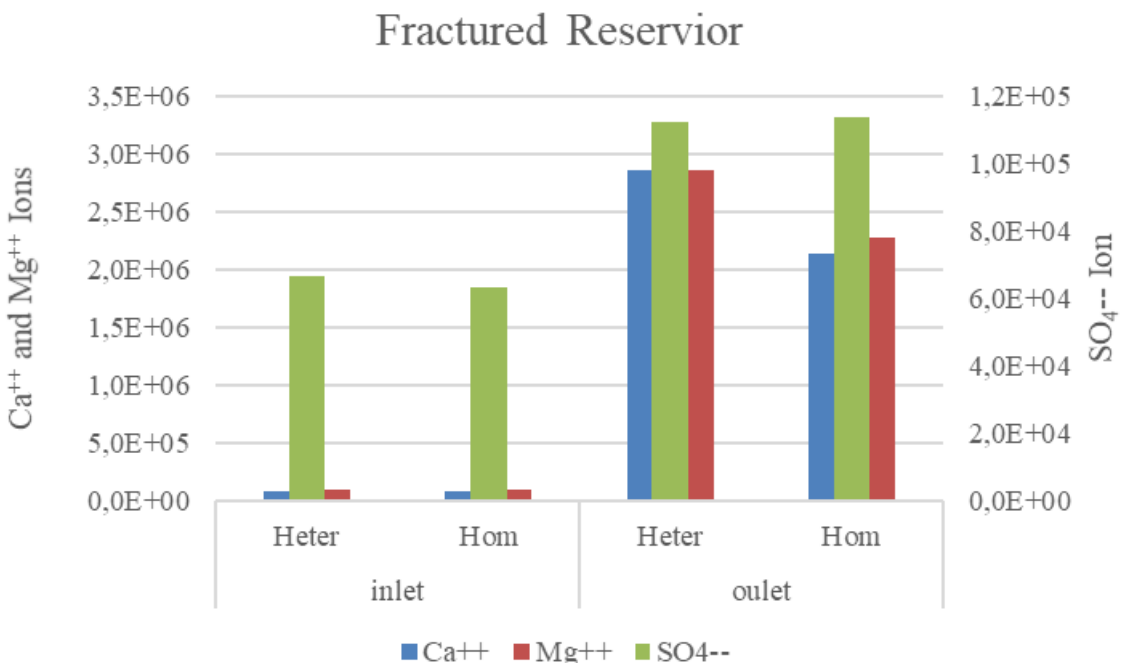


Figure 30 Aqueous Components Change in the Fractured Reservoir

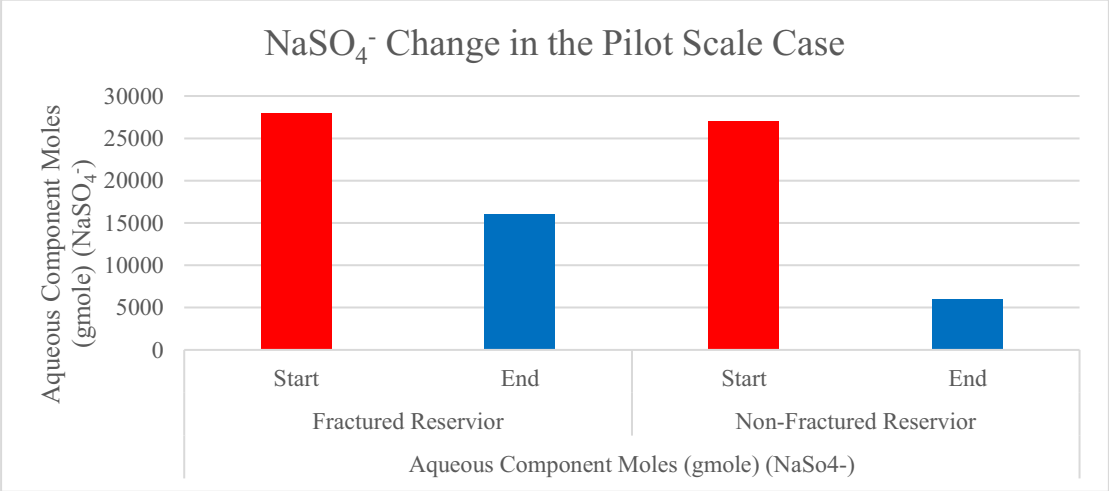


Figure 31: $NaSO_4^-$ Change in the Heterogeneous Reservoir.

#### 4.2.1.2 Mineral dissolution and Porosity Changes

##### 4.2.1.2.1 Core Scale

Dissolving carbon dioxide in water generates carbonic acid, which reacts with minerals in carbonates leading to rocks dissolution and the pore volume increase. In some cases, the results of the interaction might be precipitation, which could block the pores. In the core scale, no considerable mineral dissolution was observed, where the increase in the pore volume was less

than 0.015 % after 5 PV carbonated water injection. Figure 32 shows the changes in the pores after 5 PV. This conclusion matches the results of the experiment conducted by Soleimani et al. (2020), where they found out that the increase of the porosity is small and less than 0.5%.

The negligible change in the pore volume and the minerals could be attributed to the time and length scale in the core flooding case, where the reactions have no enough time to occur actively. From the core study alone, it can be concluded that the CSMWI has a negligible effect on the mineral dissolution, but this conclusion was disproved after the inspection of the pilot results analyzing, as will be explained in the Pilot Scale part.

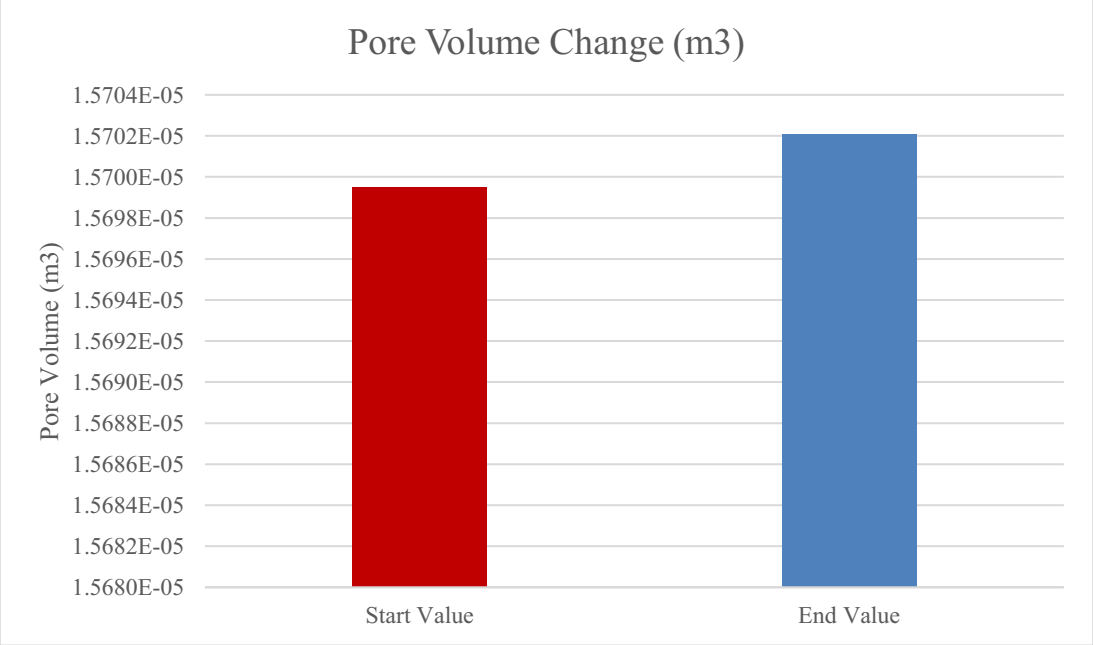


Figure 32: Pore Volume Change in the Core after 5 PVI.

#### 4.2.1.2.2 Pilot Scale

In the pilot-scale, mineral dissolution is considered to be one of the important mechanisms affecting oil recovery. The pore volume increased in the pilot-scale by 2.5-5 % in different cases based on the heterogeneity and fractures availability. As can be seen from Figure 33 and Table 7, mineral dissolution is more pronounced in the homogeneous system than the heterogeneous and fractured systems. This could be due to the consistency and uniformity of the fluid movement in the homogeneous pores. The homogeneity allows the fluid to reach all of the pores in the rock; thus, the carbonated water will be in contact with the highest specific surface area of the pores compared to the other cases of the heterogeneity and fractured systems. Furthermore, the time of the contact will be almost equal in all pores because of the regularly injected waterfront.

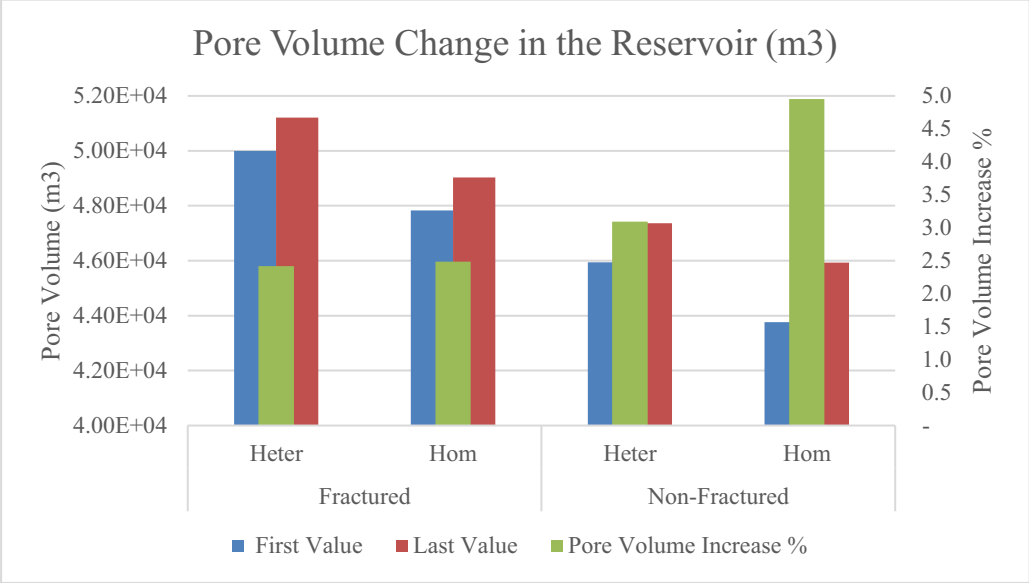


Figure 33: Pore Volume change in the Reservoir Cases (Field)

Table 7: Pore Volume Increase Values in Different Cases in the Pilot-Scale

| System | Non-Frac. Hom | Non-Frac. Het | Frac. Hom | | Frac. Het | |
|---|---|---|---|---|---|---|
| Mineral Dissolution % | 5.14 | 3.1 | 2.5 | | 2.5 | |
| | | | Fracture | Matrix | Fracture | Matrix |
| | | | 27.6 % | -0.12 % | 16 % | 1 % |

In the fractures and the high permeable part of the heterogeneous rock, the fluids will move with low velocity in the large pores, and it will be in contact with fewer surface areas of the pores than the homogeneous system. This will lead to slight active reactions occur, leading to minor mineral dissolution values. This slow movement allows the system to reach the local equilibrium state of the minerals, and to the global equilibrium, but to some extent. In the small pores, the fast movement of the fluids leads to a continuous renewal of the smart water resulting in continuous chemical reactions. These repeated actions do not allow the local or the global equilibrium to occur, thus more mineral dissolution results. In the fractured system, despite the slow water movement in the fractures, most water volume flows in the fractures imbibes into the matrix. Therefore, the reactions will be active in the fractures more than the matrices; thus, the pore volume change, and subsequently, mineral dissolution will be higher, as shown in Figure 34.

In the fractured homogeneous system, the reactions resulted in a precipitation of the minerals in the matrix (micropores), which is reflected mainly in the pore volume change as can be seen in Figure 35, which matches the results observed by Soleimani et al. (2020). This pore volume reduction might be attributed to the deposition of some minerals such as the $Na_2SO_4$ and $Na_2CO_3$ due to the small pore volume in the matrix and the low flow velocity that cannot overcome the critical velocity to carry the reaction products. This reduction occurs in

the matrix is similar to some reported experiment results (Figure 35). A reduction in the micro-pores, which refers to blockages of pores due to deposition of sulfate scales or produced fines, and an increase in the macro-pores have been reported due to mineral dissolution (Kilybay et al., 2017).

In the fractured heterogeneous reservoir, the mineral dissolution occurs in the fractures and in the large pores of the matrices as well. The effect of the heterogeneity on the recovery factor and mineral dissolution appears in this system, as shown in Figure 34. The difference between the homogeneous and heterogeneous reservoirs is that the water will flow in the fractures and the large pores in the heterogeneous rocks, thus the reactions will occur in the fractures and the large pores. The mineral precipitation in the micropores is compensated by the dissolution of the larger pores. In the fractured homogeneous reservoir, the water is flowing, as mentioned before, only in the fractures and will imbibe into the matrix pores.

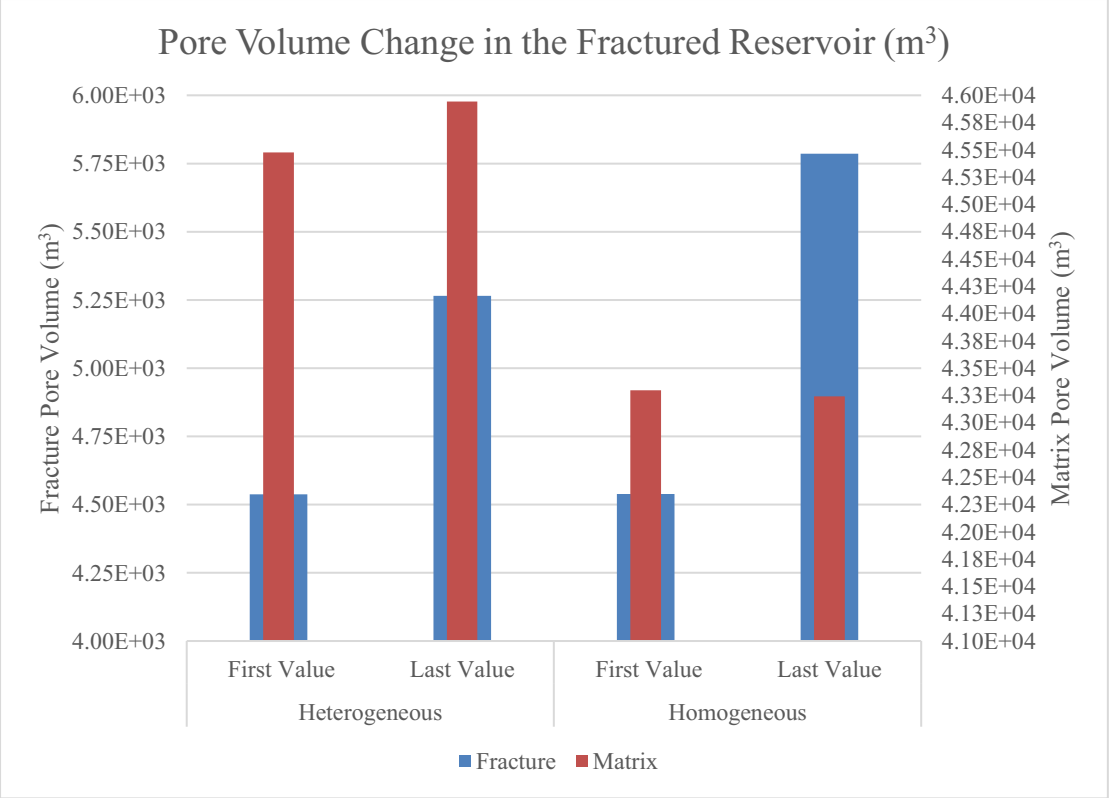


Figure 34: Pore Volume change in the Fractured Reservoir Cases (Fractures and Matrices)

Mineral dissolution change in the fracture and matrix of the fractured homogeneous reservoir is shown in Figure 35.

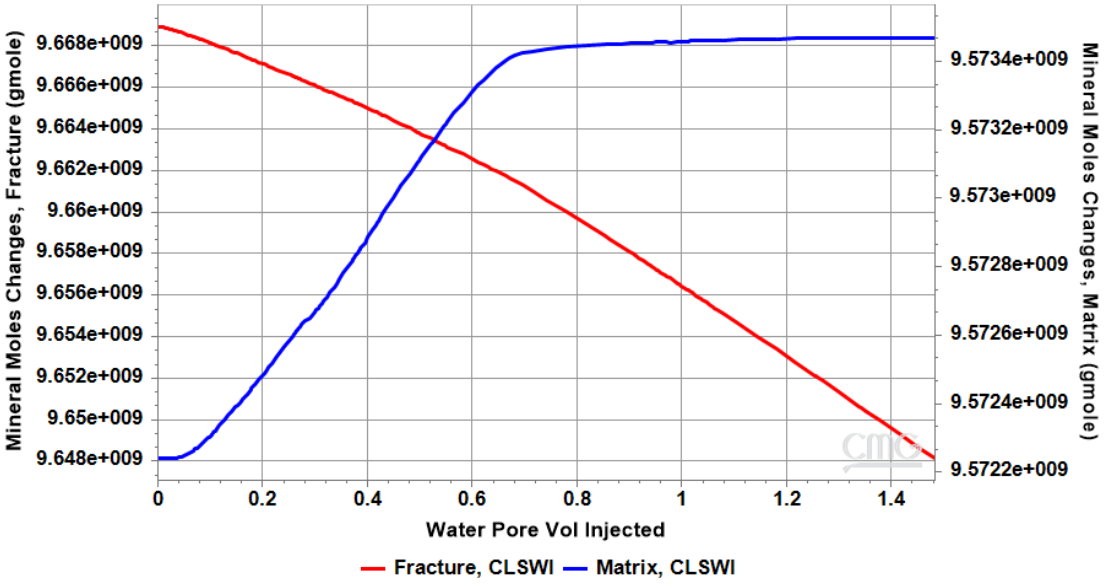


Figure 35: Mineral Dissolution in the Fractured Homogeneous Reservoir

Figure 36 depicts the mineral dissolution in the studied reservoir cases. Almost 0.1 % of the minerals have been dissolved in the fractured reservoir, and twice more minerals have been dissolved in the non-fractured reservoir. These values matched the trend of the pore volume changes in the reservoir system. These low values of the mineral dissolution might be contributing to a slight extent in the recovery factor.

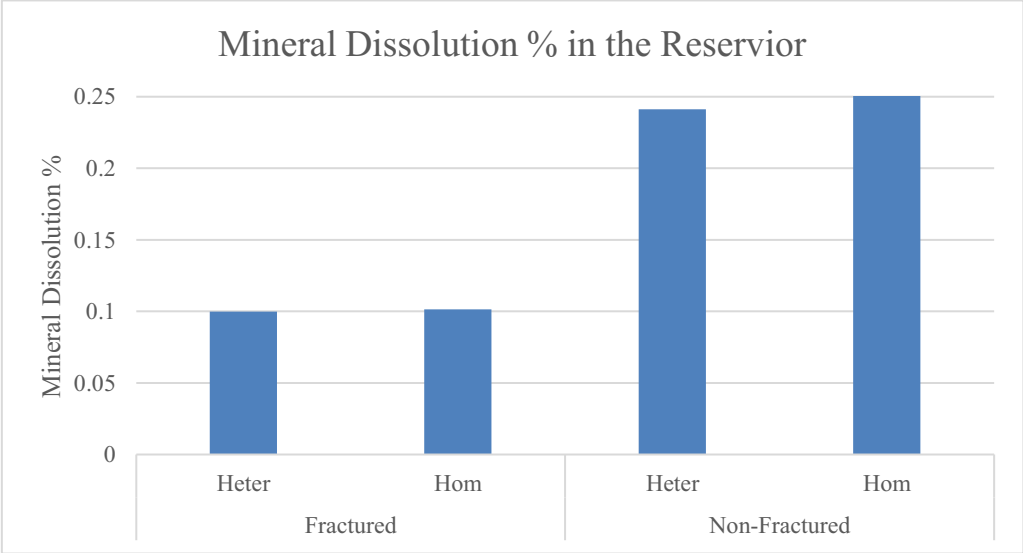


Figure 36: Mineral Dissolution % in the Several Cases of the Reservoir

The mineral dissolution is more significant in the case of the CSMWI than it is in the case of SMWI, as shown in Figure 37. In fact, the overall pore volume value in the case of SMWI is reduced, which indicates the mineral precipitation. Mineral dissolution is a potential mechanism that leads to increase RF of CSMWI.

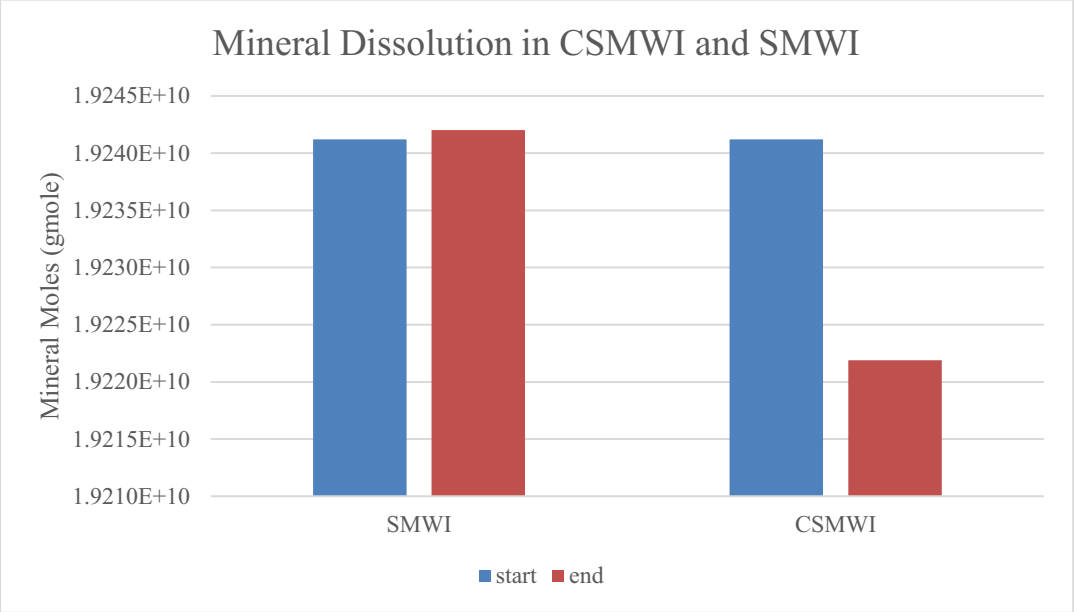


Figure 37: Mineral Dissolution in the CSMWI and SMWI

#### 4.2.1.3 Viscosity reduction

Viscosity reduction is considered to be one of the main mechanisms of the enhanced oil recovery in the CSMWI. The viscosity, in the core case, reduced in the injector and producer areas at the same value, which is 72 %. Similar reduction values in the producer and injector areas could not be reached in the pilot cases because of the inability to reach the irreducible oil after a reasonable time. Figure 38 and Figure 39 show the viscosity reduction in the core scale case. The diffusion of the $CO_2$ into the oil reduces the viscosity widely, leading to an enhancement of the sweep efficiency and the mobility of the water-oil system. An extreme reduction is reached in the inlet and outlet of the core, where it can be seen that no oil can be produced after a certain water pore volumes injection (0.1 PV and 3.4 PV in the inlet and outlet, respectively).

In the five spots model, 63.5% and 70% oil viscosity reduced has been obtained in the matrix and fracture, respectively. This reduction was in the injector area after 0.2 PV (Figure 40). In the producer area, oil viscosity did not reach the final value after 1.5 PV injection because the oil saturation in the fractures and the matrix did not reach a constant value yet (Figure 41). A round 31% and 15% oil viscosity reduction has been observed in the fractures and matrix in the producer area, respectively. This reduction of the viscosity is considered very high compared to the viscosity reduction caused by the SMWI, as can be seen in Figure 42, where SMWI reduced the oil viscosity 2.8 %. Therefore, it could be concluded that the viscosity reduction could be the main factor affecting the oil recovery in the CSMWI method.

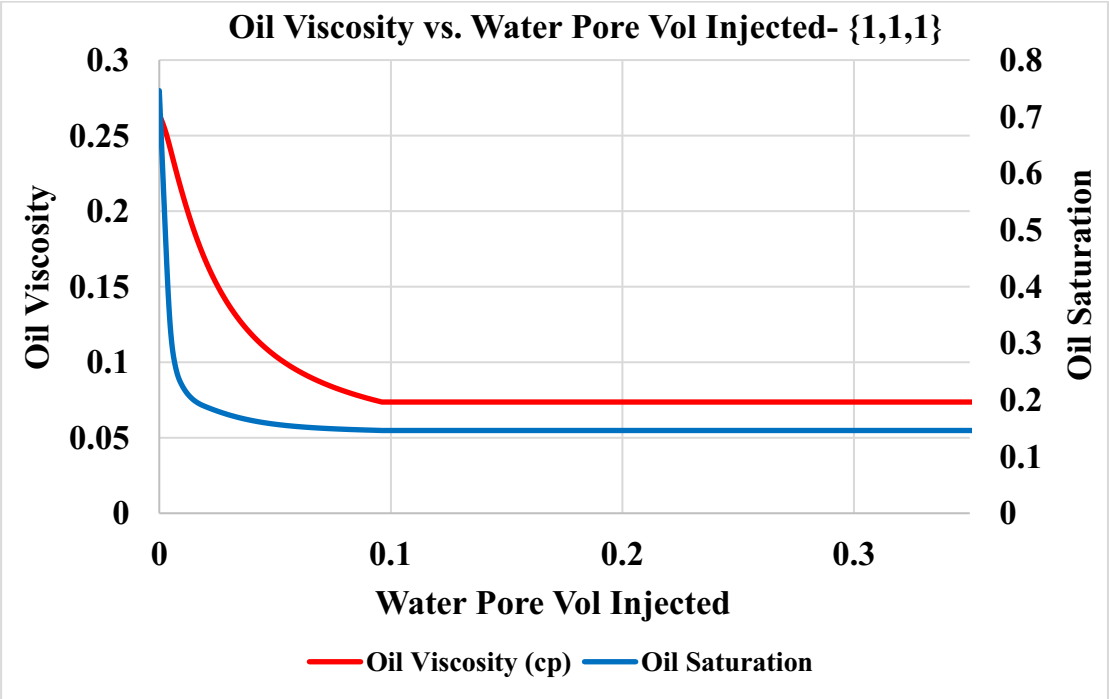


Figure 38: Oil Viscosity in the injector (inlet), Core Case

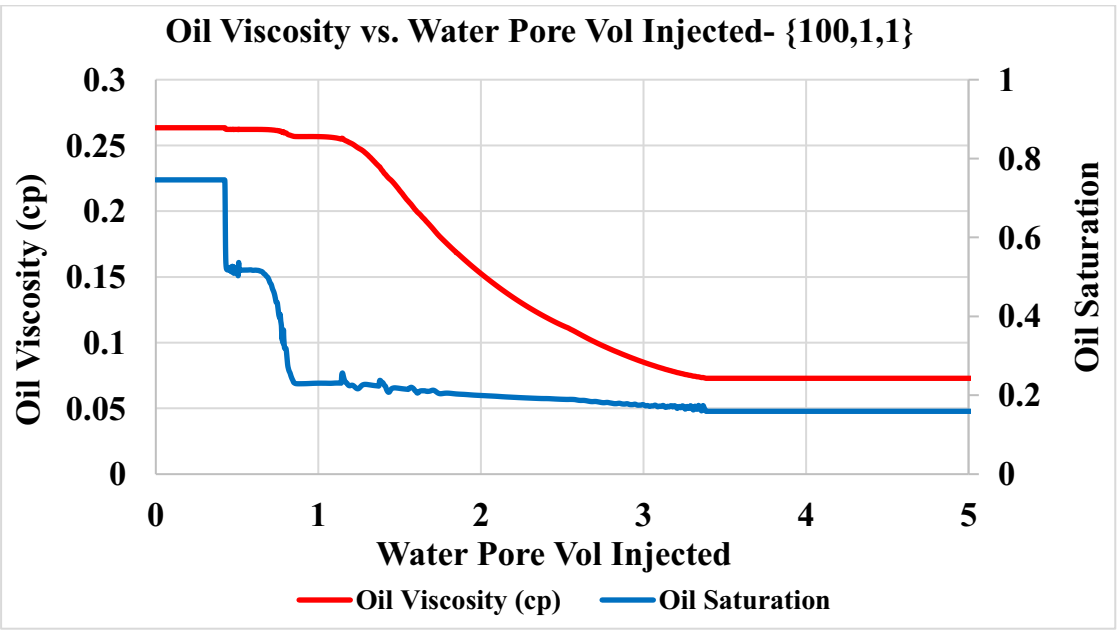


Figure 39: Oil Viscosity in the Producer (outlet), Core Case

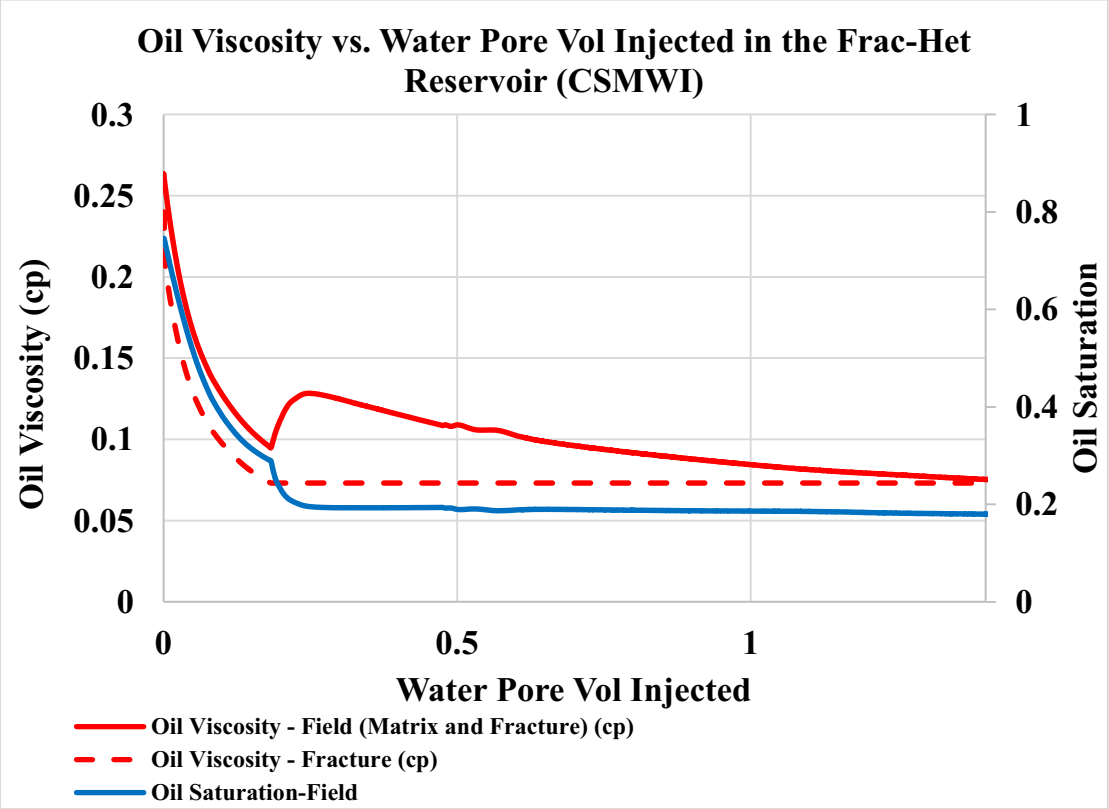


Figure 40: Oil Viscosity and Saturation in the injector, Pilot Case.

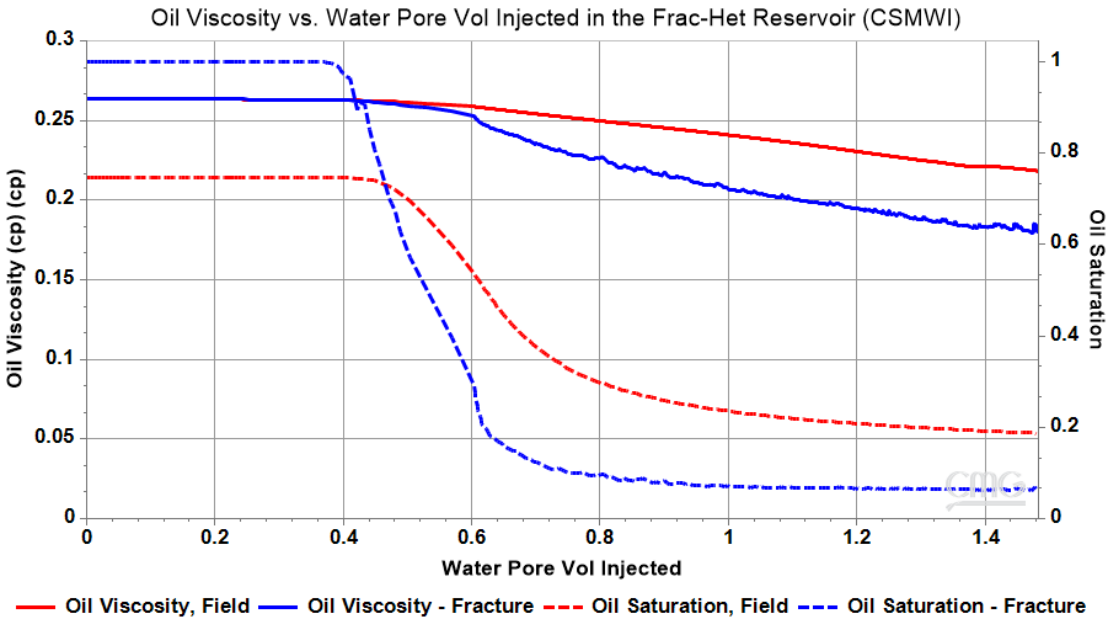


Figure 41: Oil Viscosity and Saturation in the Producer, Pilot Case

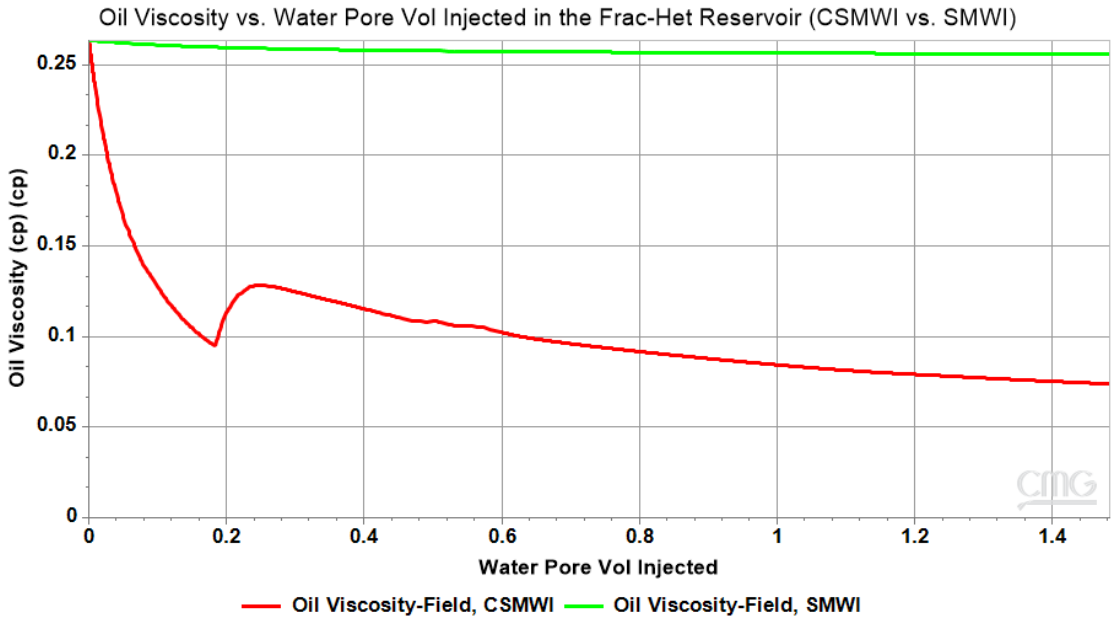


Figure 42: Oil Viscosity, in the CSMWI and SMWI cases in the Fractured Heterogeneous Reservoir

#### 4.2.1.4 Mobility Enhancement

The mobility of the water enriched with $CO_2$ will be lower than the mobility of the conventional water due to the viscosity increase of the carbonated water when the $CO_2$ is dissolved in it. Based on the mobility equation, the higher the water viscosity, the lower the mobility ratio, which means that the O-W front will be more stable, leading to more oil recovery.

$$M = \frac{K_{rw}}{K_{ro}} \frac{\mu_o}{\mu_w}$$

Where: $\mu_w$ = water viscosity, cp; $\mu_o$ = Oil viscosity, cp; $k_{rw}$ = relative permeability of water; and $k_{ro}$ = relative permeability of oil.

Furthermore, the $CO_2$ will decrease the viscosity of the oil, as explained in the Viscosity reduction part. This reduction in the viscosity leads to a more enhancement of the mobility ratio, thus the sweep efficiency.

This slower movement of the CW, due to the high viscosity, will result in a semi-stable injected waterfront and will prevent the early breakthrough and fingering phenomena. The gained stable front will be reflected in the RF of CSMWI. Figure 43 and Figure 44 depict the breakthrough of the CSMWI and SMWI in the core and the pilot, respectively. It can be obviously seen that the CSMWI has been delayed with respect to SMWI by 0.03 PV and 0.125 PV in the core and pilot, respectively. Length and time scales play the main role in the BT time of the SMWI and CSMWI in the core compared to the pilot.

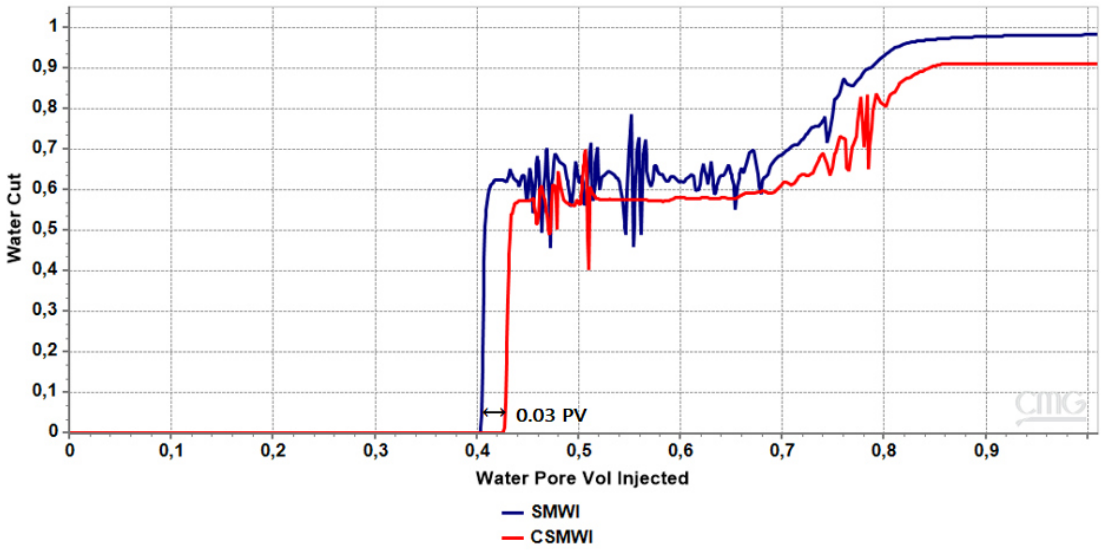


Figure 43: Water Cut in the Core Scale for SMWI and CSMWI

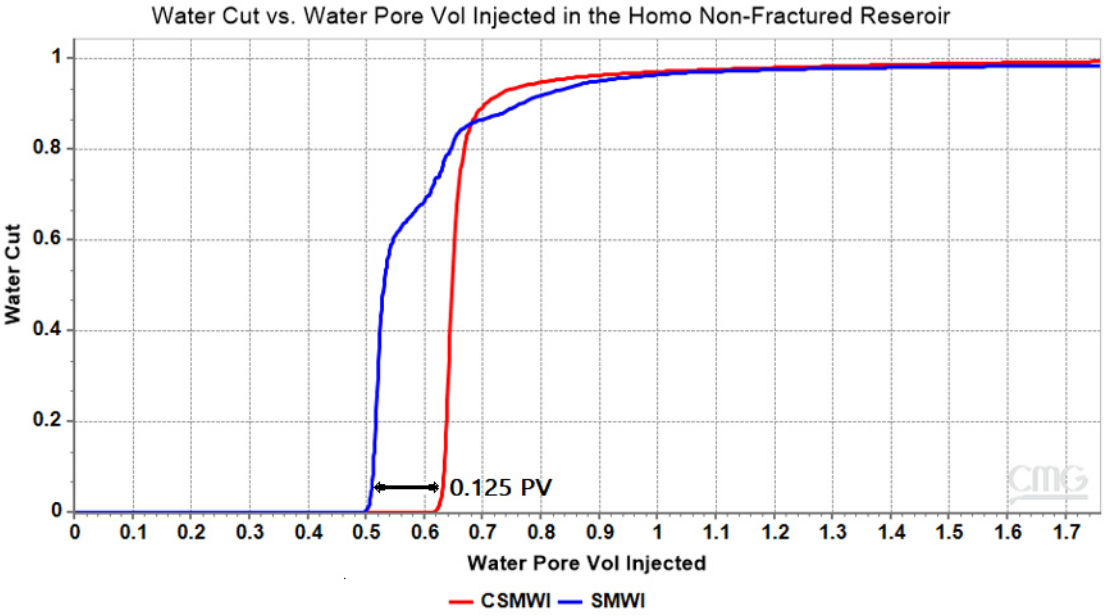


Figure 44: Water Cut in the Pilot Scale for SMWI and CSMWI

#### 4.2.1.5 Wettability alteration

Mineral dissolution results in carboxylic oil components release with its adsorbed layer of the carbonate rocks. This process and the ion exchanges lead to a change in the rock wettability by replacing sulfate ion with oil on the rock surface. This change of wettability can be seen in Figure 45 and Figure 46 in the matrix and fracture, respectively. The shifting of the curve intersection to the right side expresses the wettability alteration toward more water wet, which is one of the important enhancement oil recovery indicators.

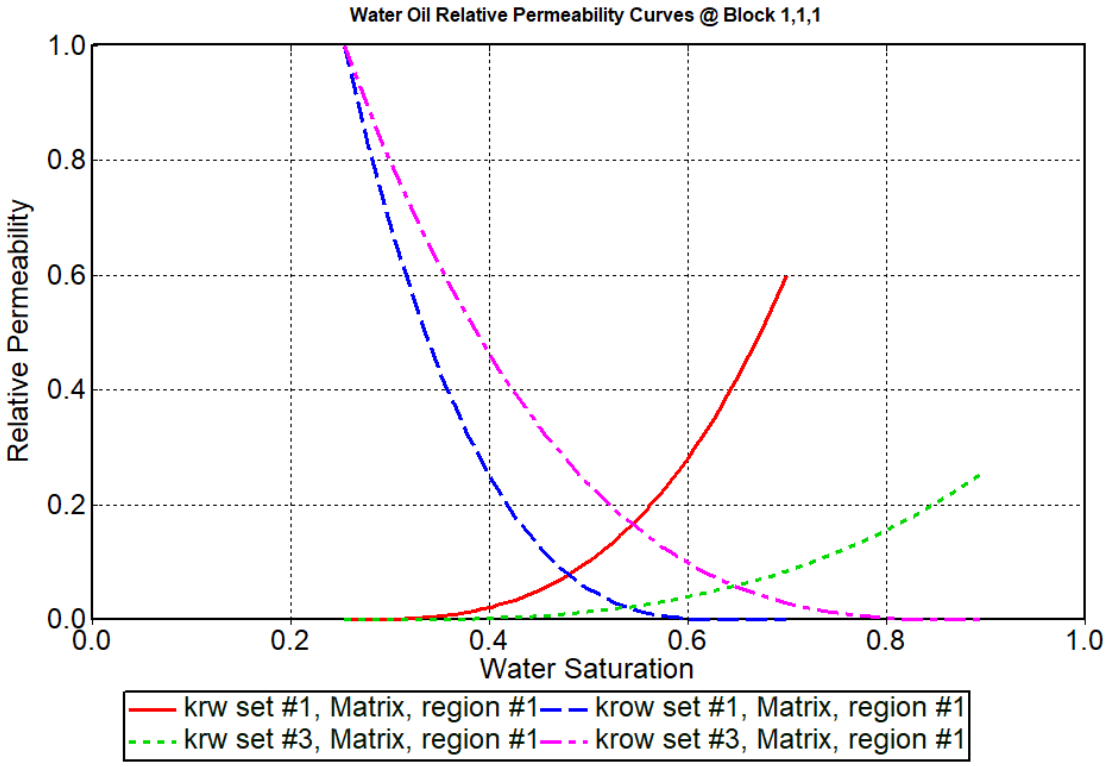


Figure 45: Wettability Alteration in the Matrix by Using CSMWI

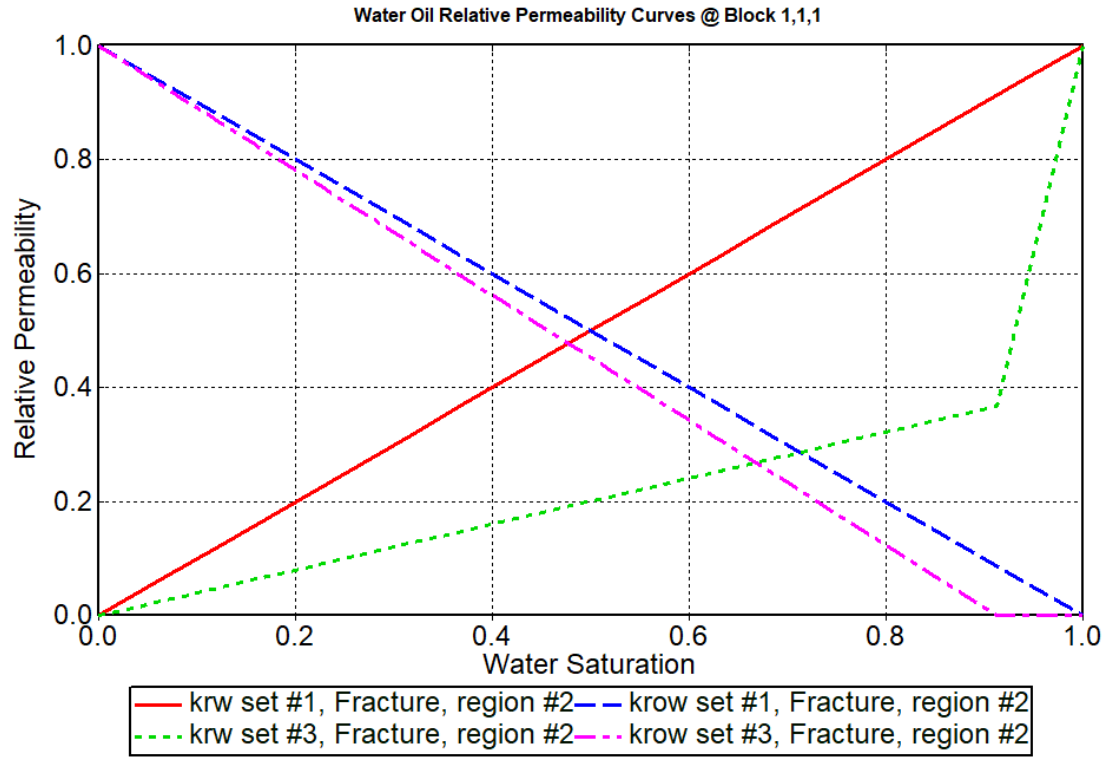


Figure 46: Wettability Alteration in the Fractures by Using CSMWI

### 4.2.1.6 PH variation

Figure 47 and Figure 48 show the PH changes during the CSMWI in the core and pilot, respectively. The reduction of the PH due to the generated acid will increase the IFT of the system (Al-Attar et al., 2013; Esene et al., 2018; Kilybay et al., 2017), preventing the rock surface wettability from being changed. Therefore, the PH reduction will not enhance the oil recovery during CSMWI, but it will impede it by increasing the IFT. This constraint will be compensated by ion exchange and mineral dissolution mechanisms, resulting in a wettability alteration.

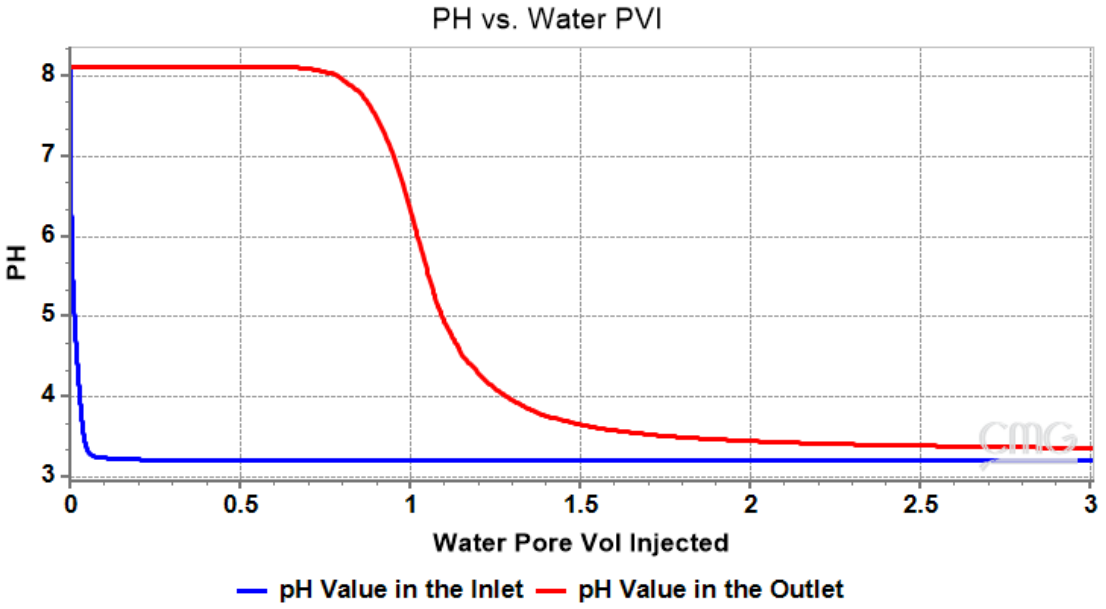


Figure 47: PH Change in the Core

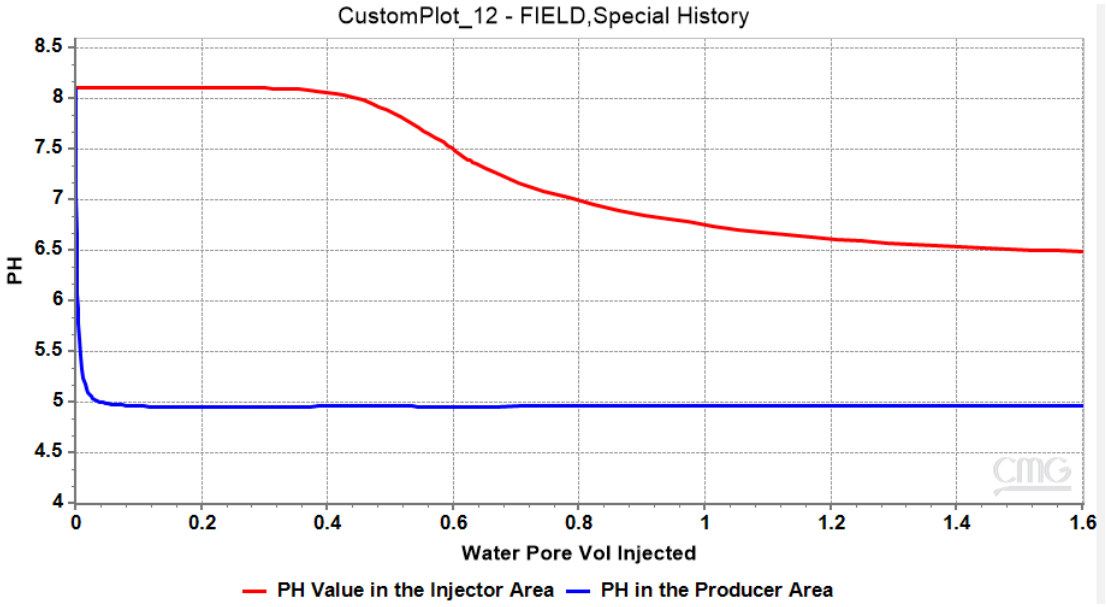


Figure 48: PH Change in the Reservoir

# Chapter 5

# Conclusion

## 5.1 Summary

The carbonated smart water injection has been demonstrated as a promising EOR method for naturally fractured carbonate reservoirs. Diluted water or LSWI cannot always be used like SMW, but the SMW has to be studied based on the formation water and minerals to find out the optimum smart composition.

CSMWI recovered more oil than SMWI, CSWI, and SWI by 14, 7.6, 26.8 % in the core scale, and in the secondary stage recovery. When CSMWI is injected in the tertiary stage, the recovery factor was less than the secondary stage by 4%. In the five spots case, the CSMWI recovered more oil than the SMWI by 5 to 8% in the studied cases based on the heterogeneity and fractures presence.

As a co-optimization method, 40% of the injected $CO_2$ was stored in the core case, while 50% of the $CO_2$ was stored in the CSWI case due to the higher residual oil saturation when the CSW is used compared with the CSMWI. In the pilot-scale case, 56% and 45.5% of the injected $CO_2$ have been permanently and safely stored in the fractured and non-fractured heterogeneous reservoirs.

Ions exchange and mineral dissolution processes proved to be pivotal mechanisms to enhance oil recovery in the CSMWI in the pilot case, but in less extent, in the core. The pore volume in the core increased only by 0.015% due to the time and length scale in the core model, which did not allow the reactions and other processes to occur effectively. In the five spots model, the pore volume increased by 2.5-5%.

Viscosity reduction is one of the main mechanisms behind the oil recovery increment when the CSMWI method is applied. CSMW decreased the oil viscosity 72% in the core scale

and 30-70% in the five spots case. The reduction of the oil viscosity enhanced the mobility ratio and thus the sweep efficiency in the system, leading to a like-piston displacement and late breakthrough time, where no fingering was observed.

Wettability alteration to more water-wet was observed when CSMWI was used, leading to more oil recovery.

## 5.2 Evaluation

This thesis paves the way for study the impact of carbonated smart water injection in naturally fractured carbonate reservoirs. Some other projects have been conducted in this field of study but only in the core scale and rarely in the pilot scale. Even those projects that shed light at the pilot-scale were not sufficient. Furthermore, no previous work studied the effect of the fractures on the CSMWI-Carbonate reservoir system. Although what has been achieved in this work, there is more need to study the mechanisms behind the effects of the CSMWI, especially experimentally. This thesis reached a good level of the aspired objectives, but further works and explanations are needed to complete and compare what has been done here.

## 5.3 Future Work

Some experiments should be performed to verify the simulation results, especially with regard to the fractured reservoirs. A combination between the CSMWI method and other EOR methods might be done, such as the Polymer-CSMWI slugs injection, to give the CSMWI more enough time to enhance the reservoir either from the geochemical reaction side or from the CO2 transfer side. More attention should be given to the oil swelling phenomenon, which is unfortunately not supported in the CMG simulator. The simultaneous transfer of the $CO_2$ from the carbonated water into the oil could not be overcome in the simulation work (at least until today), therefore the results of the simulation work still questionable until they have been proved by the experimental results.

# Chapter 6

## References

Afekare, D. A., & Radonjic, M. (2017). From Mineral Surfaces and Coreflood Experiments to Reservoir Implementations: Comprehensive Review of Low-Salinity Water Flooding (LSWF). Energy and Fuels, 31(12), 13043–13062. https://doi.org/10.1021/acs.energyfuels.7b02730

Al-Attar, H. H., Mahmoud, M. Y., Zekri, A. Y., Almehaideb, R. A., & Ghannam, M. T. (2013). Low Salinity Flooding in a Selected Carbonate Reservoir: Experimental Approach. Paper SPE 164788. EAGE Annual Conference & Exhibition.

Al Mesmari, A., Mahzari, P., & Sohrabi, M. (2016). An Improved Methodology for Simulating Oil Recovery by Carbonated Water Injection: Impact of Compositional Changes. SPE Annual Technical Conference and Exhibition. https://doi.org/10.2118/181630-MS

Andrea Saltelli, M. R. (2008). Global Sensitivity Analysis. The Primer.

Bakhshi, P., Kharrat, R., Hashemi, A., & Zallaghi, M. (2018). Experimental evaluation of carbonated waterflooding: A practical process for enhanced oil recovery and geological CO2 storage. Greenhouse Gases: Science and Technology, 8(2), 238–256. https://doi.org/10.1002/ghg.1734

Chang, Y. B., Coats, B. K., & Nolen, J. S. (1996). A Compositional Model for CO2 Floods Including CO2 solubility in water. In Society of Petroleum Engineers - Permian Basin Oil and Gas Recovery Conference, OGR 1996 (pp. 189–201). Society of Petroleum Engineers. https://doi.org/10.2118/35164-pa

Cleverson, Zendehboudi, Esene, S., Aborig, A., & Shiri, H. (2019). A modeling strategy to investigate carbonated water injection for EOR and CO 2 sequestration. Fuel, 252(April), 710–721. https://doi.org/10.1016/j.fuel.2019.04.058

De Nevers, N. (1964). A Calculation Method for Carbonated Water Flooding. Society of Petroleum Engineers Journal, 4(01), 9–20. https://doi.org/10.2118/569-pa

Eidan, A. A., Yousef, A. A., Sohrabi, M., Farzaneh, S. A., Tsolis, P., Mahzari, P., & Enezi, S. (2017). A Comprehensive Experimental Study of Pore-Scale and Core-Scale Processes During Carbonated Water Injection Under Reservoir Conditions, (April). https://doi.org/10.2118/188142-ms

Esene, C., Onalo, D., Zendehboudi, S., James, L., Aborig, A., & Butt, S. (2018). Modeling investigation of low salinity water injection in sandstones and carbonates: Effect of Na+ and SO42−. Fuel, 232(June), 362–373. https://doi.org/10.1016/j.fuel.2018.05.161

Esene, C., Rezaei, N., Aborig, A., & Zendehboudi, S. (2019). Comprehensive review of carbonated water injection for enhanced oil recovery. Fuel, 237(October 2018), 1086–1107. https://doi.org/10.1016/j.fuel.2018.08.106

Fathollahi, A., & Rostami, B. (2015). Carbonated water injection: Effects of silica nanoparticles and operating pressure. The Canadian Journal of Chemical Engineering, 93(11), 1949–1956. https://doi.org/10.1002/cjce.22289

Glen, G., & Isaacs, K. (2012). Estimating Sobol sensitivity indices using correlations. Environmental Modelling and Software, 37, 157–166. https://doi.org/10.1016/j.envsoft.2012.03.014

Haard, D. (2006). Oil and gas production handbook: An introduction to oil and gas production. An Introduction to Oil and Gas Production. https://doi.org/10.1016/S1359-0294(00)00069-8

Hamad, W. (2019). Low Salinity Water Flooding by Spontaneous Imbibition.

Hamouda, A., & Bagalkot, N. (2019). Effect of Salts on Interfacial Tension and CO2 Mass Transfer in Carbonated Water Injection. Energies, 12(4), 748. https://doi.org/10.3390/en12040748

Hickok, C. W., Christensen, R. J., & Ramsay, H. J. (1960). Progress Review of the K&S Carbonated Waterflood Project. Journal of Petroleum Technology, 12(12), 20–24. https://doi.org/10.2118/1474-g

Honarvar, B., Azdarpour, A., Karimi, M., Rahimi, A., Afkhami Karaei, M., Hamidi, H., … Mohammadian, E. (2017). Experimental Investigation of Interfacial Tension Measurement and Oil Recovery by Carbonated Water Injection: A Case Study Using Core Samples from an Iranian Carbonate Oil Reservoir. Energy and Fuels, 31(3), 2740–2748. https://doi.org/10.1021/acs.energyfuels.6b03365

Kechut, N. I., Jamiolahmady, M., & Sohrabi, M. (2011). Experimental and Numerical Evaluation of Carbonated Water Injection (CWI) for Improved Oil Recovery and CO2 Storage. Proceedings of SPE EUROPEC/EAGE Annual Conference and Exhibition, 77, 111–120. https://doi.org/10.1016/j.petrol.2011.02.012

Kechut, N. I., Riazi, M., Sohrabi, M., & Jamiolahmady, M. (2010). Tertiary Oil Recovery and CO2 Sequestration by Carbonated Water Injection (CWI). SPE International Conference on CO2 Capture, Storage, and Utilization. https://doi.org/10.2118/139667-MS

Kilybay, A., Ghosh, B., Thomas, N. C., & Aras, P. (2016). Hybrid EOR Technology: Carbonated Water and Smart Water Improved Recovery in Oil Wet Carbonate Formation. In SPE Annual Caspian Technical Conference & Exhibition. Society of Petroleum Engineers. https://doi.org/10.2118/182567-MS

Kilybay, A., Ghosh, B., Thomas, N. C., & Sulemana, N. T. (2017). Hybrid EOR Technology: Carbonated Water-Smart Water Flood Improved Recovery in Oil Wet Carbonate Formation: Part-II. SPE Oil and Gas India Conference and Exhibition. https://doi.org/10.2118/185321-MS

Kono, F., Kato, A., Shimokawara, M., & Tsushima, K. (2014). Laboratory Measurements on Changes in

Carbonate Rock Properties due to CO2-saturated Water Injection, 1–10. https://doi.org/10.2118/172013-ms

Lashkarbolooki, M., Riazi, M., & Ayatollahi, S. (2018). Experimental investigation of dynamic swelling and Bond number of crude oil during carbonated water flooding; Effect of temperature and pressure. Fuel, 214(October 2017), 135–143. https://doi.org/10.1016/j.fuel.2017.11.003

Lee, J. H. (2018). Hybrid Carbonated Low Salinity Waterflood in Calcite-Cemented Sandstone: Effects of Low pH and Salinity on Oil Production and CO2 Storage, (2008), 23–26. https://doi.org/10.1246/cl.2010.702

Lee, J. H., Jeong, M. S., & Lee, K. S. (2017). Geochemical Modelling of Carbonated Low Salinity Water Injection CLSWI to Improve Wettability Modification and Oil Swelling in Carbonate Reservoir. SPE Latin America and Caribbean Mature Fields Symposium. https://doi.org/10.2118/184915-MS

Lee, J. H., Kim, G. W., & Lee, K. S. (2017). Evaluation of Hybrid EOR as Polymer-Assisted Carbonated Waterflood in Calcite Cemented Sandstone Reservoir. OTC Brasil, 1–19. https://doi.org/10.4043/28125-MS

Luo, W., Yuan, Z., Chu, H., Zhu, Z., Zou, J., Li, X., … Liao, X. (2018). An Experimental Study on Carbonated Water Injection of Core Samples from Tight Oil Reservoirs from Ordos Basin (Russian). https://doi.org/10.2118/191474-18rptc-ru

Mahzari, P., Tsolis, P., Sohrabi, M., Enezi, S., Yousef, A. A., & Eidan, A. A. (2018). Carbonated water injection under reservoir conditions; in-situ WAG-type EOR. Fuel, 217(January), 285–296. https://doi.org/10.1016/j.fuel.2017.12.096

Mansoori, J. (1982). Compositional Modeling Of CO2 Flooding And The Effect Of CO2 Water Solubility. Retrieved from https://www.onepetro.org/general/SPE-11438-MS?sort=&start=0&q=Compositional+modeling+of+CO2+flooding+and+the+effect+of+CO2+water+solubility&from_year=&peer_reviewed=&published_between=&fromSearchResults=true&to_year=&rows=25#

Mosavat, N., & Torabi, F. (2014a). Application of CO2-Saturated Water Flooding as a Prospective Safe CO2 Storage Strategy. Energy Procedia, 63, 5619–5630. https://doi.org/10.1016/j.egypro.2014.11.595

Mosavat, N., & Torabi, F. (2014b). Experimental evaluation of the performance of carbonated water injection (CWI) under various operating conditions in light oil systems. Fuel, 123, 274–284. https://doi.org/10.1016/j.fuel.2014.01.077

Mosavat, N., & Torabi, F. (2014c). Performance of Secondary Carbonated Water Injection in Light Oil Systems. Industrial & Engineering Chemistry Research, 53(3), 1262–1273. https://doi.org/10.1021/ie402381z

Nunez, R., Vaz, R. G., Koroishi, E. T., Vidal Vargas, J. A., & Trevisan, O. V. (2017). Investigation of dissolution effects on dolomite porous media under carbonated water injection CWI. Society of

Petroleum Engineers - SPE Abu Dhabi International Petroleum Exhibition and Conference 2017, 2017-Janua.

Parkhurst, D. L., & Appelo, C. a. J. (2013). Description of Input and Examples for PHREEQC Version 3 — A Computer Program for Speciation , Batch-Reaction , One-Dimensional Transport , and Inverse Geochemical Calculations. U.S. Geological Survey Techniques and Methods, Book 6, Chapter A43, 678. https://doi.org/10.1016/0029-6554(94)90020-5

Perez, J. M., Poston, S. W., & Sharif, Q. J. (1992). Carbonated Water Imbibition Flooding: An Enhanced Oil Recovery Process for Fractured Reservoirs. https://doi.org/10.2118/24164-ms

Qiao, C., Johns, R., & Li, L. (2016). Understanding the Chemical Mechanisms for Low Salinity Waterflooding. SPE Europec Featured at 78th EAGE Conference and Exhibition. https://doi.org/10.2118/180138-MS

Ramesh, A. B., & Dixon, T. N. (1973). Numerical Simulation of Carbonated Waterflooding In A Heterogeneous Reservoir. In SPE Symposium on Numerical Simulation of Reservoir Performance. Society of Petroleum Engineers. https://doi.org/10.2118/4075-MS

Ruidiaz, E. M., Winter, A., & Trevisan, O. V. (2017). Oil recovery and wettability alteration in carbonates due to carbonate water injection. Journal of Petroleum Exploration and Production Technology, 8(1), 249–258. https://doi.org/10.1007/s13202-017-0345-z

Sanaei, A., Varavei, A., & Sepehrnoori, K. (2019). Mechanistic modeling of carbonated waterflooding. Journal of Petroleum Science and Engineering, (April), 863–877. https://doi.org/10.1016/j.petrol.2019.04.001

Seyyedi, M., & Sohrabi, M. (2016). Enhancing Water Imbibition Rate and Oil Recovery by Carbonated Water in Carbonate and Sandstone Rocks. Energy and Fuels. https://doi.org/10.1021/acs.energyfuels.5b02644

Shakiba, M., Ayatollahi, S., & Riazi, M. (2016). Investigation of oil recovery and CO2 storage during secondary and tertiary injection of carbonated water in an Iranian carbonate oil reservoir. Journal of Petroleum Science and Engineering. https://doi.org/10.1016/j.petrol.2015.11.020

Shakiba, M., Riazi, M., & Ayatollahi, S. (2015). Oil Recovery and CO2 Storage through Carbonated Water Injection Process ; Experimental Investigation on an Iranian Carbonate Oil Reservoir Oil Recovery and CO 2 Storage through Carbonated Water Injection Process ; Experimental Investigation on an Iranian. The 1st National Conference on Oil and Gas Fields Development (OGFD).

Sohrabi, M., Emadi, A., Farzaneh, S. A., & Ireland, S. (2015). A Thorough Investigation of Mechanisms of Enhanced Oil Recovery by Carbonated Water Injection. SPE Annual Technical Conference and Exhibition. https://doi.org/10.2118/175159-MS

Sohrabi, M., Riazi, M., Jamiolahmady, M., Kechut, N. I., Ireland, S., & Robertson, G. (2011). Carbonated Water Injection (CWI) - A productive way of using CO2 for oil recovery and CO2 storage. Energy

Procedia, 4, 2192–2199. https://doi.org/10.1016/j.egypro.2011.02.106

Soleimani, P., Shadizadeh, S. R., & Kharrat, R. (2020). Experimental investigation of smart carbonated water injection method in carbonates, 22, 1–22. https://doi.org/10.1002/ghg.1948

Yousef, A. A., Al-Saleh, S. H., Al-Kaabi, A., & Al-Jawfi, M. S. (2011). Laboratory Investigation of the Impact of Injection-Water Salinity and Ionic Content on Oil Recovery From Carbonate Reservoirs. SPE Reservoir Evaluation & Engineering, 14(05), 578–593. https://doi.org/10.2118/137634-PA

Zhang, P., Tweheyo, M. T., & Austad, T. (2007). Wettability alteration and improved oil recovery by spontaneous imbibition of seawater into chalk: Impact of the potential determining ions Ca2+, Mg2+, and SO42-. Colloids and Surfaces A: Physicochemical and Engineering Aspects, 301(1–3), 199–208. https://doi.org/10.1016/j.colsurfa.2006.12.058

Zhang, Y., & Sarma, H. (2012). SPE 161631 Improving Waterflood Recovery Efficiency in Carbonate Reservoirs through Salinity Variations and Ionic Exchanges: A Promising Low-Cost "Smart-Waterflood" Approach.

Zhao, H., Dilmore, R., Allen, D. E., Hedges, S. W., Soong, Y., & Lvov, S. N. (2015). Measurement and Modeling of CO2 Solubility in Natural and Synthetic Formation Brines for CO2 Sequestration. https://doi.org/10.1021/ES505550A.S001

Zuo, L., & Benson, S. M. (2014). CO2 Exsolution – challenges and Opportunities in Subsurface Flow Management. Energy Procedia, 63, 5664–5670. https://doi.org/10.1016/J.EGYPRO.2014.11.599